The Dissertation Committee for Claudia Isela Torres Garibay Certifies that this is the approved version of the following dissertation:

MANUFACTURING OF INTERMEDIATE-TEMPERATURE SOLID OXIDE FUEL CELLS USING NOVEL CATHODE COMPOSITIONS

Committee:

Desiderio Kovar, Supervisor

Arumugam Manthiram

David L. Bourell

Harovel G. Wheat

John R. Howell

MANUFACTURING OF INTERMEDIATE-TEMPERATURE SOLID OXIDE FUEL CELLS USING NOVEL CATHODE COMPOSITIONS

by

Claudia Isela Torres Garibay, B.S., M.S.

Dissertation

Presented to the Faculty of the Graduate School of

The University of Texas at Austin

in Partial Fulfillment

of the Requirements

for the Degree of

Doctor of Philosophy

The University of Texas at Austin

May, 2007

Dedication

Para mis padres, Armando y Elia,

que siempre han estado ahí por mí,

apoyando ilimitadamente mis sueños.

Mi red de seguridad. Viento bajo mis alas.

Sin ellos no sería quien soy, ni estaría donde estoy.

y sobre todas las cosas

AMDG

Acknowledgements

This project would not be possible with out the guidance, support, encouragement and patience of my advisor, Dr. Desi Kovar, to whom I am deeply thankful. I would also like particularly to thank Dr. Arumugam Manthiram for his advice during this project. I must recognize the invaluable assistance of people like Dr. Ki-Tae Lee, who trained me in many of the methods used in this work; Dr. Ronald Dass, from whom I learned some of the chemical synthesis techniques and always had a wise word to share; and Jung Hyun Kim, for precious "thinking aloud" conversations.

My most sincere appreciation to everybody at the Texas Materials Institute for their help and friendship, particularly former and current Kovar's research group members: Jue Wang who introduced me to tape casting; Sven Kerzenmaher who build the fuel cell test set up; James Ma who took the pictures in Appendix A; Andre Albert, who became my personal coach on to the proper and improper uses of English language; and Jesus Gallegos and Jim Mikulak for his advice. Special thanks to Dr. Kenneth Ralls and my former and current ME111L TA colleagues for their support.

A big thank you to my family, members of UGAP group at UCC, and my dear friends who are always a phone call away. Your love fuels my life.

Financial support provided by Conacyt, Mechanical Engineering Department and the Institute of Advance Technology has been highly appreciated during my doctoral studies.

MANUFACTURING OF INTERMEDIATE-TEMPERATURE SOLID OXIDE FUEL CELLS USING NOVEL CATHODE COMPOSITIONS

Publication No._____

Claudia Isela Torres Garibay, Ph.D.

The University of Texas at Austin, 2007

Supervisor: Desiderio Kovar

The development of intermediate temperatures solid oxide fuel cells (IT-SOFC) with YSZ electrolytes imposes a double requirement in their manufacturing. First, the electrolyte has to be kept as thin as possible to minimize ohmic polarization losses. Second, the cathode compositions used must exhibit an adequate catalytic activity at the operating temperature (600 – 800 ºC). Current methods to manufacture thin YSZ electrolytes require complex processes, and sometimes costly equipment. Cathode compositions traditionally used for high temperature solid oxide fuel cells, such as $(La,Sr)MnO_3$ do not exhibit good catalytic properties at intermediate temperatures. These challenges present areas of opportunity in the development of original manufacturing techniques and new cathode compositions. This study presents a low-cost fabrication

procedure for IT-SOFC using tape casting, co-firing and screen printing. The electrochemical performance of the cells is evaluated using a known cathode composition for IT-SOFC, such as $La_{0.6}Sr_{0.4}CoO_{3-\delta}$ (LSC), novel perovskite oxides, such as $Nd_{0.6}Sr_{0.4}CoO_{3-\delta}$ (NSC), and perovskite-related intergrowth oxides compositions, like $Sr_{0.7}La_{0.3}Fe_{1.4}Co_{0.6}O_{7-\delta}$ (SLFCO7) and $LaSr_3Fe_{1.5}Co_{1.5}O_{10-\delta}$ (LSFCO10). The impact of conductivity is studied by substituting Fe for Co in the case of the perovskite oxides, with compositions such as $La_{0.6}Sr_{0.4}Co_{0.5}Fe_{0.5}O_{3-\delta}$ (LSCF), and $Nd_{0.6}Sr_{0.4}Co_{0.5}Fe_{0.5}O_{3-\delta}$ (NSCF) and by infiltration of NSCF with silver. The effect of the cathode sintering temperature is studied using LSC and LSCF cathodes. It is found that there is generally a correlation between cell performance and conductivity. However, the microstructure of the cathode is also important in determining cell performance by tailoring the cathode sintering temperature. IT-SOFC with SLFCO7 cathodes show a performance comparable to cells with LSFC cathode. In the case of LSFCO10, the performance loss associated with its lower conductivity compared to LSC can be more than offset by tailoring the microstructure.

Table of Contents

List of Tables

List of Figures

Chapter 1: Introduction

Society has relied heavily on the exploitation of fossil resources for the last 200 years to meet energy requirements. However, to maintain sustainable development, it is imperative that alternatives are found to meet energy demands while significantly reducing the level of emissions. Fuel cells are one of the best examples of "green technologies" that can provide such alternatives. A fuel cell is an electrochemical device that converts chemical energy directly into electrical energy while producing little or no harmful by-products.[1-4]

1.1 Fuel Cells Advantages

Fuel cells are a versatile alternative for independent electrical generation.[1,2] In terms of efficiency, fuel cells surpass heat engines, like internal combustion engines, for two reasons. First, fuel cells operate isothermally; therefore they are not subject to the limitations of the Carnot cycle. Second, no additional conversion of energy is required to produce electricity in the electrochemical reaction of fuel cells.

Different types of fuel cells cover a great range of operation temperatures. Although hydrogen is the most common fuel used, some types of fuel cells are also able to operate on hydrogen reformed from hydrocarbons, or even directly on hydrocarbons. Water vapor and heat are the by-products when hydrogen is used as fuel.

In other cases, the levels of emissions are very low. Waste heat can also be used, further increasing the efficiency of a fuel cell system.

Minimal maintenance is required for fuel cells because they do not have moving components and their performance is free of noise and vibration. They offer great siting capability as they can be placed in a variety of locations, and their modularity makes their power output easily scalable by connecting fuel cells in series.

Fuel cells offer advantages with respect to batteries, which are also electrochemical devices.[1-3] Reactants are part of the structure of a battery; once they are consumed, the battery has to be recharged or replaced. In principle, a fuel cell can operate as long as the externally stored reactants are fed into the reaction areas and the reaction products are removed. Fuel cells only provide the sites for the electrochemical reaction to occur. The life span of a fuel cell is also potentially longer as ideally no reactions occur at their electrodes.

1.2 FUEL CELLS CLASSIFICATION

The main components of a fuel cell are a fuel electrode (anode), an oxidant electrode (cathode), both separated by an ion-conducting electrolyte.[1-4] Fuel cells can be classified according to their operation temperature, cell operating fuels and/or design features;[5] nevertheless the most common classification is based on the type of electrolyte, as different kinds of ions can be conducted by different types of electrolytes. Table 1.1 summarizes the characteristics of different types of fuel cells.[4]

Polymer electrolyte fuel cells, alkaline fuel cells, and phosphoric acid fuel cells operate in the low-temperature range. Molten carbonate fuel cells and solid oxide fuel cells are high temperature fuel cells. For solid oxide fuel cells, temperatures below 800 ºC are considered intermediate operation temperatures.

Table 1.1. Characteristics of different types of fuel cells (adapted from Minh[4]).

	Polymer Electrolyte Fuel Cell	Alkaline Fuel Cell	Phosphoric Acid Fuel Cell	Molten Carbonate Fuel Cell	Solid Oxide Fuel Cell
Electrolyte	Ion-exchange membrane	Mobilized or immobilized KOH	Immobilized liquid H_3PO_4	Immobilized liquid molten carbonate	Ceramic
Operating Temperature (ºC)	80	65-220	205	650	600-1000
Charge Carrier	H^+	OH^-	H^+	CO_3^{2-}	O^{2-}
External reformer for CH_4	Yes	Yes	Yes	No	No
Prime cell components	Carbon-based	Carbon-based	Graphite-based	Stainless Steel-based	Ceramic
Catalyst	Platinum	Platinum	Platinum	Nickel	Oxide perovskites or metal ceramic composites
Product water management	Evaporative	Evaporative	Evaporative	Gaseous product	Gaseous product

1.3 SOLID OXIDE FUEL CELLS

Solid oxide fuel cells (SOFC) exhibit various advantages over other types of fuel cells.[1,2,6] The use of a solid electrolyte instead of a liquid one makes SOFC easier to maintain, and there are no pore flooding or catalyst wetting problems.[1] The electrolyte is made usually from yttria doped zirconia (YSZ), a highly chemically and thermally stable material.[7] At high temperatures, YSZ can serve as a solid-state electrolyte as it becomes sufficiently conductive to oxide ions, while remaining non-conductive to electrons.

A major benefit of SOFC is that hydrocarbons can be directly used as fuel in a SOFC,[1-4] without the need for further transformation. The high operating temperature ensures that fuels will spontaneously internally reform and then oxidize rapidly to chemical completion without the need for specialized and expensive catalysts, as can be seen in Table 1.1. The lack of high-activity catalysts that can be easily poisoned also gives SOFC a high tolerance to impurities. SOFC can achieve the highest total energy efficiency among all types of fuel cells. The use of a solid oxide electrolyte reduces corrosion problems. Generated heat can be easily utilized in a simple and economical way.

1.3.1 Historical Background of SOFC

There has been great development of SOFC technologies in the last forty years, but fuel cells have been around for many years.[1,2,8] In 1839 Sir William Grove

demonstrated the operating principle of fuel cells by reversing the electrolysis of water. His cell used dilute sulfuric acid as electrolyte and operated at room temperature.[9] By the end of the century, certain oxide compositions, such as the so-called Nernst mass, were identified as ionic conductors at high temperatures.[10] The Nernst mass consisted of zirconia doped with 15 % yttria which is an insulator at room temperature, an ionic conductor when red hot (600 – 1000 °C) and both an electronic and ionic conductor at white heat (~ 1500 °C). Schottky suggested the use of the Nernst mass as a fuel cell solid electrolyte in 1935.[11] The operation of the first SOFC was demonstrated two years later, in 1937, by Baur and Preis, using magnesia- or yttria-stabilized zirconia as electrolytes at temperatures higher than 1000 °C.[12]

The study of yttria-doped zirconia electrolytes continued for the next decades, but it was until the early 60's when real efforts for practical applications of SOFC were made. Since then, research has focused on improving the design as well as the materials used in the components of the cells.

1.3.1 Operation Principle

The operating principle of a fuel cell[1,2,5,13] is shown in Figure 1, using common reactants for SOFC. A fuel, such as hydrogen, is fed to the anode and an oxidant, such as oxygen from air, is fed to the cathode. Hydrogen is oxidized at the anode and electrons are released to an external circuit, providing DC current to a load. Oxygen is reduced at the cathode, accepting incoming electrons from the external circuit. The

circuit is closed by oxygen ions that diffuse through the electrolyte to the anode interface where they react with the hydrogen ions to produce water vapor as a reaction product.

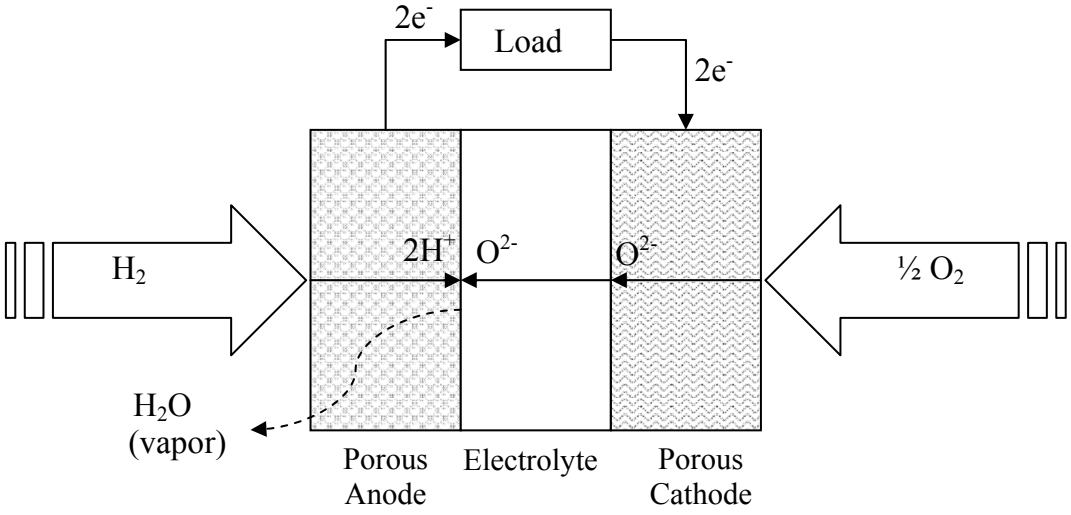

Figure 1.1. Operating principle of a SOFC

The half reactions at the electrodes and the overall reaction in the cell are:

Cathode	½ O_2	+	$2e^-$	→	O^{2-}
Anode	H_2	+	O^{2-}	→	$H_2O + 2e^-$
Cell	H_2	+	½O_2	→	H_2O

The efficiency ε of a fuel cell is the ratio of the electrical energy produced by the cell to the chemical energy of the reaction. The energy output is expressed as the Gibbs free energy change ΔG of the combustion reaction of the fuel. The chemical energy of the reaction is expressed in terms of enthalpy change ΔH or heat of combustion of the fuel. Thermodynamically

$$\varepsilon = \frac{\Delta G}{\Delta H} = \frac{\Delta H - T\Delta S}{\Delta H} = 1 - \frac{T\Delta S}{\Delta H} \tag{1.1}$$

where ΔS is the entropy change of the reaction at the temperature T.

The net work done by a cell, or the standard electromotive force (emf) E^0 of a cell, is measured as the voltage between the electrodes in open circuit conditions and when all species involved in a reversible reaction are in their standard state. In terms of the standard Gibbs free energy change ΔG^0 of the combustion reaction, the standard cell voltage is

$$E^0 = \frac{-\Delta G^o}{nF} \tag{1.2}$$

where n is the number of electrons involved in the reaction and F is Faraday's constant. In the above example, if hydrogen and oxygen at standard conditions combine to produce water vapor, the standard Gibbs free energy change ΔG^0 for the reaction is -

228.5 kJ/mol. Therefore, the standard cell voltage in open circuit conditions should be 1.18 V. However, when there is a load connected to the electrodes, the reversible cell voltage E_{cell} is less than the standard cell voltage E^0. The reversible voltage E_{cell} is given by the Nernst equation. If the fuel used is hydrogen, the reversible cell voltage is

$$E_{cell} = \frac{-\Delta G}{2F}$$

$$E_{cell} = \frac{-\left(\Delta G^0 + RT \ln \dfrac{p(H_2O)}{p(H_2)p(O_2^{1/2})}\right)}{2F}$$

$$E_{cell} = E^o - \frac{RT}{2F} \ln \frac{p(H_2O)}{p(H_2)p(O_2)^{\frac{1}{2}}} \tag{1.3}$$

where R is the gas constant, and $p(H_2O)$, $p(H_2)$ and $p(O_2)$ are the partial pressures of the species at the anode and cathode.

The driving force for a SOFC is the difference in oxygen partial pressure on either side of the electrolyte. The SOFC can be considered as an oxygen concentration cell, as the oxygen partial pressure on the anode side is extremely low, corresponding to the value of the dissociation of water vapor ($H_2 + ½\ O_2 \leftrightarrow H_2O$). In this case,

$$E_{cell} = \frac{RT}{2F} \ln \frac{p(O_2)_{cat}^{1/2}}{p(O_2)_{an}^{1/2}} \tag{1.4}$$

Equation (1.4) gives the voltage for a reversible oxygen concentration cell with an oxide ion transport number of 1, in other words, with a pure ionic conductor. If the oxygen partial pressure is kept constant at the cathode (*cat*), E_{cell} is a function of only the oxygen partial pressure at the anode (*an*). The presence of oxygen in contact with the anode side of the cell decreases E_{cell}.

In an operating cell, the real voltage output V drops from the ideal E_{cell} as the current density I drawn from the cell increases by an amount known as polarization or overpotential, η. The total polarization η, which reflects the additive effects of three main types of polarization: activation polarization η_{a}, ohmic polarization η_{Ω}, and concentration polarization η_{c}. Mathematically

$$V = E_{cell} - \eta_a - \eta_\Omega - \eta_c \tag{1.5}$$

The dominant mechanism of polarization is a function of the current density. A plot of V versus I (I-V curve) depicts how V is affected by η, as can be seen in Figure 1.2. The voltage output at zero current density is known as the open circuit voltage (OCV).

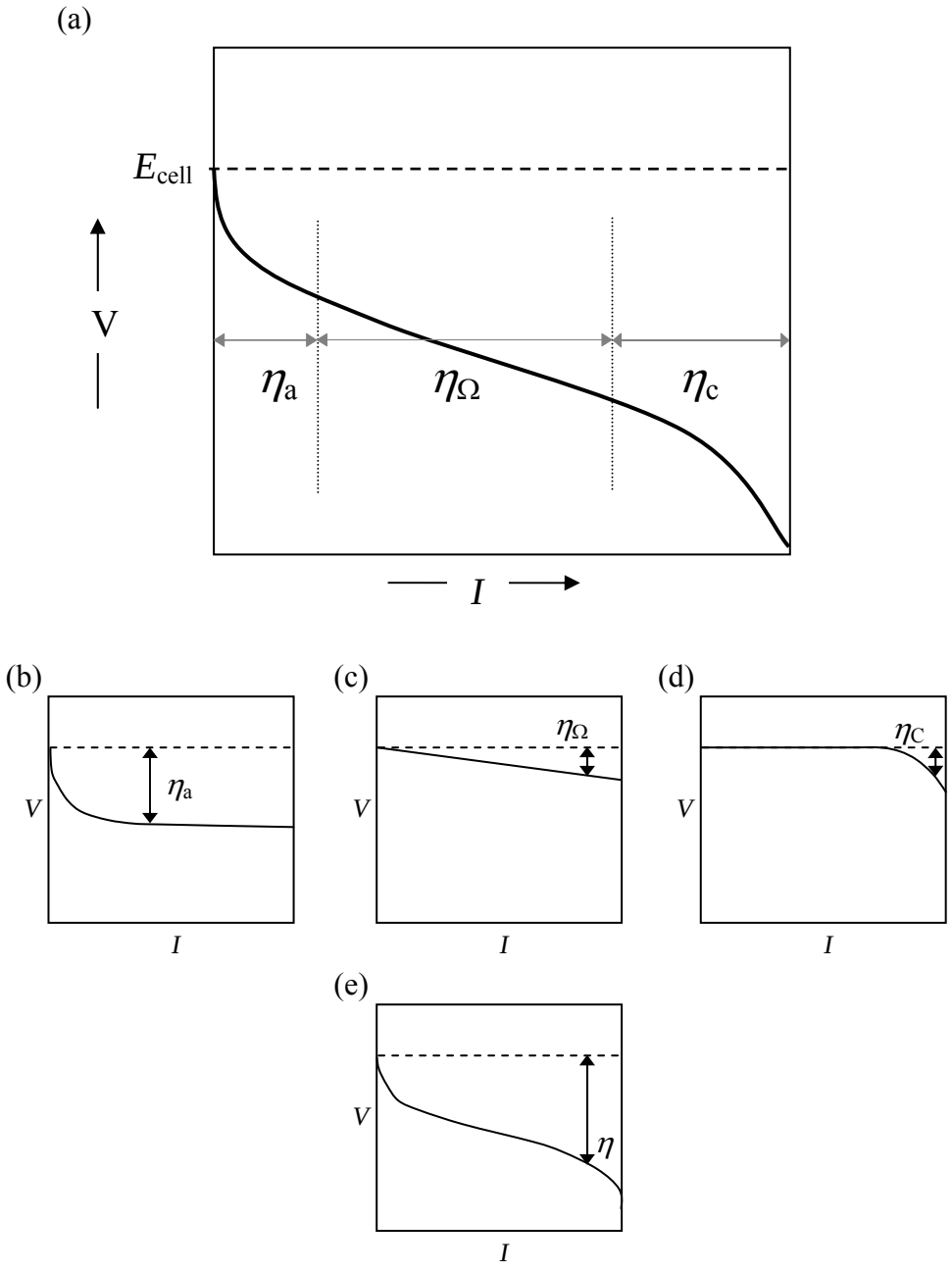

Figure 1.2. (a) I-V plot showing the dominant polarization mechanisms as a function of current density, and the specific effects of the (b) activation polarization, (c) ohmic polarization, (d) concentration polarization, and (e) the additive effect of them in the output voltage (Adapted from Minh[2] and Pukrushpan[14]).

Activation polarization η_a is related to the reaction rates at the electrodes. For a SOFC operating on hydrogen and oxygen, η_a is dominated by the kinetics of the reaction at the cathode, because the hydrogen oxidation at the anode is very fast.[1] Cathodic activation polarization is affected by the microstructure of the cathode, number of active sites temperature, atmosphere, and current density.[15] The relationship of η_a with current density is linear only at very low values of I.

$$\eta_a = \left| \frac{RT}{nFI_o} \right| I \tag{1.6}$$

where I_0 is the exchange current density which results from the balanced charged transfers between the electrodes and the electrolyte during open circuit conditions.

The ohmic polarization η_Ω is caused by ionic resistance at the electrolyte, mixed ionic and electronic resistances at the electrodes, and contact resistance at the interfaces. In a SOFC, the resistivity ρ of the electrodes is small compared to the ionic resistivity of the solid electrolyte ρ_e. Assuming that the contact resistance is negligible, the ohmic polarization is a direct function of the electrolyte thickness l_e:

$$\eta_\Omega = I \, \rho_e \, l_e \tag{1.7}$$

The resistances of SOFC components are commonly expressed in terms of area specific resistance (ASR). ASR is the resistance per unit area. In this way, η_Ω is simply

$$\eta_\Omega = I\, ASR_e \tag{1.8}$$

ASR is constant at all temperatures, and can be found from the slope of the I-V curve at low temperatures.[16]

Concentration polarization η_c, also known as diffusion polarization, is present at high current densities. It is caused by mass transport difficulties due to differences in the concentration of the reactant gases in the bulk and at the surfaces of the electrodes. When diffusion is the only transport mechanism, the voltage declines rapidly. It is then when the limiting current density I_L is reached. If there is no activation polarization at the electrodes, η_c is given by

$$\eta_c = \frac{RT}{nF}\ln\left(1-\frac{I}{I_L}\right) \tag{1.9}$$

1.3.2 SOFC components

Each one of the components of the SOFC is critical in itself and there are certain requirements that each one of them must meet for a SOFC to operate properly. They should be stable in many ways.[2] The thermal expansion coefficient (TEC) between the components must be closely matched. Components cannot react at

fabrication temperature of the fuel cell which is higher than the operating temperature. Ease of fabrication and low cost also must be considered when selecting materials for fuel cells.

1.3.2.1 Electrolyte

This is the first material selected when designing fuel cells. The electrolyte is a gas-tight layer that exhibits chemical, phase, morphological and dimensional stability in both reducing and oxidizing atmospheres.[2] It allows the transport of ions, specifically O^{2-} ions in SOFC.[1,2,17] The ionic conductivity of the electrolyte should be as high as possible and remain constant over time, while its electronic conductivity should be negligible.

Yttria-stabilized zirconia (YSZ) is the most widely used electrolyte material for high temperature SOFC. Other oxide-ion conductors with a fluorite structure and better ionic conductivity at lower temperatures have been explored as potential electrolyte materials.[1,2,17] However, they present practical disadvantages with respect to YSZ such as higher electronic conductivity, chemical instability over certain oxygen partial pressure values, cost, and difficulties in processing. Some perovskites, brownmillerites and hexagonal structure oxides, have also been recently studied,[17] but YSZ remains the most widely used electrolyte material.[2]

YSZ posses a fluorite structure; cations occupy the corners and face-centered positions of a cube and anions occupy the tetrahedral sites. The highest ionic conductivity of YSZ is achieved by doping cubic zirconia (ZrO_2) with 8 mol % of

yttria (Y_2O_3), the minimum amount required to stabilize the cubic zirconia. This composition is commonly known as 8YSZ. The ionic conductivity is the result of oxygen vacancies produced to compensate the electronic imbalance created by the substitution of a fraction of Zr^{4+} in zirconia by Y^{3+}.[1,2,17] At 1000 °C, the ionic conductivity of 8YSZ is 0.13 S/cm, and decreases to 0.09 S/cm after annealing for 1000 hours.[18] The electronic conductivity is negligible at SOFC operation temperatures and pressures.

YSZ exhibits properties particularly desirable in planar cell configurations,[2,17,18] such as a high bend strength of 300 MPa at room temperature and 230 MPa at 1000 °C, high fracture toughness of 3 $MPa \cdot m^{1/2}$, and a nearly constant TEC from 20 °C to 1500 °C of 10.3 x 10^6 /K.[19]

There are three ways to increase the flux of ions through the electrolyte: by increasing the temperature, by reducing the thickness or by the development of materials with higher ionic conductivity.[1] Given the current trend of decreasing the operation temperature, reducing the thickness of the electrolyte is the obvious choice since YSZ meets other requirements. Ishihara et al.[17] suggested that for an electrolyte with a resistance of 0.2 Ωcm^2 in a cell with efficiency greater than 50 % and operating at 700 °C, the thickness of the electrolyte should be less than 50 microns. Reductions in operating temperature require further decreases in electrolyte thickness.

1.3.2.2 Anode

The anode is a porous component in contact with the electrolyte on one side and a current collector on the other. The current collector side of the anode is exposed to a reducing environment at high temperatures during the operation of the SOFC. Various important processes take place in the anode that place strict requirements on the microstructure and materials in the anode.[20] First, the reaction sites where the oxidation of the fuel takes place must be active. Second, it must allow fuel to be delivered and by-products to be removed from the surface sites. Finally, electronic transport must occur in the anode from the electrolyte/anode reaction sites to the current collector and also some ionic transport towards the electrolyte interface.

The operating conditions of the SOFC impose stringent requirements on the materials used in the anode.[2,20] The anode must be dimensionally and chemically stable under reducing environments while exhibiting chemical compatibility and closely matched TEC with the electrolyte and the current collector. In addition, at least 30 vol % connected porosity is required to allow the fuel pass through the anode and for the elimination of reaction products. Lastly, good particle contact is important to provide electronic and ionic mass transport since the anode materials must be excellent electronic conductors and good ionic conductors.

The most commonly used material in the manufacturing of SOFC is a Ni/YSZ cermet[21] because it fulfills fairly well the anode requirements and it has a low cost. To produce the cermet, a NiO/YSZ composite is first produced. Before SOFC operation, and sometimes in situ, the NiO is reduced to metallic Ni, which provides an electronic

path. YSZ constitutes the skeleton of the anode, providing mechanical stability, allowing ionic transport and contributing to the presence of triple phase boundaries (TPB) which is where the reaction occurs.

Variations in the NiO/YSZ ratio allow tailoring of the desired characteristics of the cermet, such as electronic conductivity, thermal expansion coefficient and degree of porosity. It is very important to find the optimum ratio of NiO (and therefore Ni) to YSZ to maximize the performance of the fuel cell.[22] The optimum NiO content is usually 40 vol %, which correspond to 30 vol % Ni after reduction. Higher Ni content decreases the IR resistance as the IR resistance is sensitive to the contact area of nickel on the electrolyte. On the other hand, polarization resistance relates to the Ni/YSZ ratio and it is very low at 30 vol. % Ni. The mismatch in the coefficient of thermal expansion between NiO and YSZ is very low when the volume percentage of NiO in the cermet is 40 %. Given the volume fraction *v* of the components, the coefficient of thermal expansion of the cermet can be calculated according to the logarithmic rule of mixtures.

$$\ln(TEC_{NiO/YSZ}) = v_{NiO} \ln(TEC_{NiO}) + v_{YSZ} \ln(TEC_{YSZ}) \quad (1.10)$$

1.3.2.3 Cathode

The cathode is the other porous component of the SOFC in contact with the electrolyte and a current collector. The side of the cathode in contact with the current

collector is where the oxidant is supplied to the SOFC, and it is in the cathode where the reduction of the oxidant occurs.[1,2,17] The cathode must exhibit dimensional and chemical stability under oxidizing environments, and chemical compatibility and close matching of the TEC with the electrolyte and the current collector. In addition, the cathode must have the highest electronic conductivity possible in order to minimize ohmic losses as well as a good catalytic activity to reduce activation polarization.

There are few materials that meet the requirements to be used as cathode materials. Platinum was used in at the beginning of the development of SOFC, but its cost makes it unreasonable for practical uses. A realistic alternative has been the use of conductive metal oxides with a perovskite structure. From this class of materials, strontium-doped lanthanum manganite has been preferred over other compositions due to its high electrical conductivity in reducing atmospheres, low reactivity with YSZ, and tolerable thermal expansion mismatch with other cell components.

Perovskites are cubic structures with a chemical formula ABO_3, in which a large cation, A, is located in the center position, surrounded by 8 smaller cations, B, in the corners of the cube and 12 oxygen atoms in the edge centered positions of the cube.

$La^{3+}Mn^{3+}O^{2-}{}_3$ has an orthorhombic structure at room temperature.[2,17] Oxidation of Mn^{3+} to Mn^{4+} at 600 °C increases the oxygen content. The stoichiometry of oxygen strongly affects the crystallography of the material, and in this case there is a crystallographic transformation to the rhombohedral structure. Substituting small amounts of La^{3+} by Sr^{2+} increases the concentration of Mn^{4+} and therefore the oxygen content, allowing the existence of rhombohedral $LaMnO_3$ at lower temperatures.

Changes in the oxygen stoichiometry must be avoided especially during fabrication, as this may affect the dimensional stability of the cathode.

In the high-temperature operation range, $La_{1-x}Sr_xMnO_{3-\delta}$ (LSM) has been the preferred choice for SOFC cathodes due to its chemical [23] and mechanical [24] stability in the presence of YSZ electrolyte, high oxygen diffusivity [25], and mixed ionic-electronic conductivity [26].

1.3.3 SOFC geometry

There are two main configurations for a SOFC: tubular and planar.[2] Tubular and planar designs have been evaluated, with the former being more structurally stable, but the latter having a better performance in terms of power density per mass or volume and lower fabrication costs.[2,27,28] In the case of fuel cell stacks, the dense components, electrolyte and interconnect can be fabricated independently to avoid difficulties in the co-sintering, allowing multiple manufacturing options. For example, screen printing can be used to produce the electrodes on a sintered tape cast electrolyte.

1.3.4 Seals

Seals are required at the electrodes to prevent oxidant and fuel from mixing. Gas leakage is a major problem in the testing of SOFC.[29] Air leakage into the anode compartment decreases the reversible voltage value, as mentioned in section 1.3.1. Compressive seals lead to non-uniform stress distribution resulting in cracking of the

layers. Glass or glass-ceramics seals are preferred over other ceramic materials because: (1) they are easy to place due to their softness at elevated temperatures, (2) stresses induced during the process or by differences in thermal expansion may be relaxed at the operating temperatures, (3) at lower temperature the rigid glass limits the risk of fracture due to handling, (4) cracks in glass seals can be healed by heat treatment and (5) the stoichiometry can be varied to tailor the properties of the glass seal. All of these are further incentives to reduce the 1000 ºC operating temperature, as most glasses are not able to withstand such high temperatures.

1.3.5 Disadvantages of SOFC

The high operating temperature of a SOFC represents a challenge as it hastens the breakdown of cell components.[2,3,30] Mechanical stresses are enhanced at high temperatures due to mismatch in the TEC between the cell components. In addition, interfacial reactions may occur at high temperatures during fabrication and operation of the cells. All this makes the materials selection critical for the components to survive over the lifetime of the SOFC.[2,3,31]

1.4 INTERMEDIATE-TEMPERATURE SOLID OXIDE FUEL CELLS (IT-SOFC)

The current trend in the development of SOFC is to be able to operate at intermediate temperatures, in the range of 600 to 800 °C. Decreasing the operating temperature for SOFC would bring some advantages[6,27,31,32]: the overall cost of the

SOFC can be decreased as interconnects, heat exchangers, and structural components could be fabricated from relatively inexpensive metal components rather than the oxides that are currently used. The use of low-cost materials reduces the total cost of the SOFC. The reduced operation temperature would also enhance durability of SOFC by reducing the temperature variations experienced by the components during thermal cycling.

1.4.1 Requirements

The main problem with decreasing the operating temperature is the drop in the cell voltage due to the increased polarization losses, particularly at the electrolyte. This issue is addressed with a double requirement in design of intermediate-temperatures SOFC (IT-SOFC): first, the electrolyte must be very thin and second, the cathode materials must have an adequate level of catalytic activity at the intermediate operation temperatures. From a design point of view, thinner components represent a challenge for structural stability and manufacturability of the fuel cell.

1.4.2 Thin Electrolytes Manufacturing Techniques

The fabrication of SOFC is based in the manufacturing of their component layers. There are a wide variety of techniques. Factors such as design, characteristics of the raw materials, compatibility between subsequent techniques, availability of

equipment and cost, will determine which process is the best to use for each SOFC configuration. Table 1.2[6] shows a classification of the most common methods.

Thinner electrolytes can compensate for the reduction in the ionic conductivity of YSZ at reduced operating temperatures. In order to exhibit sufficient ionic conductance, the thickness of the electrolyte should not exceed about 15 μm. A variety of techniques have been proposed to produce electrolytes of reduced thickness for solid oxide fuel cells. Common examples in the literature are chemical vapor deposition (CVD) [6,33], electrochemical vapor deposition (EVD)[6,33], electrostatic assisted vapor deposition (EAVD)[34], electrophoretic deposition[35], cathodic electrodeposition[36], colloidal deposition[37], spark-plasma sintering[38], spin coating[39], centrifugal casting[16], spray coating[40], tape calendaring[41], and DC magneton sputtering[6,42]. Most of these techniques require special facilities that result in increased manufacturing costs. An established technology, such as tape casting, is cost efficient, but it has until now been used primarily to produce electrolyte-supported SOFC thick electrolytes.[6] Screen printing and tape casting are called "thick film techniques" but they can also be used to produce films from 10 to 150 μm as the components of self-supported SOFC.

For screen printing, a ceramic powder, an organic binder and a plasticizer are mixed to form a viscous paste that is forced through the open meshes of a screen and deposited onto a substrate. Parameters that affect the final result are: particle size and form, surface properties, packing density of the powder, sintering temperature, time and atmosphere.[6]

A slurry similar to the one used for screen printing is prepared for tape casting. Green tapes of different thickness are produced using a device called a doctor blade. The resulting flexible tape can be cut to size, corrugated, or otherwise formed prior to firing. This technique has been used for the fabrication of large area, thin, flat ceramic layers for monolithic and planar SOFC with YSZ electrolytes and cermet anodes.[2,6]

Table 1.2. Methods for deposition of thin ceramic films.[6]

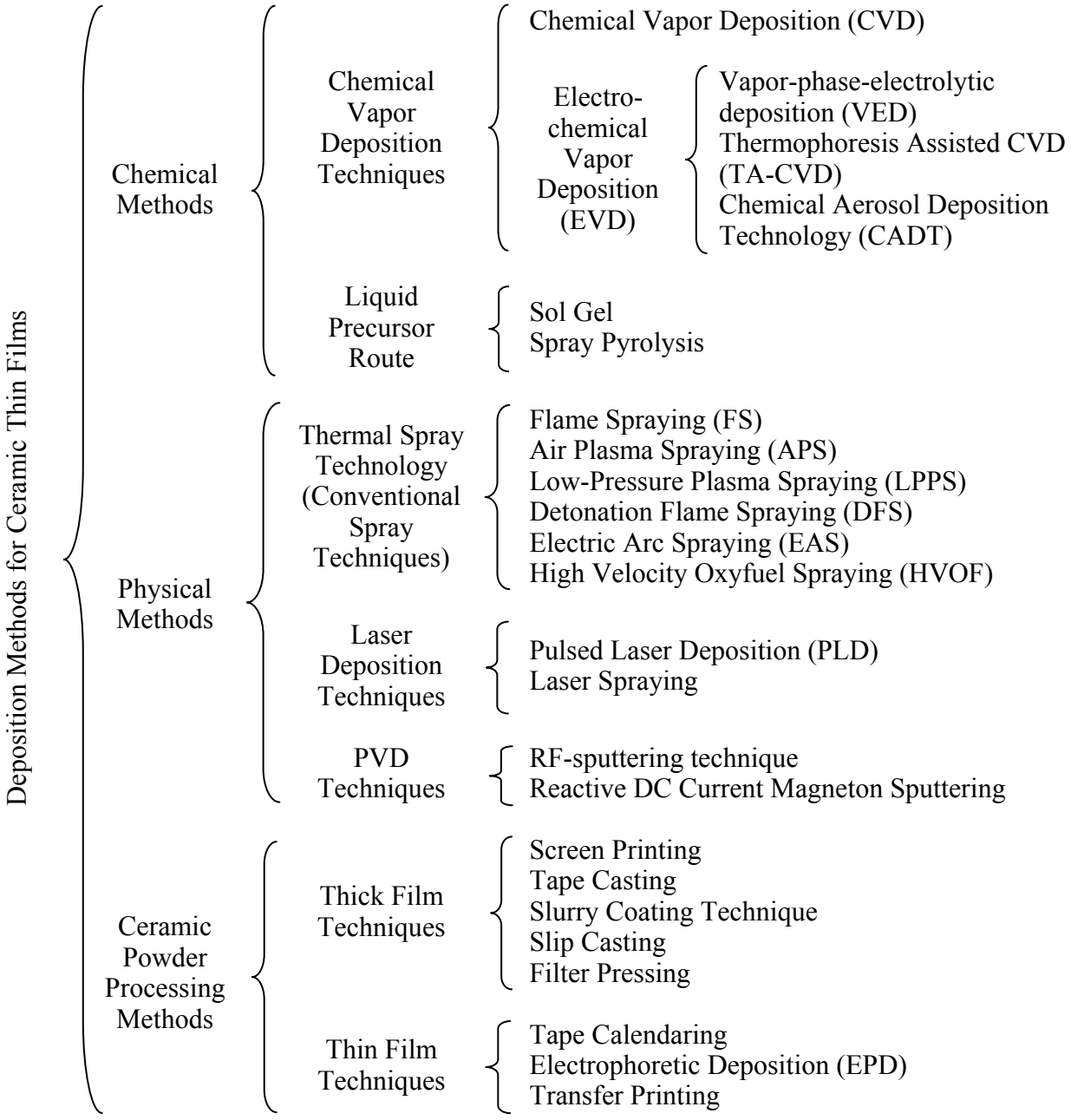

1.4.3 Current Status

The use of lower operating temperatures requires the use of new material compositions for the cathodes. LSM has been the most common cathode material used in SOFC, but its catalytic activity decreases dramatically in the intermediate range of operation temperatures,[25,43] particularly during long duration tests.[44] In an effort to obtain similar or improved performance at intermediate operation temperatures, new compositions have been explored. These materials should show an adequate mixed conductivity below 800 °C, and still be compatible in all other aspects with the electrolyte material. For this reason, other perovskite materials[45,46], and perovskite-related intergrowth structures[47] have been investigated as candidates for IT-SOFC cathodes.

Ni/YSZ cathode can be used over a wider range of temperatures than LSM. This continues to be a common anode material for IT-SOFC.

Few groups have used both tape casting to produce SOFC with thin electrolytes and LSM as the cathode material. For example, Ohrui et al. [48] has produced cells with a electrolyte thickness of 15 μm and achieved a power density of 0.45 W/cm^2 at 1000 °C; whereas the thickness of the electrolyte in the cells produced by Simner et al. [44] was 10 μm and the power density was between 0.20-0.35 W/cm^2 at 800 °C.

1.5 SCOPE OF THIS STUDY

There are two main aspects in this work: first, the development of a manufacturing method to produce IT-SOFC using an economically advantageous process that can be easily scaled; second, the testing of IT-SOFC with cathode compositions that exhibit an adequate catalytic activity at intermediate temperatures, and have a smaller TEC mismatch with the electrolyte.

The anode and electrolyte material that are used in this study are the same as those used for high temperature SOFC. The first objective is the production of anode-supported, flat IT-SOFC with thin electrolytes by tape casting, co-firing and screen printing. The second objective is to test the performance at 600 ºC, 700 ºC and 800 °C of thin-electrolyte IT-SOFC focusing on cathode materials with low TEC: perovskite oxides and perovskite-related intergrowth oxides that have been suggested as the cathode materials for IT-SOFC [45-47,49]. The compositions to be studied are:

Perovskite oxides:

- $Nd_{0.6}Sr_{0.4}CoO_{3-\delta}$ (NSC)
- $Nd_{0.6}Sr_{0.4}Co_{0.5}Fe_{0.5}O_{3-\delta}$ (NSCF)
- $Nd_{0.6}Sr_{0.4}Co_{0.5}Fe_{0.5}O_{3-\delta}$-Ag composite (NSCF-Ag)

Perovskite-related intergrowth oxides:

- $Sr_{2.7}\ La_{0.3}Fe_{1.4}Co_{0.6}O_{7-\delta}$ (SLFCO7)
- $LaSr_3Fe_{1.5}Co_{1.5}O_{10-\delta}$ (LSFCO10)

Specific details on these compositions will be given in the appropriate sections.

Chapter 2: Experimental Procedures

The first part of this chapter is devoted to the manufacturing of the IT-SOFC. Each one of the components of the cell and materials used will be addressed, as well as the overall preparation of the cells. The later part of this chapter will deal with the characterization techniques used to analyze the performance and microstructure of the cells.

2.1 MANUFACTURING OF IT-SOFC

To achieve the objectives of this work, SOFC with thin electrolytes were produced using tape casting, screen printing and co-firing. Figure 2.1 shows a summary of the manufacturing processes that were followed to produce IT-SOFC. The biggest challenge faced in the fabrication of SOFC is maintaining the structural stability of the individual components as well as of the whole assembly during fabrication and operation.[21] The thermal expansion coefficient of adjacent materials must also be matched to avoid cracking; thin layers produced by tape casting are difficult to handle, and they tend to curl during sintering.

The anode and electrolyte materials were prepared by tape casting from commercially available materials. The interlayer and cathode materials were produced in our laboratory. Details on the synthesis of the cathode materials will be given later in the corresponding chapter.

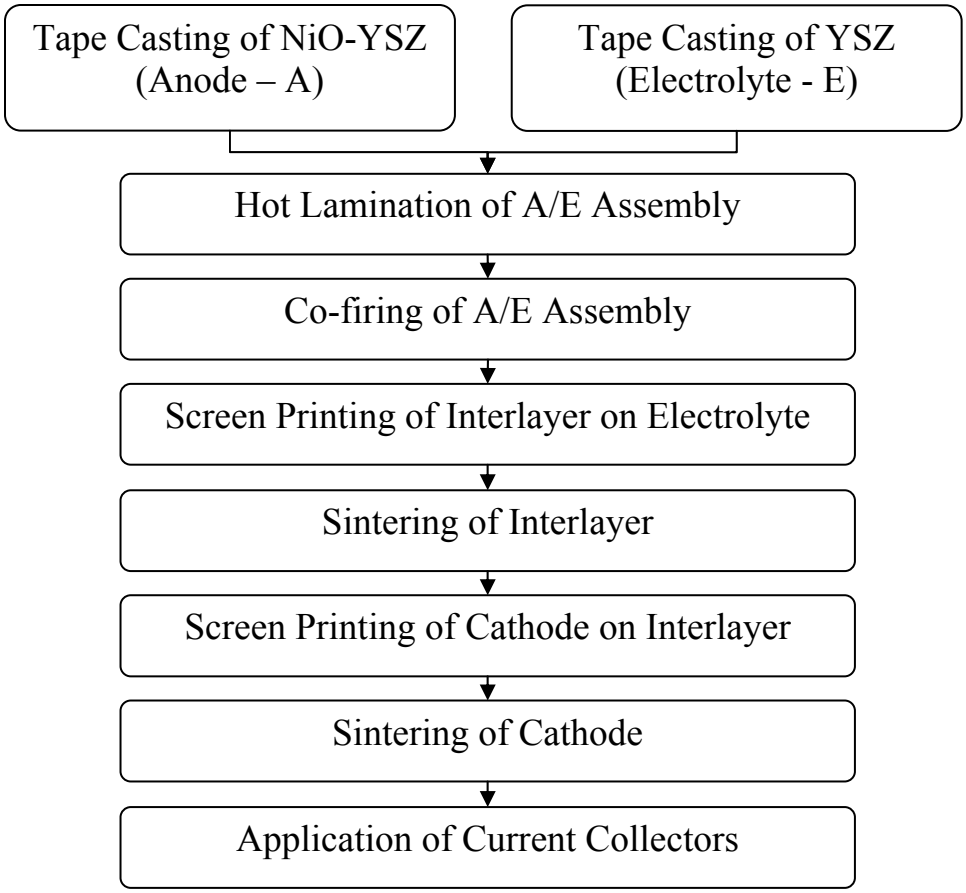

Figure 2.1. Manufacturing process.

2.1.1 YSZ Electrolyte

The electrolyte slurry was prepared from 8 mol% YSZ (8YSZ) (Tosoh) following the formulation given by Mukherjee et al.[7] The composition of the slurry is given in Table 2.1. The ceramic powder was dispersed by ball milling for 12 hours with phosphate ester (PE) (Crompton Chemicals Co., Emphos PS-21A), in an azeotropic mixture of methyl ethyl ketone (MEK) (Fisher Chemical, Certified ACS)

and ethanol (EtOH) (Aaper Alcohol, USP absolute 200 proof). Then, the slurry was ball-milled for 24 more hours with an organic binder, polyvinyl butyral (PVB) (Solutia, Butvar B-98) and two plasticizers, polyethylene glycol (PEG) (Carbowax, 200) and benzyl butyl phthalate (BBP) (Ferro Co., Santicizer® 160).

Table 2.1. Electrolyte slurry for tape casting.[7]

Component	Function	ρ (g/cc)	Wt %	Vol %
8-YSZ	Ceramic Powder	5.9	45.0	10.4
EtOH	Solvent	0.79	22.2	38.5
MEK	Solvent	0.8	22.2	38.0
PE	Dispersant	1.05	0.7	0.9
PVB	Binder	1.1	4.2	5.2
PEG	Plasticizer	1.1	4.6	5.7
BBP	Plasticizer	1.12	1.1	1.3

The resulting slurry was manually tape cast on a glass substrate using a doctor blade with a gap of 100 μm. After drying, the tapes were smooth, without defects, and were easy to remove from the substrate and to handle.

2.1.2 NiO/YSZ Anode

The slurry for the NiO/YSZ anode was made by first dispersing ceramic powders in a solvent system with the dispersant for 24 hours. Consecutive ball milling with the binder and plasticizer was performed for additional 24 hours. The resulting

slurry was tape cast onto a glass substrate with a doctor blade with a 400 μm gap, unless otherwise noted.

Several different formulations were studied in order to find the best composition. An ideal anode would have a TEC similar to that of the electrolyte, an adequate level of porosity, and be easy to handle during the assembly of the cells. The volume fraction of the components of each of the compositions that were studied is shown in Table 2.2.

Table 2.2. Volume fractions of anode slurries studied.

	Composition #	1	2	3	4	5	6	7	8	9
Function	Component									
Ceramic Powder	NiO	0.105	0.106	0.069	0.058	0.051	0.045	0.056	0.097	0.096
	8-YSZ	0.090	0.091	0.059	0.050	0.044	0.038	0.048	0.082	0.082
Solvent	EtOH	0.259	0.261	0.261	0.276	0.280	0.321	0.310	0.270	0.283
	Toluene	0.354	0.355	0.355	0.374	0.410	0.446	0.455	0.396	0.415
Dispersant	PE	0.019	0.019	0.019	0.010	0.010	0.012	0.009	0.043	0.021
Binder	PVB	0.065	0.060	0.128	0.116	0.095	0.083	0.052	0.052	0.052
Plasticizer	BBP	0.108	0.109	0.109	0.116	0.110	0.055	0.071	0.060	0.050
$\frac{\text{NiO}}{\text{YSZ}}$	ratio	$\frac{54}{46}$	$\frac{54}{46}$	$\frac{54}{46}$	$\frac{54}{46}$	$\frac{54}{46}$	$\frac{54}{46}$	$\frac{54}{46}$	$\frac{54}{46}$	$\frac{54}{46}$
$\frac{\text{Binder}}{\text{Plasticizer}}$	ratio	0.60	0.55	1.18	1.00	0.86	1.50	0.74	0.86	1.03
$\frac{\text{Powders}}{\text{Solids}}$[1]	ratio	0.75	0.77	0.50	0.48	0.50	0.50	0.67	0.77	0.77
Solids load:	$\frac{\text{Powders}}{\text{All}}$[1]	0.20	0.20	0.13	0.11	0.10	0.08	0.10	0.18	0.18

2.1.2.1 Effect of the binder

Composition # 1 was made following the procedure given by Zhitomirsky et al.[50] and using the same starting materials: NiO (Inco, grade F) and 8YSZ (Tosoh) as ceramic powders, EtOH (Aaper Alcohol, USP absolute 200 proof) and Toluene (EM Science, GR ACS) as solvents, Butvar B-79 (Solutia) as binder and Santicizer 160

[1] Solids = Ceramic Powders + Binder

(Ferro) as dispersant. The only difference was the kind of dispersant used: Emphos PS21-A (Crompton Chemicals Co.) instead of fish oil. The resulting tape was sticky and it proved difficult to remove from the glass.

The function of the binder is to maintain the position of the ceramic powders in the tape after solvent drying.[51] The binder has a great effect in the mechanical properties of the green tape. For the second composition, the amount of binder was slightly reduced in order to ease the removal of the tape from the substrate. Everything else remained the same, excepting that in this case, NiO was bought from another supplier (Acros, Black 76 % Ni). The resulting slurry was tape cast in four different ways:

a) using a doctor blade with a 150 μm gap onto glass.

b) using a doctor blade with a 400 μm gap onto glass.

c) using a doctor blade with a 150 μm gap onto an 8YSZ tape.

d) using a doctor blade with a 150 μm gap onto an 8YSZ tape.

The 8YSZ tape used in cases c) and d) was tape cast using a doctor blade with a 400 μm gap and it was dry.

The NiO/YSZ tapes started drying as soon as they were tape cast. Discs of 2.54 cm (1") diameter were punched for all of the tapes. From cases a) and b), it was found that the thicker the tape, the more difficult it was to remove from the glass substrate. Samples from specimens c) and d) were easily removed. These ones were placed in a

---

[1] All = Ceramic Powders + Solvents + Dispersant + Binder + Plasticizer.

tubular furnace to pyrolyze the organic binder using the following firing schedule: from room temperature to 130 ºC at 3 ºC/min, to 275 ºC at 0.33 ºC/min, to 500 ºC at 0.66 ºC/min, to 600 ºC/min at 1.66 ºC/min, to room temperature at 2 ºC/min. Both specimens exhibited cracks at the time when they were removed from the furnace. The formation of cracks during pyrolysis was likely due to the mismatch between the TEC of the electrolyte and the anode.

For the next trial, the relative volume of binder was increased with respect to the ceramic powder loading with the expectation that this would cause the anode tapes to shrink more uniformly when co-fired with the electrolyte tapes. The resulting formulation was composition # 3. The volume fractions of ceramic powders and binder were 1:1. The anode tapes produced with composition # 3 had a good appearance, but they were rubbery, very deformable and difficult to remove from the glass substrate.

2.1.2.2 Effect of the plasticizer

Mistler[51] recommends keeping the binder-to-plasticizer ratio larger than 1. The effect of the variation of the relative volume of the plasticizer while keeping the same volume fraction of ceramic powders and binder was studied in compositions 4, 5 and 6. The tape was less rubbery and easier to handle when the binder-to-plasticizer ratio decreased; but when the amount of plasticizer was increased, the tapes showed an orange peel appearance soon after being tape cast. As a result, the binder to plasticizer volume ratio was kept less than 1 for composition # 7.

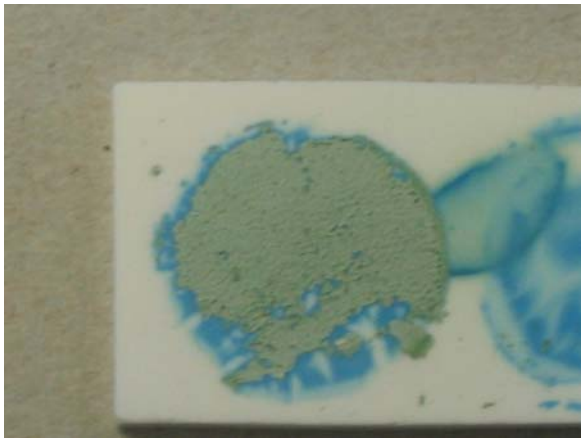

Figure 2.2. A/E assembly after pyrolysis. Anode was prepared with anode composition # 6.

In this last formulation, the ratio of ceramic powder volume fraction to the solids fraction was the same as in the slurry used for the electrolyte. This slurry was tape cast using two different gap thicknesses. The tapes cast with a 400 μm gap doctor blade developed orange peel, whereas the tapes cast with a 150 μm gap doctor blade had a nice appearance but were easily deformable. Some discs were punched from the thick tape. Two discs of anode material were laminated with one disc of the electrolyte material and co-fired following the schedule mentioned previously. The specimen exhibited internal cracks after pyrolysis.

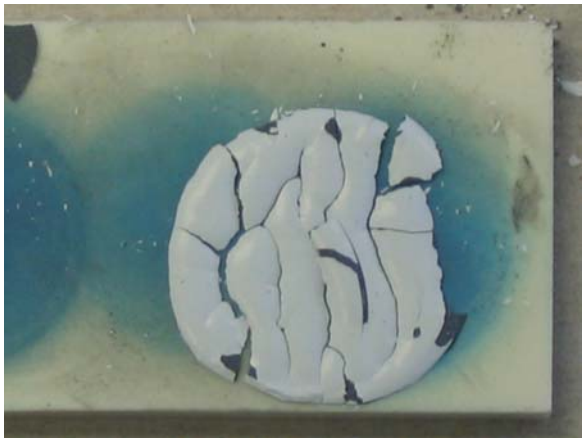

Figure 2.3. A/E assembly after pyrolysis. Anode was prepared with anode composition # 7.

2.1.2.3 Effect of the powder load

Composition # 8 was made following a formulation for powders with low surface area in an oxidizing atmosphere found in Mistler et al.[51] The main difference from previous formulations was an increase in the volume fraction of ceramic powders and dispersant. Tapes cast with 400 and 150 μm gap doctor blade had a smooth appearance, although they were slightly difficult to handle. Discs were punched and laminated with the electrolyte material. There were no major cracks during pyrolysis.

Combinations of different 8YSZ and NiO powders with different particle size were tested to find the best match. The processability of the anode/electrolyte (A/E) assemblies improves when using a coarser 8YSZ (Stanford). However, in terms of electronic conductivity of the anode, it is better to have similar particle sizes for the

NiO and YSZ, so there is a good dispersion and the Ni particles are in contact with each other after reduction. Tapes prepared with 8YSZ from Stanford and NiO from Acros previously coarsened for 2 hours at 1000 ºC were too rubbery to be used. The best tape was achieved when using 8YSZ from Tosoh and NiO from J.T. Baker.

Adjustments to the volume fractions of the dispersant and plasticizers lead to composition # 9, which resulted in the one we used in the manufacturing of our cells.

This whole process shows the importance of using the right proportions in tape casting formulations. The importance of the volume ratios of the binder and plasticizer in the slurry can be particularly seen when comparing composition # 2 and 9.

2.1.2.4 Processing of Anode

The anode was prepared using a mixture of NiO (J.T. Baker) and 8 mol% YSZ (Tosoh) at a volume ratio of 54:46. The weight ratio of NiO and YSZ was 57:43, which should result in a 40 % volume of Ni in the anode after reduction.[52] This corresponds to a porosity level of 42 %, which is adequate to allow gas diffusion while maintaining good electronic conductivity according to the percolation theory.[20,53]

Table 2.3. Anode slurry for tape casting (adapted from Mistler[51]).

Component	Function	ρ (g/cc)	Wt %	Vol %
NiO (Baker)	Ceramic Powder	6.67	35.4	9.6
8-YSZ (Tosoh)	Ceramic Powder	5.9	26.6	8.2
Ethyl alcohol	Solvent	0.79	12.3	28.3
Toluene	Solvent	0.805	18.4	41.5
PE	Dispersant	1.05	1.2	2.5
PVB (Butvar B79)	Binder	1.083	3.1	5.2
BBP	Plasticizer	1.12	3.1	5.0

To reduce the presence of imperfections due to trapped air in the slurry, the glass substrate where the tapes were cast was placed with the tape side down for drying.

2.1.3 Interlayer material

The interlayer material $Ce_{0.9}Gd_{0.1}O_{2-\delta}$ (GDC) was prepared using glycine-nitrate combustion synthesis (GNP).[54] A stoichiometric amount of Gd_2O_3 was diluted in HNO_3. The solution was diluted with distilled water and $(NH_4)Ce(NO_3)_6$ was added. After the addition of glycine to the solution, small amounts of it were heated. Excess water evaporated until it exhibited a gel consistency, followed by auto-ignition. The resulting pale-yellow ashes were fired at 600 ºC for 5 hours to remove any carbon residues.

2.1.5 Cell preparation

A detailed description of the cell preparation process is presented in Appendix A. A summary is presented here.

After drying, 22.2 mm (7/8") diameter discs were punched from the anode and electrolyte tapes. Six discs of the anode material and one of the electrolyte material were stacked and hot laminated in a manual 12 ton force Spectropress® for 10 minutes at 85 ºC and 19.3 MPa to produce an anode/electrolyte assembly. The assemblies were covered in non-stick, coated, ultra-heavy duty barbecue aluminum foil (All-Foils, Inc.) and placed between ¼" thick polycarbonate plates to protect them during lamination.

The organics were pyrolyzed by heating slowly at 20 ºC/h from room temperature to 160 ºC, followed by 40 ºC/h to 400 ºC, 100 ºC/h to 500 ºC, and cooled at 2 ºC/min. The anode/electrolyte assembly was then co-fired for 2 h at 1400 ºC. Heating and cooling ramps during the entire manufacturing process were 2 ºC/min. To maintain the flatness of the assembly during pyrolysis, they were covered by graphite and placed with the anode side facing up on a flat layer of coarsened YSZ in an alumina crucible. The coated specimens were covered by more coarsened YSZ that was later flattened. Finally, an alumina plate was placed on top. During co-firing, an additional mass was placed on top of the alumina plates to produce a pressure of 500 Pa on each cell.

A GDC interlayer was applied by screen printing on the co-fired electrolyte. The interlayer paste was a mixture of GDC powder with an organic vehicle (W. C. Heraeus, V-006) in equal amounts. The interlayer/anode/electrolyte assembly was then

fired for 2 h at 1300 ºC. Cathodes were applied on the sintered interlayer by screen printing in three passes. The applied paste was a mixture of the cathode powder and an organic vehicle (W. C. Heraeus, V-006) in a weight proportion of 3:2. The cathodes were sintered for 2 h. The sintering temperature for each cathode composition was determined using a reactivity test. Details are given in section 2.2.

Prior to electrochemical testing, platinum current collectors were attached to the electrodes. The current collector consisted of a 5 mm x 5 mm platinum gauze interweaved and welded with a 0.005" diameter platinum wire. A small amount of platinum ink (Heraeus, CL11-5100) was applied to the contour of the gauze before it was placed on the electrode. First, a current collector was applied on top of the cathode, followed by a second current collector applied on the anode at an angle of 90° with respect to the first one. The fuel cell with the current collectors was then fired at 900 ºC for 30 minutes to remove organic products in the platinum ink.

2.2 CHARACTERIZATION TECHNIQUES

2.2.1 X-Ray Diffraction (XRD)

X-ray diffraction was used to confirm the stoichiometry of the interlayer and cathode materials synthesized in our laboratory as well as to characterize the reactivity between components of the IT-SOFC. The equipment used was a Philips X'PERT diffractometer. The measurements were made using a rotary stage and monochromatic

Cu Kα radiation. The diffracted intensity was recorded from 2θ = 10 º- 90 º with a step size of 0.05 º and 2 seconds as the step time.

2.2.2 Scanning Electron Microscopy (SEM)

The microstructure of the IT-SOFC was analyzed with scanning electron microscopy of the fracture surfaces with a JEOL model LSM-5610. Prior to observation, the specimens were broken manually and sputtered for 30-40 seconds with a Pt-Au conductive layer.

2.2.3 Electrochemical Characterization

2.2.3.1 Seal formation

The quality of the seal is critical to prevent leaks and achieve an OCV value close to the predicted by the Nernst equation. Prior to the electrochemical test, the fuel cell was attached to two alumina rings using a glass paste made with 95 wt % glass powder with a high TEC (Specialty Glass, SP737 TF-200) and 5 wt % of Duco cement. At least 3 grams of such paste were used per cell. The glass powder and Duco cement were mixed with acetone until a homogeneous consistency was achieved. Each one of the alumina rings had to be fully joined with the electrolyte or the anode respectively by the glass paste to compensate for any curvature in the cell. The alumina ring in contact with the anode was attached to the alumina tube of the testing set up with a

small amount of Duco cement. Electrical connections were made through the Pt and glass paste was applied surrounding the alumina rings and the top section of the tube, as shown in Figure 2.4.

The set up was heated at 2 ºC/min until it reached 875 ºC, slightly above the softening point of the glass. The temperature was held for a couple of hours, and then decreased at 2 ºC/min until the first operation temperature, 800 ºC.

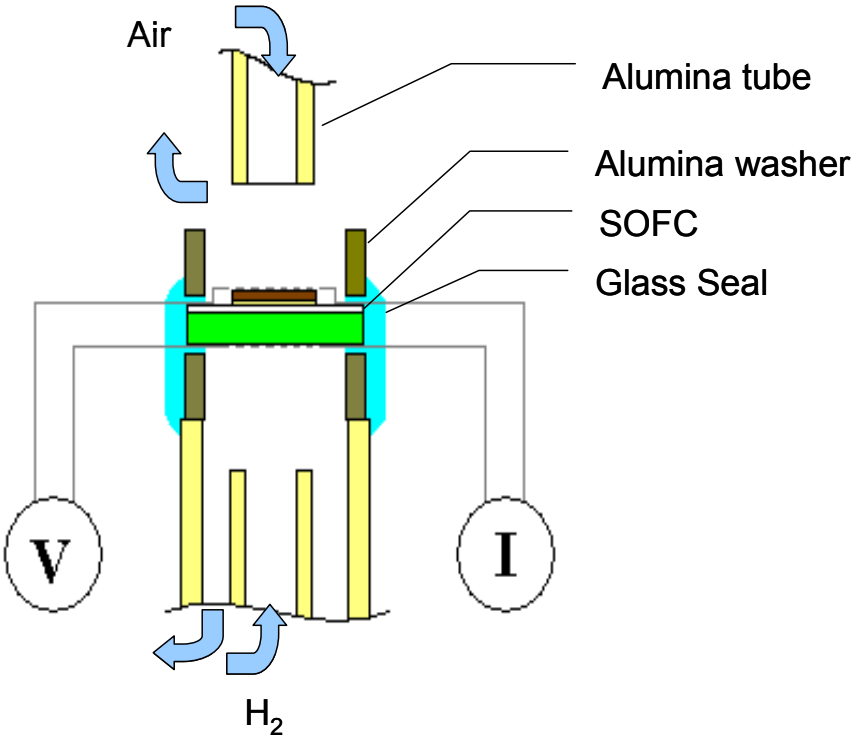

Figure 2.4. Schematic of SOFC testing set up.

2.2.3.2 Anode reduction

Nitrogen gas was injected to the anode side of the setup to check for the presence of leaks. If no leaks were present, the system was purged with nitrogen to deplete oxygen from the atmosphere on the anode side. After at least a couple of hours of running under 100 sccm of nitrogen and if no leaks were found, the nitrogen supply was slowly decreased and replaced by hydrogen. In the mean time, air was gradually supplied to the cathode until the flux was 100 sccm. The reduction of NiO to Ni in the anode took place in the presence of the hydrogen at 800 ºC. Once the OCV had stabilized at its maximum value, the electrochemical test was performed.

2.2.3.3 Electrochemical performance evaluation

The electrochemical tests were performed at three different temperatures: 800 ºC, 700 ºC and 600 ºC. Each one of the cells was tested at these temperatures in a descending order and then in an ascending order. Humidified H_2 (~ 3 % H_2O at 30 ºC) was supplied as the fuel to the anode and O_2 as the oxidant to the cathode at 100 sccm. I–V measurements were performed in situ using an Arbin BT2000 battery fuel cell test station. At least two cells of each cathode composition tests were performed for each material at each temperature.

Chapter 3: IT-SOFC with Perovskite Cathodes: $Ln_{0.6}Sr_{0.4}Co_{1-y}Fe_yO_3$ (Ln = La, Nd, y = 0, 0.5) cathodes

3.1 CATHODE MATERIALS EVOLUTION

As mentioned in Chapter 1, $La_{1-x}Sr_xMnO_{3-\delta}$ (LSM) exhibits multiple advantages as a cathode material for high temperature SOFC.[23-26] However, LSM is not an attractive candidate to be used for IT-SOFC because, at temperatures below 900 ºC, the activation polarization of LSM increases considerably.[55] To improve the catalytic activity at intermediate temperatures, Mn has been substituted with Co resulting in a material with better performance at low temperatures.[56,57] However, lanthanum cobaltites exhibit a high TEC[58] which is undesirable. A trade off between conductivity and TEC is achieved by partially substituting Co for Fe, resulting in a $(La,Sr)(Co,Fe)O_3$ perovskite cathode material.[58]

In an attempt to reduce the TEC of cathode materials for IT-SOFC, studies have been performed on cathodes with other lanthanides different from lanthanum in their A sites.[59-61] Even though neodymium cobaltites do not exhibit the highest catalytic activity in the series, the TEC is decreased because the ionicity of the Nd-O bond is smaller than for the La-O bond. Further studies have shown that the conductivity of $Nd_{1-x}Sr_xCoO_3$ is optimized when the amount of dopant is $x = 0.4$.[62] In an attempt to reduce the TEC even more, studies have been performed on the effect of Fe in the B

sites of $Nd_{0.6}Sr_{0.4}Co_{1-y}Fe_yO_3$.[46] However, the conductivity of this material is reduced relative to the undoped compound. From this series, the smallest reduction in conductivity occurs when y = 0.5. Impregnation of $Nd_{0.6}Sr_{0.4}Co_{0.5}Fe_{0.5}O_3$ with silver has also been attempted using $La_{0.8}Sr_{0.2}Ga_{0.8}Mg_{0.2}O_{3-\delta}$ (LSGM) electrolytes in order to achieve a high electrical conductivity while maintaining a low TEC.[63] Thus, a number of novel cathode materials have been studied using thick LSGM electrolytes which have relatively poor conductance at intermediate operating temperatures. These compounds have not been studied, however, at intermediate temperatures using YSZ electrolytes. Since it is possible that the ohmic polarization at the electrolyte may be dominant beyond low current densities for electrolytes with poor conductance due to the large electrolyte thickness, it is necessary to study the behavior of these materials using a high conductance electrolyte to know the best performance achievable. If YSZ is used, it is important to use a thin YSZ electrolyte, which has good conductance.

The objective of this work is to evaluate the electrochemical performance of IT-SOFC using thin YSZ electrolytes with high conductance and the following perovskite cathode compositions:

- $Nd_{0.6}Sr_{0.4}CoO_{3-\delta}$ (NSC)
- $Nd_{0.6}Sr_{0.4}Co_{0.5}Fe_{0.5}O_{3-\delta}$ (NSCF)
- $Nd_{0.6}Sr_{0.4}Co_{0.5}Fe_{0.5-\delta}$ - Ag (NSCF-Ag)

Since the performance on SOFC are very sensitive to experimental parameters including gas pressures and fluxes, cell geometry, and material microstructure, to draw

comparisons to the work of others, it is necessary to test different cathode compositions using an identical cell geometry and experimental apparatus. Thus, although they have higher TEC and therefore are less desirable for IT-SOFC the following cathode compositions were also studied so that comparisons could be made with well-studied materials:

- $La_{0.6}Sr_{0.4}CoO_{3-\delta}$ (LSC)
- $La_{0.6}Sr_{0.4}Co_{0.5}Fe_{0.5}O_{3-\delta}$ (LSCF)

3.2 EXPERIMENTAL PROCEDURE

IT-SOFC were prepared with the procedure detailed in Chapter 2. The synthesis and characterization of the specific perovskite cathode compositions are explained in the following sections.

3.2.1 Synthesis and Characterization of $Ln_{0.6}Sr_{0.4}CoO_{3-\delta}$ (Ln = La, Nd)

LSC and NSC were synthesized by solid state reaction. The starting materials were La_2O_3 (Alfa Aesar) (for LSC), Nd_2O_3 (Alfa Aesar) (for NSC), $SrCO_3$ (Alfa Aesar) and Co_3O_4 (GFS Chemicals). The first step in the preparation of each one of these compounds was to dry the lanthanide oxide starting material for 2 hours at 1000 ºC to determine the weights necessary to obtain the stoichiometric mass required for the synthesis of LSC and NSC. The dried lanthanide oxide was mixed using an agate

mortar and pestle with the required amounts of $SrCO_3$ and Co_3O_4. The mixtures were then fired in air for 48 hours for the LSC and for 72 hours for the NSC, with an intermediate grinding every 24 hours. Finally, the powders were dry ball milled or hand ground using ethanol with an agate mortar and pestle to achieve the desired particle size. The composition of the powders was confirmed by XRD and the particle size was observed by SEM (Figure 3.1).

3.2.2 Synthesis and Characterization of $Ln_{0.6}Sr_{0.4}Co_{0.5}Fe_{0.5}O_{3-\delta}$ (Ln = La, Nd)

LSCF and NSCF were synthesized by co-precipitation. The starting materials were La_2O_3 (Alfa Aesar) (for LSCF), Nd_2O_3 (Alfa Aesar) (for NSCF), $SrCO_3$ (Alfa Aesar), $Co(CH_3COO)_2{\cdot}H_2O$ (Spectrum) and $Fe(CH_3COO)_2$ (GFS Chemicals). The first step in the preparation of each one of these compounds was to dry the lanthanide oxide starting material for 2 hours at 1000 ºC and weigh it shortly after to determine the stoichiometric mass required for the synthesis of LSCF and NSCF. Required amounts of $SrCO_3$ and the acetates are dissolved in a dilute solution of the lanthanide oxide in nitric acid. A 10 % (w/v) solution of equal amounts of KOH and K_2CO_3 were added slowly until the pH reached a value equal to or greater than 11 which caused the precipitation of the metal ions as carbonates and hydroxides. The precipitates were filtered and washed with deionized water several times. The products were dried overnight in an oven, and then calcined in air at 500 ºC for 5 hours. The calcined powders were ground with an agate mortar and pestle. The powders were fired in air

for 24 hours at 1200 ºC. Finally, the powders were dry ball milled or hand ground using ethanol with an agate mortar and pestle to achieve the desired particle size distribution. The composition of the powders was confirmed by XRD and the particle size was observed by SEM (Figure 3.2).

3.2.3 Synthesis of $Nd_{0.6}Sr_{0.4}Co_{0.5}Fe_{0.5}O_{3-\delta}$ - Ag

NSCF powders were prepared by co-precipitation as described in the previous section and applied by screen printing to IT-SOFC as explained in Chapter 2. Prior to application of the current collector, the NSCF cathodes were loaded with 0.1 mg/cm^2 (~ 0.5 wt %) of Ag by impregnation. A solution of $AgNO_3$ (Alfa Aesar, ACS 99.9+%) in a 1:1 (v/v) mixture of ethanol and water was used. The amount of solution required for impregnation was calculated according to the silver content in the solution and the cathode mass. The cathode mass was calculated from the weight difference of the cell before screen printing the cathode and after cathode sintering.

$$Solution\ volume\ for\ impregnation = \frac{(Required\ mass\ of\ metal\ cation)}{(Mass\ of\ metal\ cation\ per\ mole)(Concentration\ of\ solution)}$$

A 0.2 M solution was used to impregnate ~ 1 mg cathodes using a micropipette by successive depositions of small amounts of the solution.

3.2.4 GDC Interlayer

For each one of the perovskite cathodes, reactivity tests were conducted by mixing with an agate mortar and pestle the cathode material with an equal weight of 8YSZ. The mixture was fired for 2 hours at different temperatures and then analyzed by XRD. The peaks of the resulting XRD pattern were identified according the PDF cards of the mixed powders. Any other peak not corresponding to these compositions was considered to correspond to reaction products. The XRD patterns showed evidence of chemical reactions between the perovskite materials and 8YSZ at temperatures lower than 1000 ºC. Sintering cathodes at temperatures that low compromises the bonding between the cathode and the electrolyte and therefore higher temperatures are required. Thus, a buffer layer (interlayer) that reacts with neither the cathode nor the electrolyte material must be used with this system so that higher cathode sintering temperatures can be used.

The material selected as the interlayer was $Ce_{0.9}Gd_{0.1}O_{2-\delta}$ (GDC). GDC has a cubic fluorite structure and exhibits mixed conductivity.[64,65] The electronic conductivity of GDC is significant at high temperatures and under reducing atmospheres, but it can be considered an ionic conductor under oxidizing environments at intermediate temperatures. GDC has been previously investigated for use as an electrolyte material, but mechanical degradation in mixed oxidizing/reducing atmospheres[20] and low open circuit voltage (OCV) values due to reduction of GDC by H_2[65] are considerable disadvantages. However, doped ceria has successfully been used

as a barrier layer for lanthanum cobaltite-based cathodes that react with zirconia.[65,66] Thus, samples were prepared to determine if GDC could be used as a barrier layer for the perovskite cathodes used in this study.

GDC was prepared using a glycine nitrate combustion synthesis technique[54] as described in Chapter 2. Reactivity test were conducted with each one of the cathode compositions to determine the maximum temperature that a cathode/interlayer/electrolyte could be subjected to without causing reactions between the constituents. This temperature was used to determine the optimum sintering temperature of the cathodes.

3.3 RESULTS

In general, the ball milled powders are finer than the ones that were hand ground using and agate pestle and mortar. The particle size of the LSC powders 0.5 – 5 μm (Figure 3.1, top); LSCF powders, 0.5 – 10 μm (Figure 3.1, bottom); NSC powders, 1 – 10 mm (Figure 3.2, top); and NSCF, 0.5 – 10 μm (Figure 3.2, bottom).

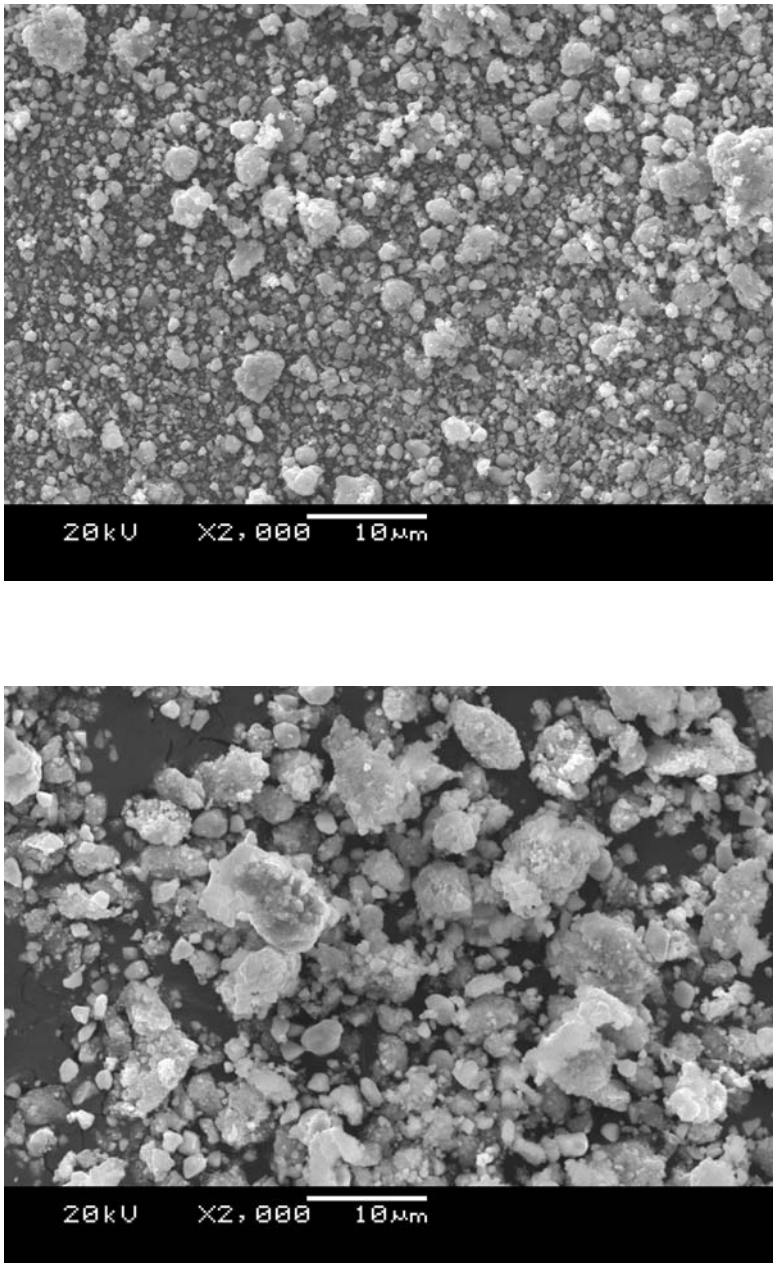

Figure 3.1. SEM of LSC (top) and LSCF (bottom) powders produced by solid state reaction and dry ball-milling.

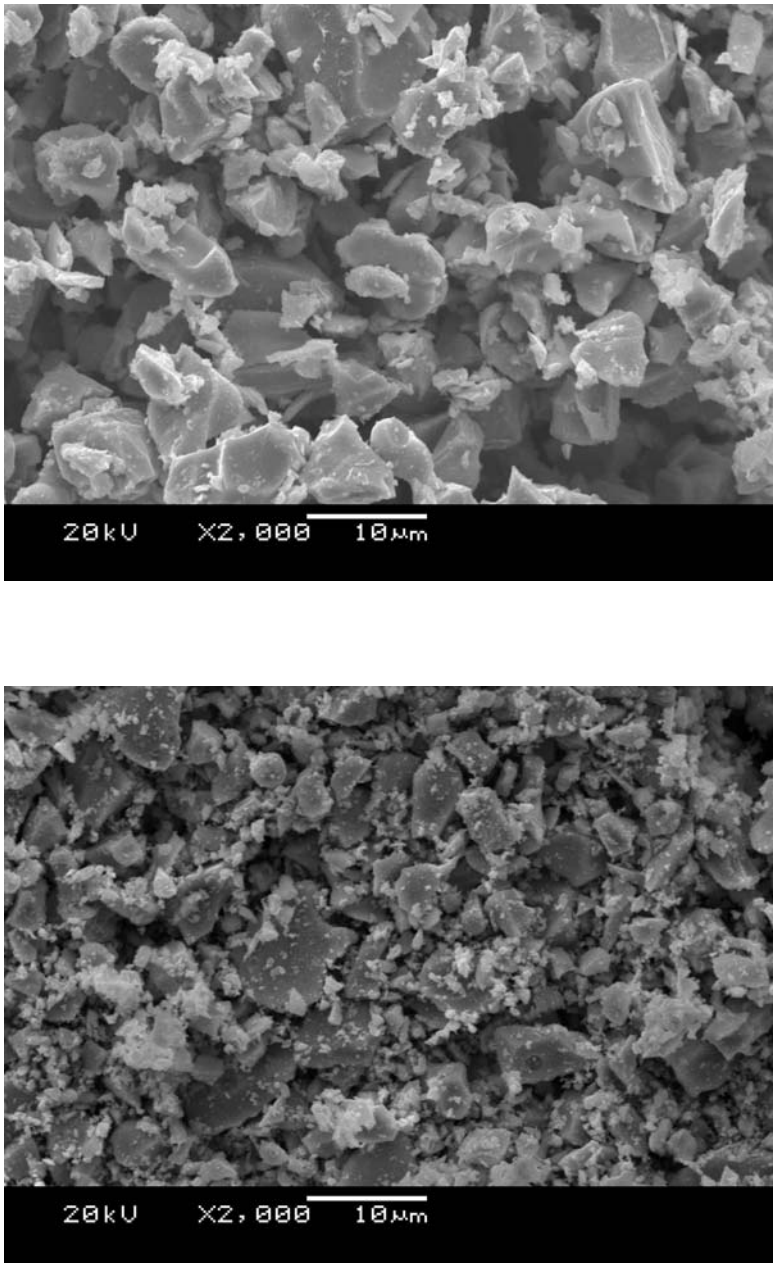

Figure 3.2. SEM of NSC (top) and NSCF (bottom) powders produced by solid state reaction and manual grinding using a mortar and pestle.

Reactivity tests for NSC and NSCF with YSZ (Figures 3.3 and 3.4 respectively) showed that these cathode materials cannot be used directly on a YSZ electrolyte because they react with the electrolyte. Similar observations of chemical reactions between LSC and LSCF and YSZ have been reported previously.[21,60]

Further reactivity tests were conducted between each one of these cathode compositions and GDC. XRD patterns of these tests are shown in Figures 3.5 to 3.8. The optimum sintering temperature for the cathode was determined based on the highest temperature at which there were no evidence of reaction products between the cathode material and GDC. Thus, the optimum sintering temperatures for NSC was determined to be 1100 ºC while for NSCF the optimum sintering temperature was determined to be 1200 ºC.

As a basis for comparison with Nd-based cathode materials, both LSC and LSCF cathodes were sintered at both 1000 ºC and 1100 ºC to study the effects of the sintering temperature on the performance of the cell and to compare with cells with NSC and NSCF cathodes.

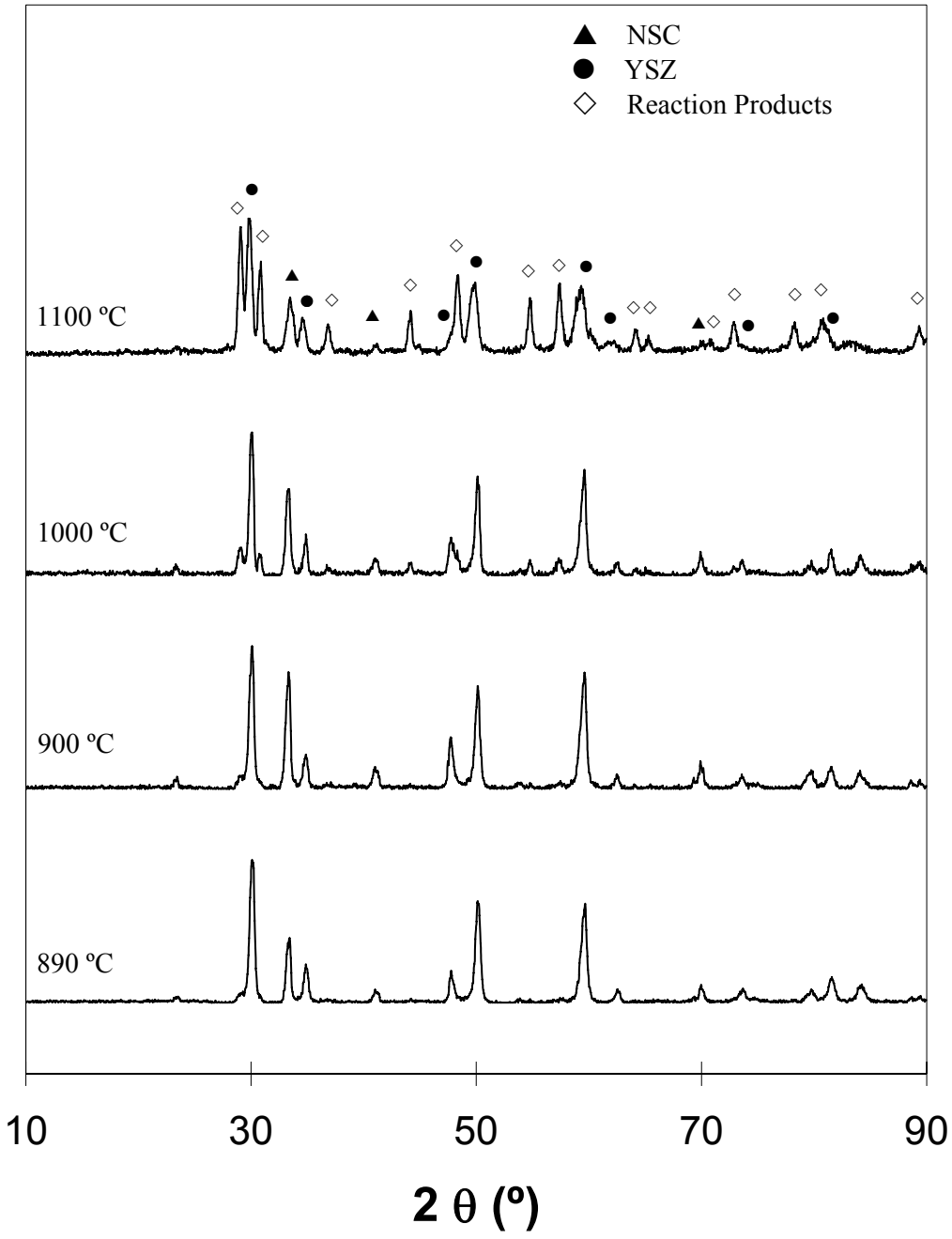

Figure 3.3. Reactivity test for NSC and YSZ.

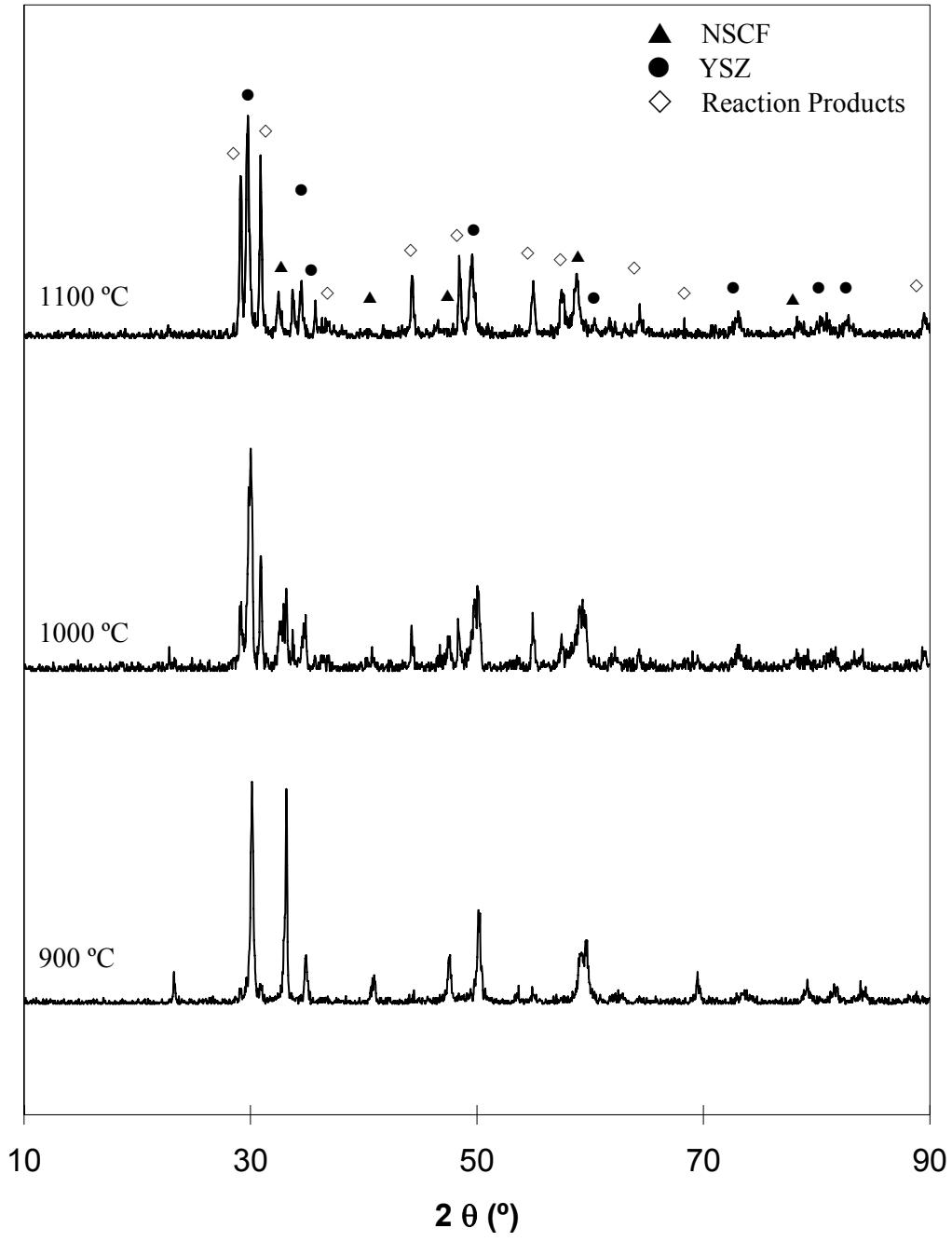

Figure 3.4. Reactivity test for NSCF and YSZ.

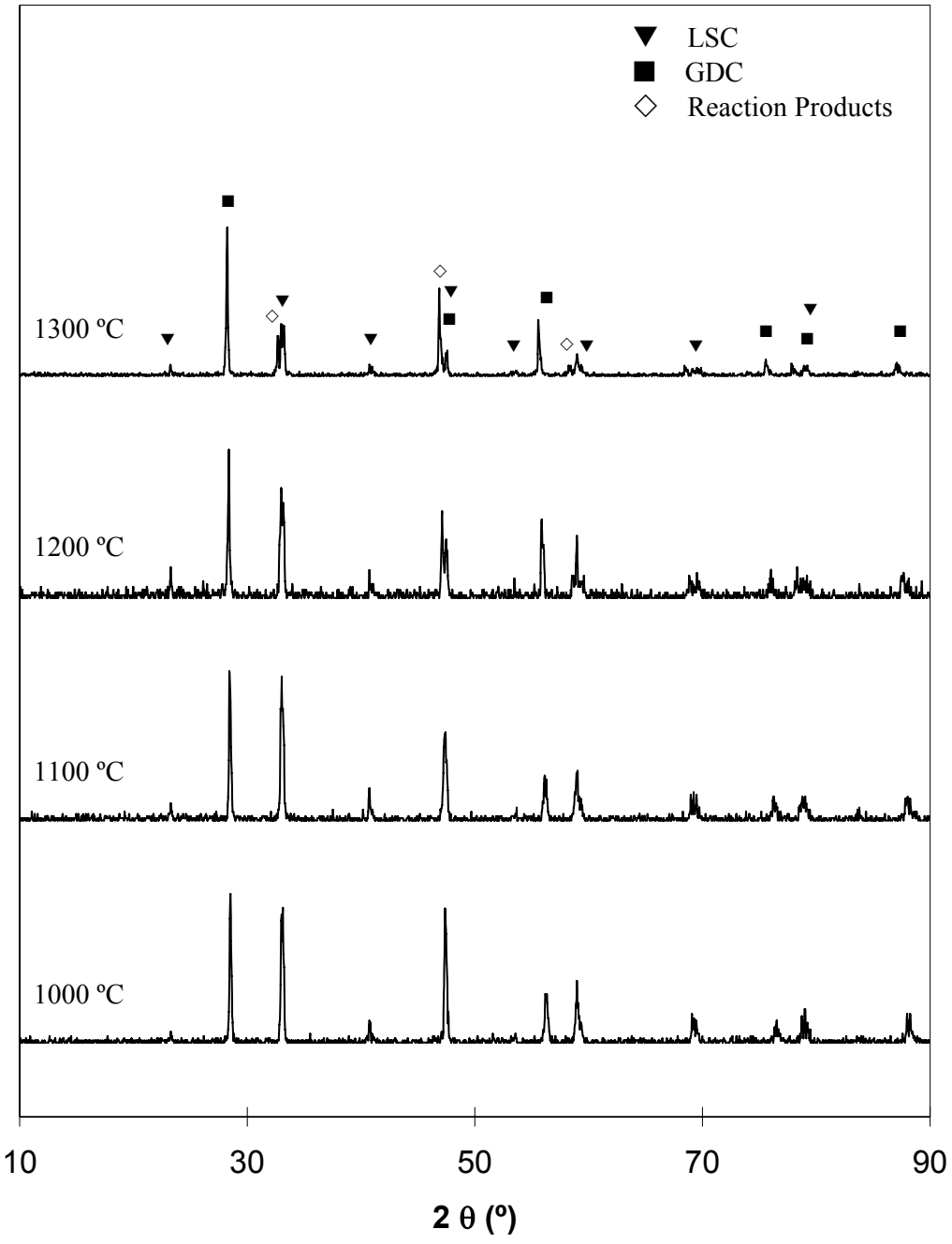

Figure 3.5. Reactivity test for LSC and GDC.

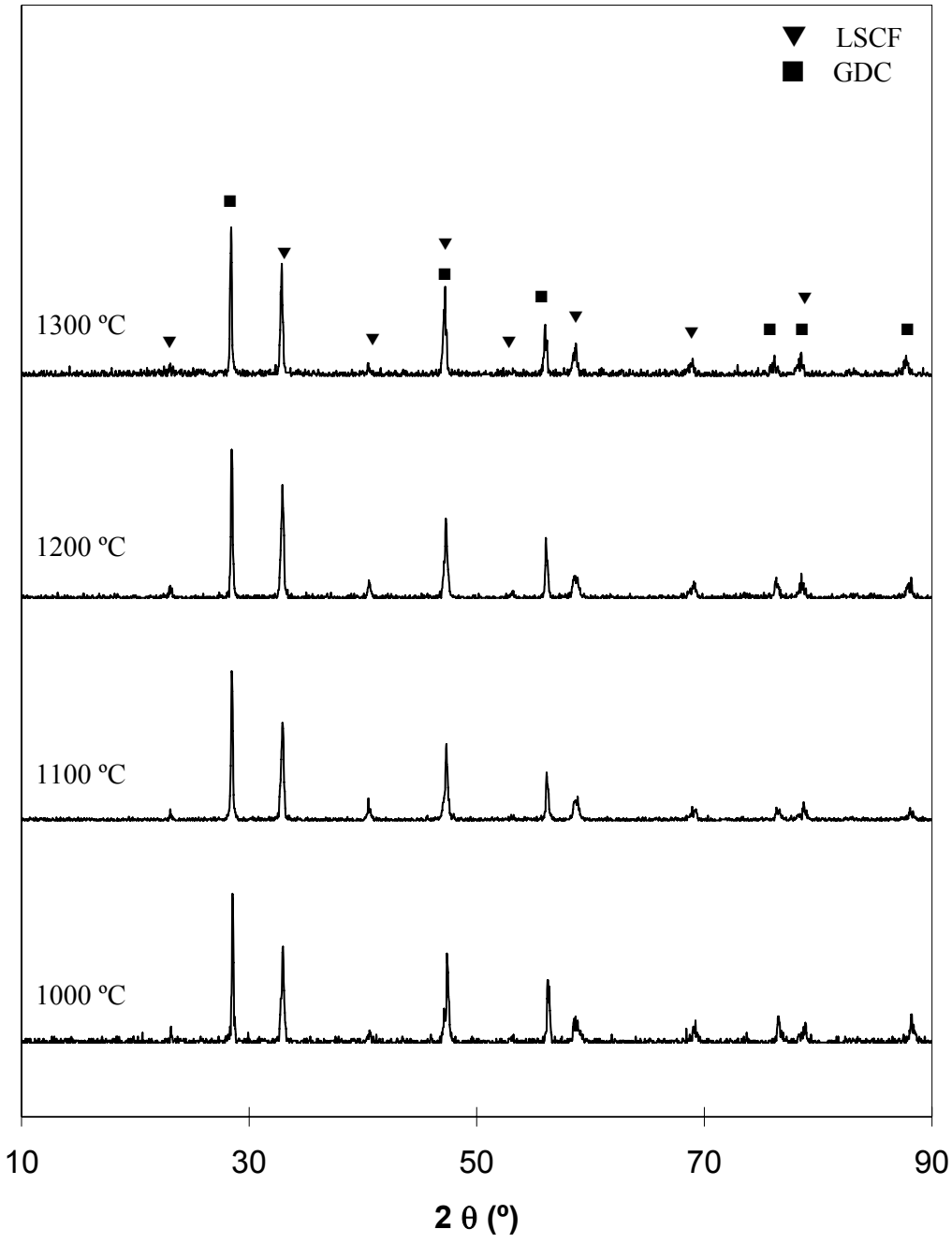

Figure 3.6. Reactivity test for LSCF and GDC.

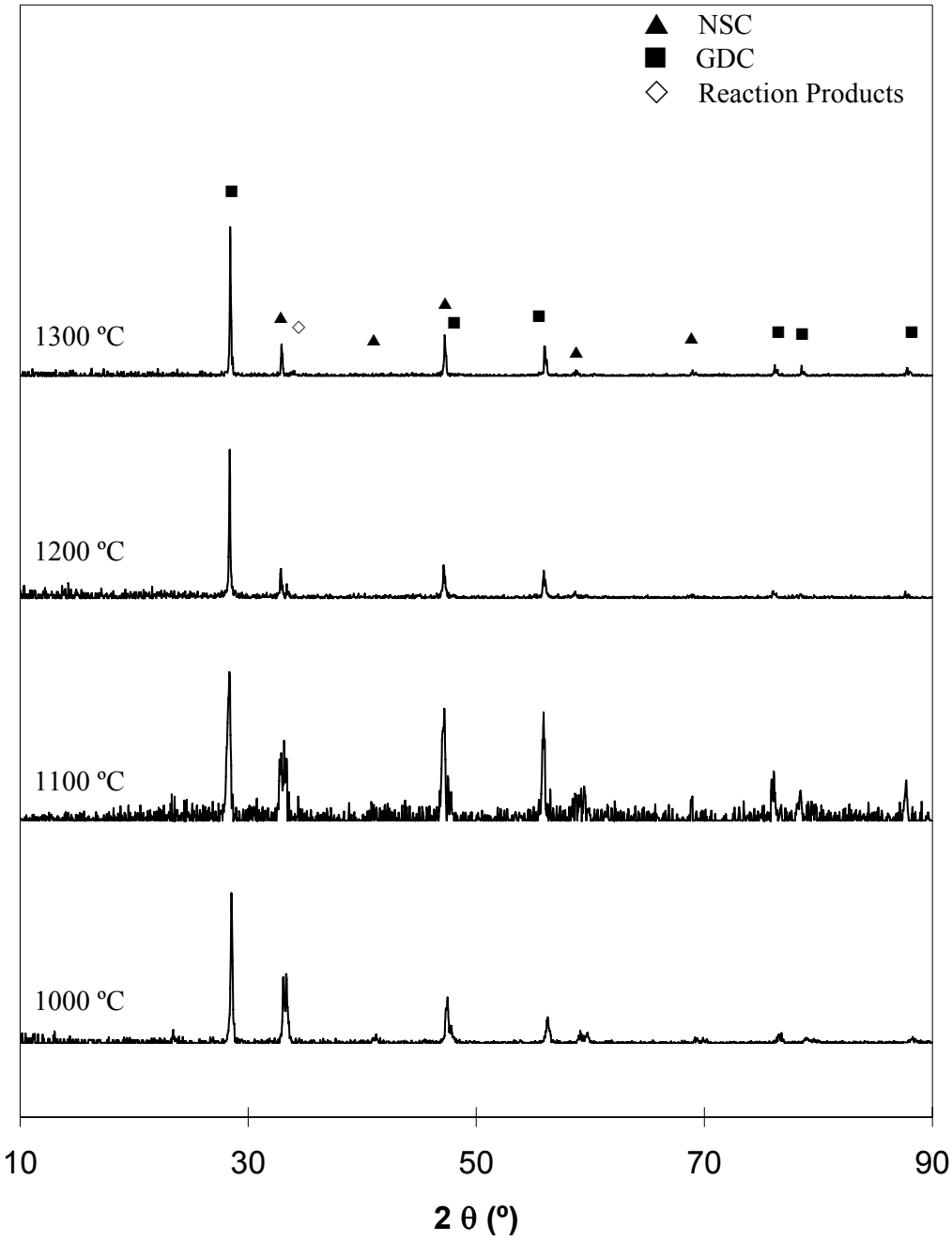

Figure 3.7. Reactivity test for NSC and GDC.

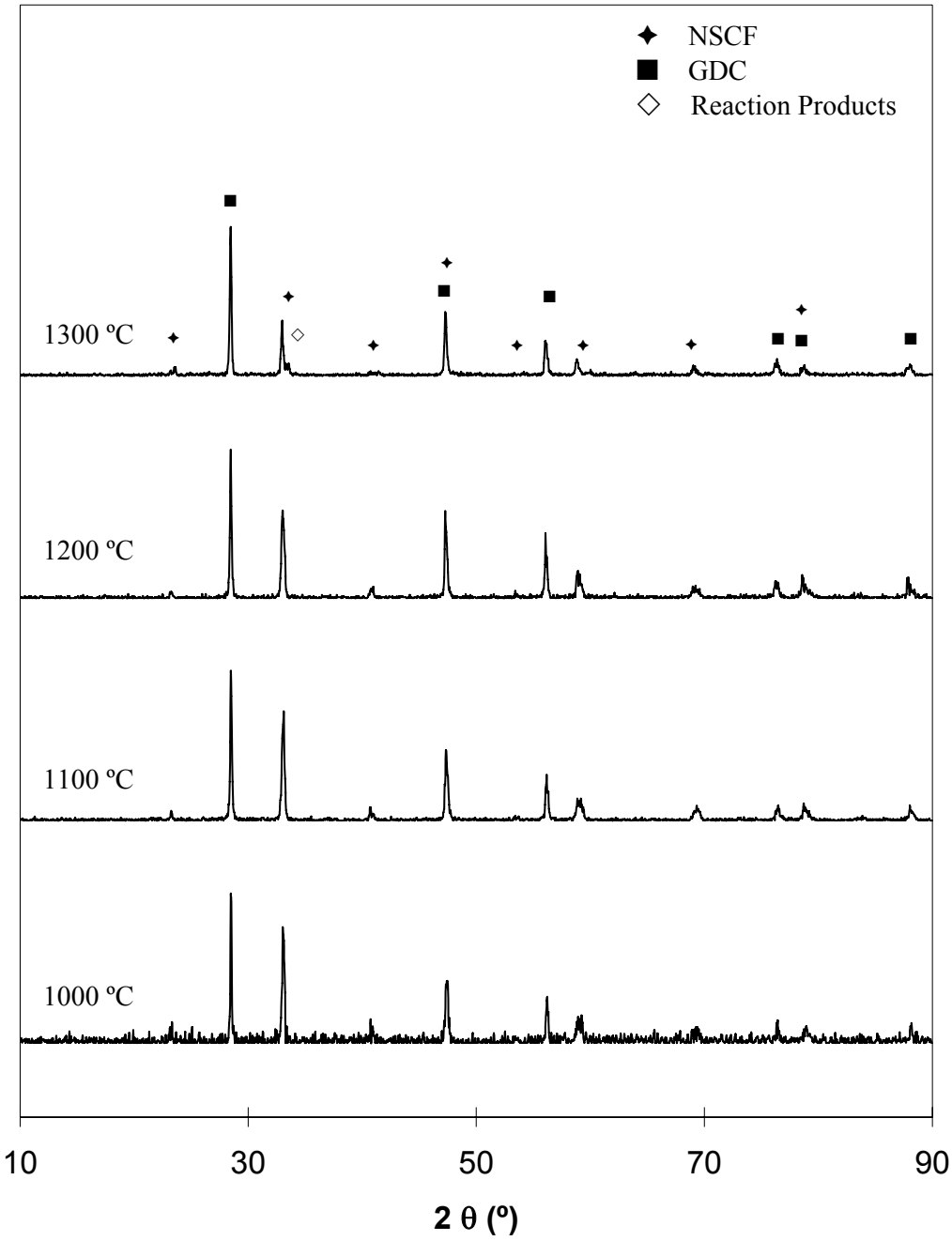

Figure 3.8. Reactivity test for NSCF and GDC.

IT-SOFC were prepared and tested following the procedures described in Chapter 2. I-V traces and power density curves of individual specimens can be found in Appendix C. The average maximum power densities for each composition and temperature are shown in Table 3.1. The number after LSC and LSCF is the temperature at which the cathodes were sintered. The electrochemical performances of representative cells are shown in Figures 3.9 to 3.15.

Table 3.1 Maximum power densities (W/cm^2) obtained at operating temperatures of 600 ˚C – 800 ˚C for IT-SOFC using perovskites cathodes.

Cathode	800 ºC	700 ºC	600 ºC
LSC1000	0.549	0.232	0.069
LSC1100	0.344	0.148	0.049
LSCF1000	0.378	0.159	0.045
LSCF1100	0.274	0.120	0.040
NSC	0.404	0.192	0.065
NSCF	0.173	0.066	0.021
NSCF-Ag	0.213	0.083	0.023

From Table 3.1, it is apparent that, at a given sintering temperature, the LSC-based cells prepared at the sintering temperature of 1000 ºC exhibit the highest performance at all of the operating temperatures that were studied. Comparing the results for LSC-based cells sintered at 1000˚C and 1100˚C (Figures 3.9 and 3.10), a reduction in peak power density of between 29-37% is observed, depending on the operating temperature, when the sintering temperature of the cathode is increased.

Similar observations are observed for LSCF-based cells sintered at 1000˚C and 1100˚C (Figures 3.11 and 3.12) where a 11-28% reduction in peak power is observed upon increasing the sintering temperature. Thus, a higher cathode sintering temperature does not result in better performance.

Comparing the results for the NSC-based cells to that for the LSC-based cells, the peak power densities for the NSC-based cells sintered at 1100˚C (Figure 3.13) lie above that for the LSC-based cells sintered at the same temperature (Figure 3.10). However, the performance of the NSC-based cells sintered at 1100˚C lie below that for LSC-based cells sintered at 1000˚C (Figure 3.9).

Comparing the results of the NSCF-based cells (Figure 3.14) to that of the NSC-based cells (Figure 3.13), we see a significant reduction in the peak power densities at all operating temperatures. Impregnating the NSCF cathode with silver results in significant improvements in power densities (Figure 3.15) compared to the unimpregnated NSCF-based cells (Figure 3.14), particularly at high operating temperatures. However, the Ag-impregnated, NSCF-based cells still exhibit reduced power densities compared to NSC (Figure 3.15 vs. Fig. 3.13).

.

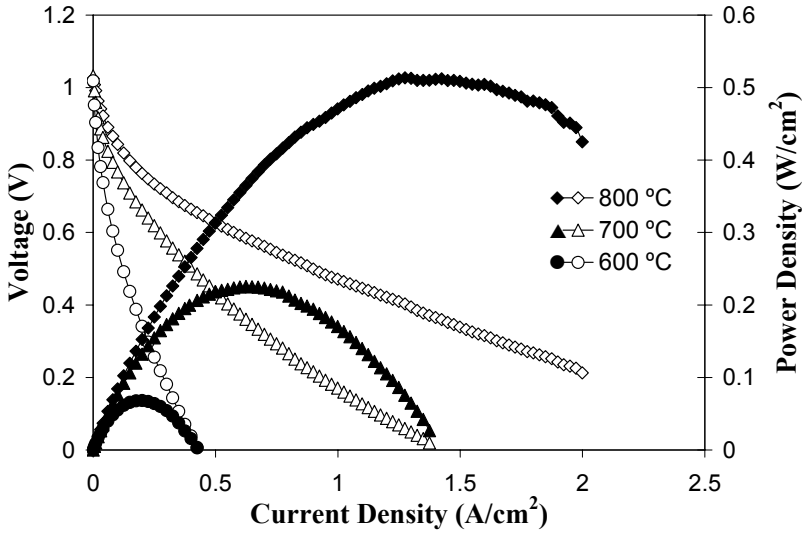

Figure 3.9. I-V curves (open symbols) and power densities (closed symbols) of IT-SOFC with LSC cathodes fired at 1000 ºC.

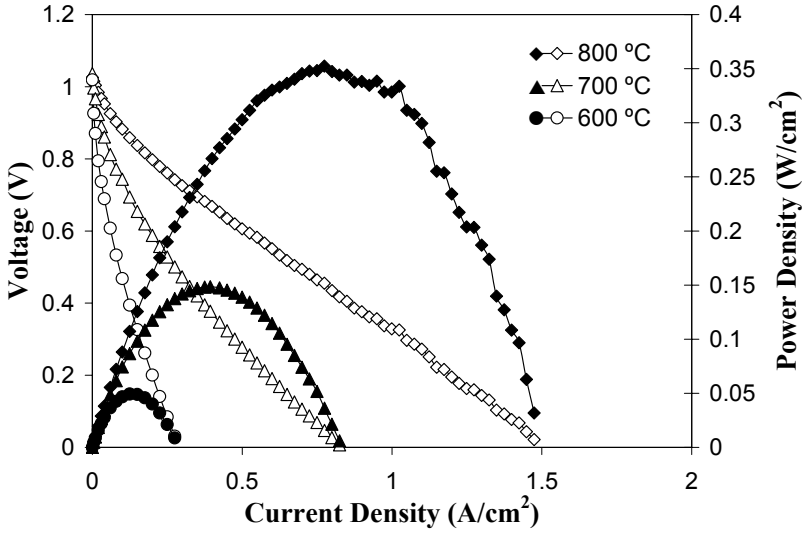

Figure 3.10. I-V curves (open symbols) and power densities (closed symbols) of IT-SOFC with LSC cathodes fired at 1100 ºC.

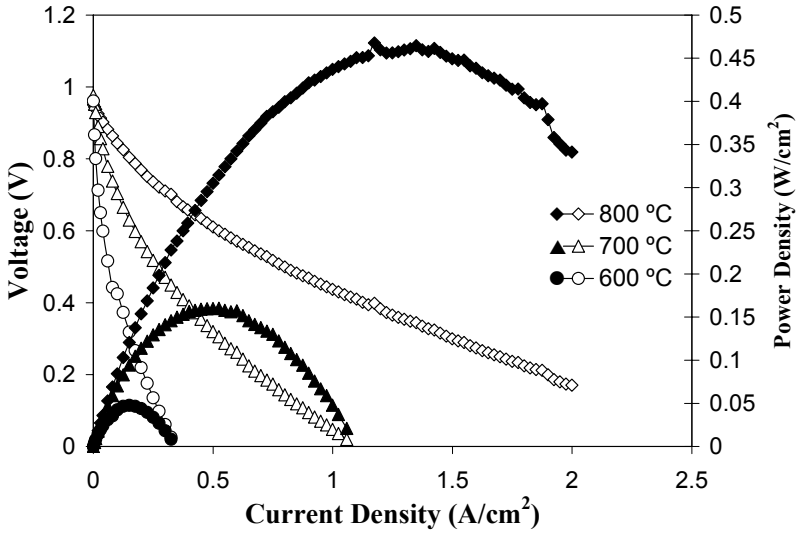

Figure 3.11. I-V curves (open symbols) and power densities (closed symbols) of IT-SOFC with LSCF cathodes fired at 1000 ºC.

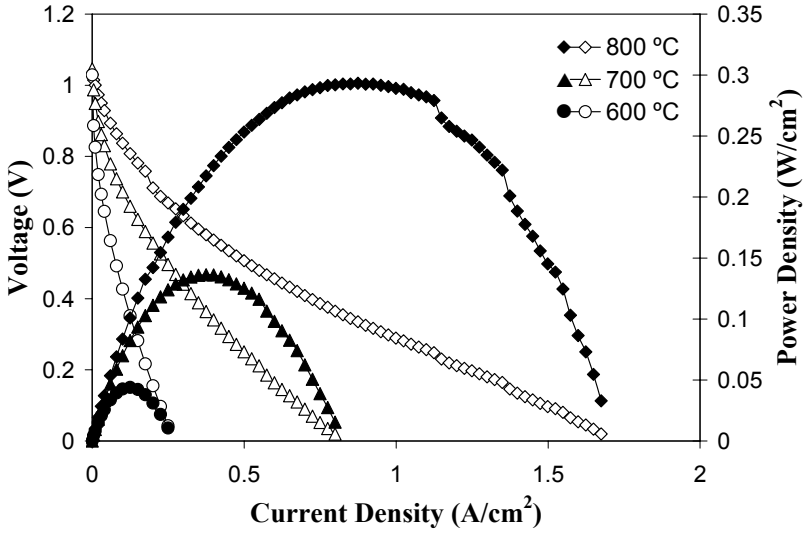

Figure 3.12. I-V curves (open symbols) and power densities (closed symbols) of IT-SOFC with LSCF cathodes fired at 1100 ºC.

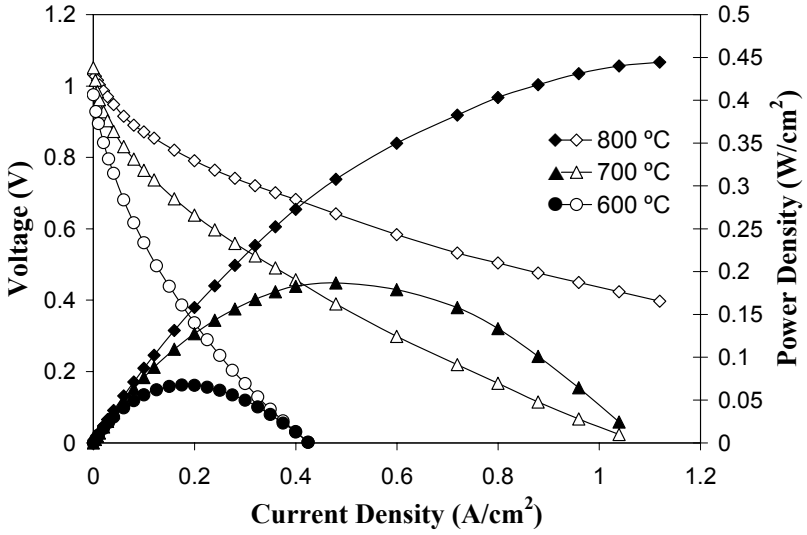

Figure 3.13. I-V curves (open symbols) and power densities (closed symbols) of IT-SOFC with NSC cathodes.

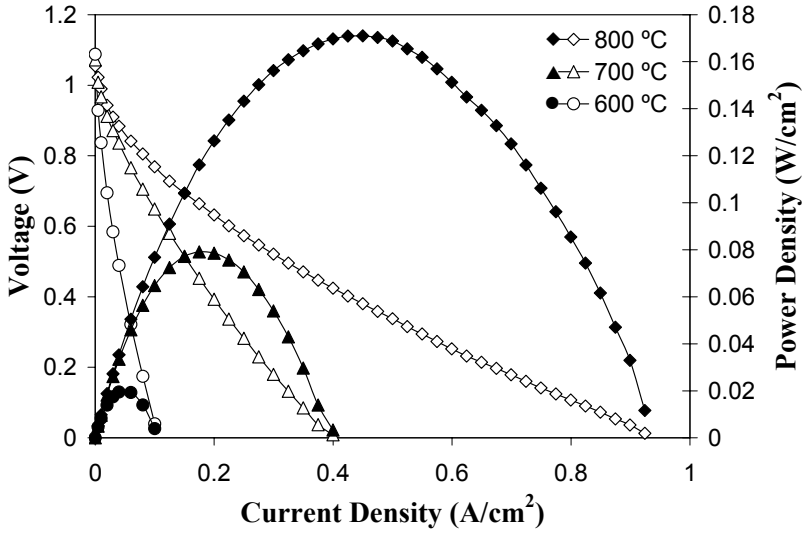

Figure 3.14. I-V curves (open symbols) and power densities (closed symbols) of IT-SOFC with NSCF cathodes.

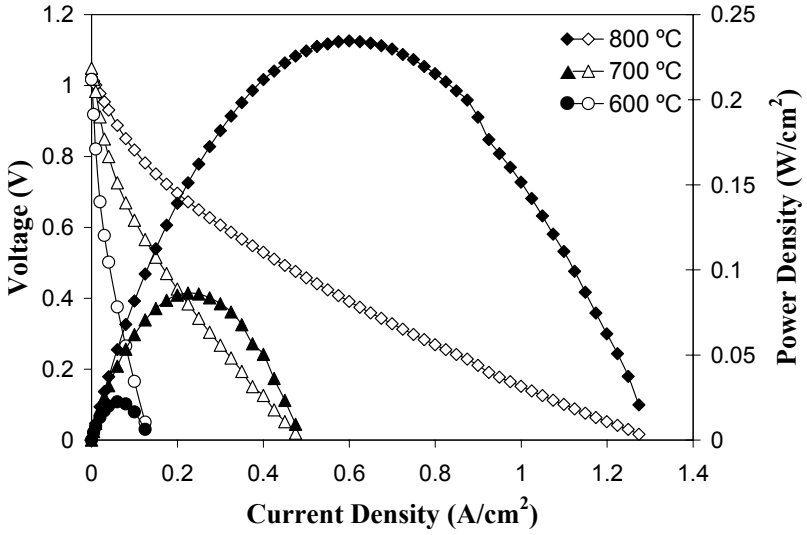

Figure 3.15. I-V curves (open symbols) and power densities (closed symbols) of IT-SOFC with NSC-Ag.

3.4 DISCUSSION

3.4.1 Influence of Cathode Sintering Temperature for LSC and LSCF

From Table 3.1, it is apparent that the sintering temperature of the cathode significantly influences the performance of the cell. As discussed in Chapter 1, the cathode must have both excellent electrical conductivity and high catalytic activity. Increasing the sintering temperature may result in a reduction in the porosity of the cathode due to densification which would in turn increase the electrical conductance of the cathode and thus should improve cell performance. This would be most apparent at moderate currents where performance is limited by ohmic polarization. The reduction

in porosity may also lead to increased concentration polarization and thus a reduction in performance that would be apparent at high currents. However, increasing the sintering temperature may also result in particle coarsening which would reduce the total number of reaction sites and therefore result in an increase in the activation polarization at low current but have little effect at high currents. Thus, a comparison of the I-V curves at low and high currents should allow us to determine the cause of the reduction in performance that was observed in LSC and LSCF-based cells when the cathode sintering temperature was increased. Since concentration polarization does not have a strong effect on the power density of SOFC,[2] we will focus on comparing the I-V curves at low to moderate current densities. Figures 3.16, 3.17 and 3.18 show the initial portion of I-V traces at 800 ºC, 700 ºC and 600 ºC in which the voltage values are an average of the results for each cathode composition. The voltage value at zero current density corresponds to the OCV. As mentioned in Chapter 1, OCV results from the difference in oxygen pressures between the cathode and the anode sides of the cell and it is not related to the intrinsic performance of the cell, although it can affect the maximum power density. Thus, The OCV value reflects the quality of the glass seal which may be affected by deviations from flatness of the cell, glass paste composition and application method. It can be seen that I-V traces for LSC and LSCF-based cells have a steeper initial slope as the cathode sintering temperature increases.

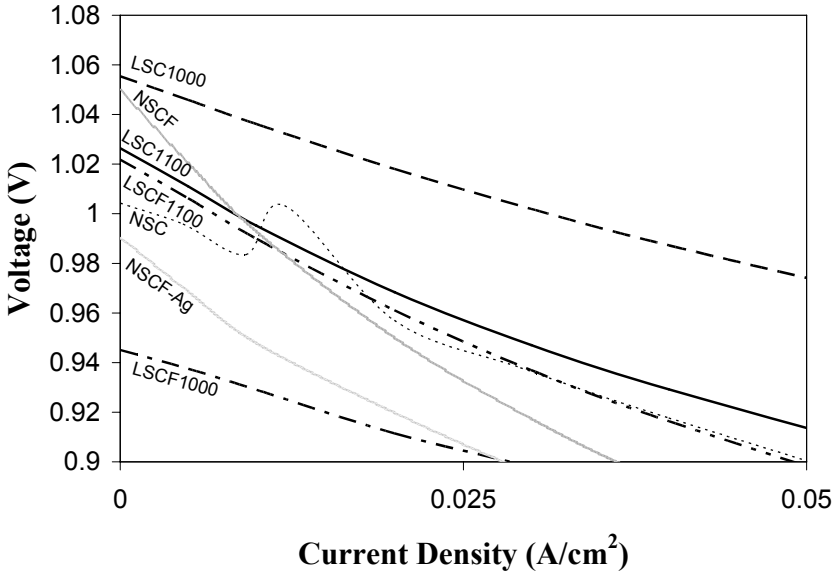

Figure 3.16. Comparison of average I-V traces at low current densities at 800 ºC.

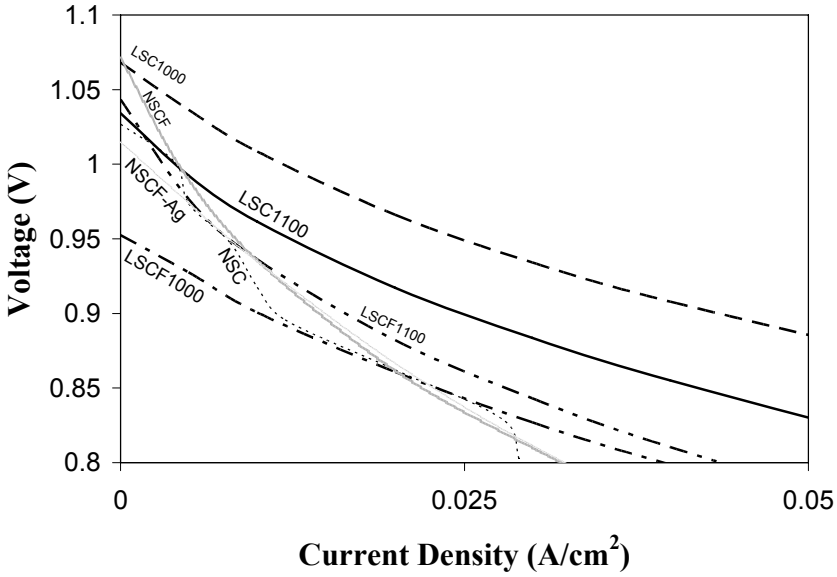

Figure 3.17. Comparison of average I-V traces at low current densities at 700 ºC.

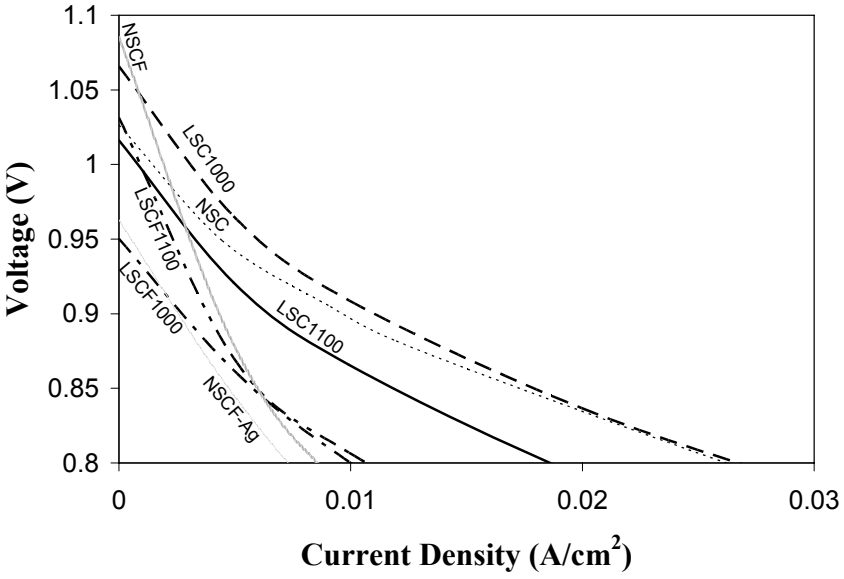

Figure 3.18. Comparison of average I-V traces at low current densities at 600 ºC.

In general, the activation polarization increases at lower operation temperatures. The observed decrease in performance with increasing sintering temperature of the LSC and LSCF-based cells at low currents is consistent with increased activation polarization due to particle coarsening and a concomitant decrease in the number of reaction sites that are available in the cathode. Although densification and its associated increase in conductivity likely also occurs to offset some the loss in performance due to the reduction in the number of reaction sites, the observed decrease in performance suggests that that the performance of these cells is dominated by particle coarsening rather than densification. The coarsening of the LSC cathode can be

appreciated by comparing Figures 3.19 (a) and (b); and LSFC cathodes is illustrated by comparing Figures 3.20 (a) and (b).

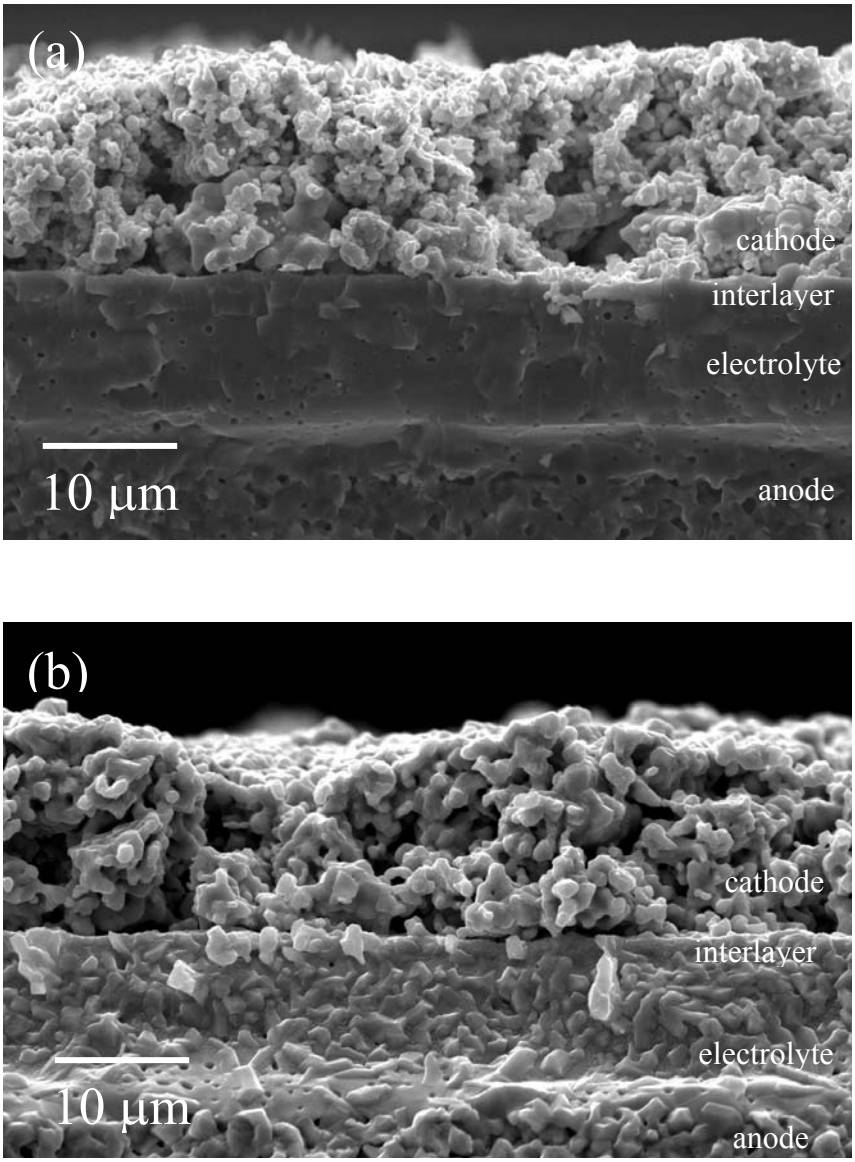

Figure 3.19. SEM of IT-SOFC with LSC cathodes fired at (a) 1000 ºC, and (b) 1100 ºC.

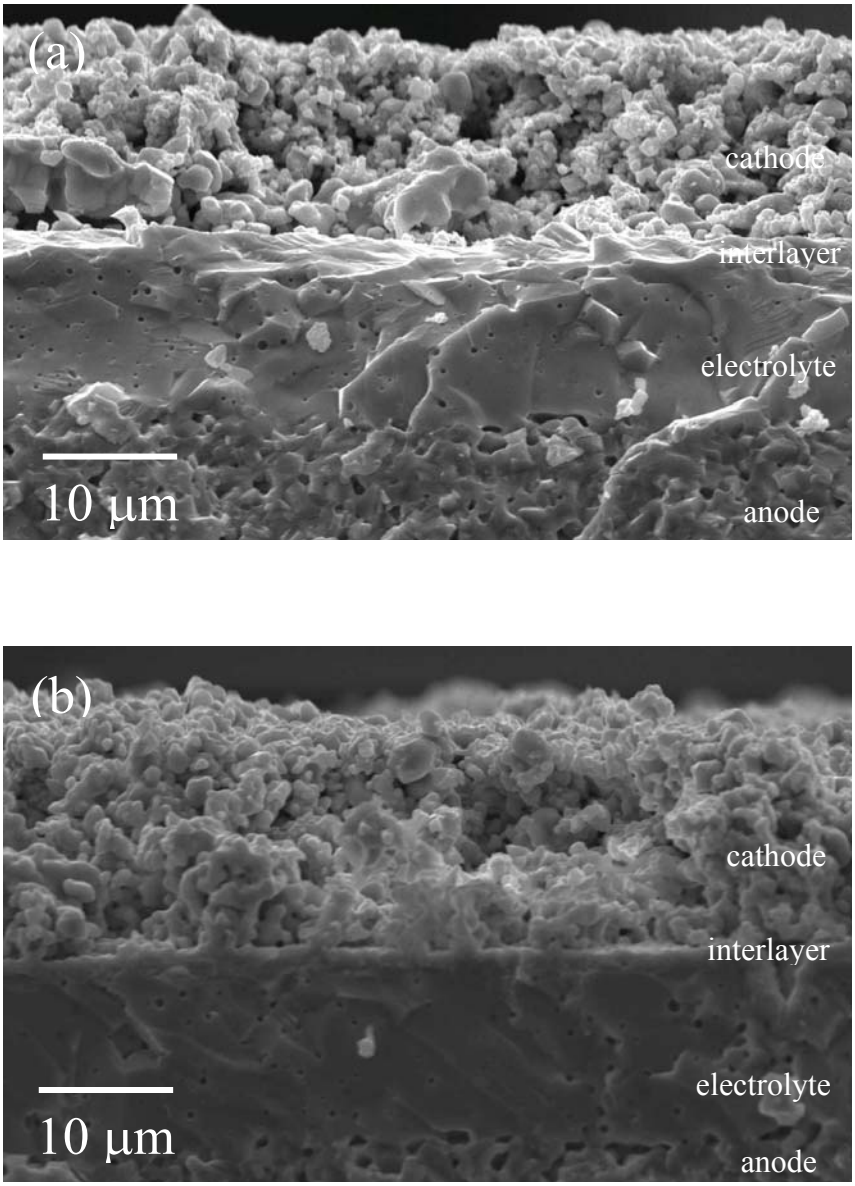

Figure 3.20. SEM of IT-SOFC with LSCF cathodes fired at (a) 1000 ºC, and (b) 1100 ºC.

3.4.2 Comparison between NSC and LSC-Based Cells

Substituting lanthanum by neodymium in the cathode composition has a positive effect on the performance of the cell even though the conductivity and electrocatalytic activity for oxygen reduction reaction are higher for LSC than for NSC.[61] This effect has not been observed in SOFC with thick LSGM electrolytes because the conductivity of LSC is only approximately two orders of magnitude larger than the conductivity of NSC (see Appendix B). It is likely that the effects of chemistry on conductivity are being masked by small differences in microstructure that occur during processing or sintering.

3.4.3 Comparison between LSC and LSCF-Based Cells and NSC and NSCF-Based Cells

Figures 3.21 (a) and (b) show micrographs of fracture surfaces of cells with NSC and NSCF cathodes. The decrease in the performance on cells with Fe-doped cathodes is expected, given that substitution of Co by Fe causes a decrease in the conductivity of the perovskite of ~ 32 % (LSC1000 vs LSFC1000), ~ 20 % (LSC1100 vs LSFC1100), and ~ 63 % (NSCF vs NSCF). The I-V curves for all the cells have a positive curvature, except at very high current densities. The negative of slope of the curve at very low current densities represents the area specific resistance of the cell. This resistance involves the ohmic resistance of the electrolyte and the effective charge transfer resistance that is a measure of the activation energy of the cathode. Given the thickness of the electrolyte and interlayer and its ionic resistivity, we can see that the

major contributor to this overpotential is the conductivity of the cathode. The fact that the slope of the I-V curves for Fe-doped cathodes is more pronounced than for when the cathode has only Co in the B sites is clear evidence that the presence of Fe decreases the conductivity of the cathode, leading to higher ohmic polarization at moderate currents.

The very poor performance of the NSCF-based cells sintered at 1200 ˚C relative to the LSCF-based cells sintered at 1100 ˚C and 1000 ˚C suggests that the higher sintering temperature used to produce the NSCF-based cells may have decreased the number of reaction sites, leading to activation polarization. This suggests that a lower sintering temperature for the NSCF-based cells may lead to improved performance.

3.4.4 Influence of Impregnation of NSCF with Ag

Figure 3.21 (c) shows the fracture surface of a IT-SOFC with NSCF-Ag cathode. The poor performance of the Fe-doped perovskites-based cells relative to the undoped NSC and LSC-based cells suggests that developing a strategy for improving the electrical conductivity of the cathode materials should improve cell performance. This was attempted by impregnating NSCF with silver which should cause an increase in electrical conductivity of the cathode by creating a continuous Ag phase with high electrical conductivity. Comparison of the NSCF and the NSCF-Ag confirms that the presence of the conducting Ag increases the performance of the cell by reducing the

activation polarization of the cathode. However, the performance of the NSCF-based cell impregnated with silver is still below that for the undoped NSC-based cells.

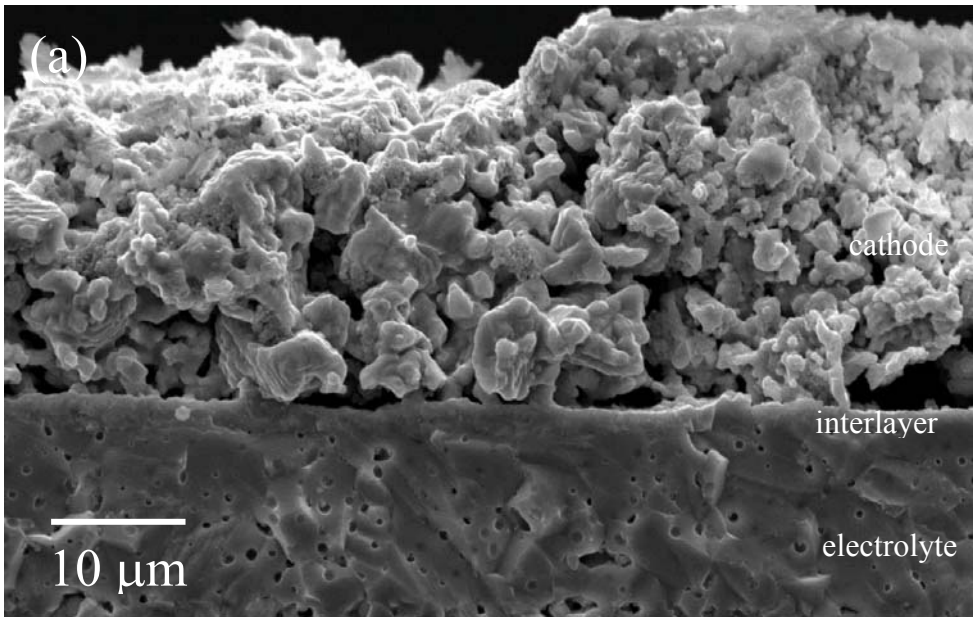

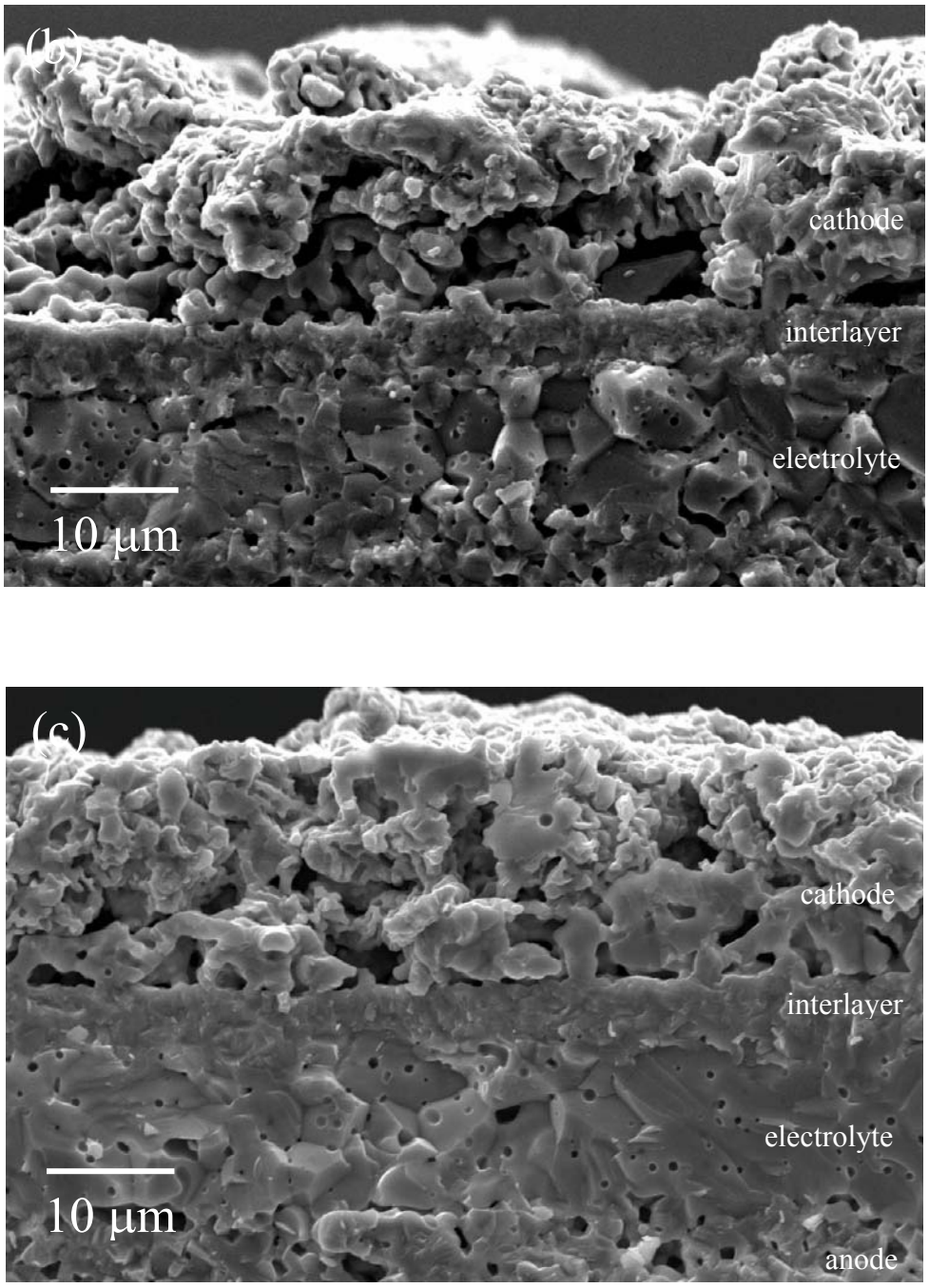

Figure 3.21. SEM of IT-SOFC with (a) NSC, (b) NSCF, and (c) NSCF-Ag cathodes.

3.4 CONCLUSIONS

These results show that the sintering temperature of the cathode plays an important role in determining cell performance for perovskite-based cathodes. Increasing the cathode sintering temperature results in a reduction in cell performance that was attributed to particle coarsening. The increase in the particle size and neck diameter during coarsening reduces the number of active reaction sites in the cathode. However, it is expected that very low sintering temperatures would also result in poor performance due to poor conductivity due to poor connectivity between the particles and the large fraction of pores. Thus, an optimum cathode sintering temperature must be determined for each cathode composition.

Although the performance of cells made NSC cathodes are comparable to those of cells produced with LSC cathodes, NSC cathodes offers another advantage for IT-SOFC because NSC has a lower TEC mismatch with YSZ. The lower TEC mismatch may result in reduced long-term degradation that is typically observed during thermal cycling of SOFC.[21] Although NSCF cathodes exhibit an even lower TEC mismatch with YSZ than NSC, the performance of this cathode is very low and thus it is not a good candidate for IT-SOFC cathodes. However, impregnation of the NSCF cathodes with silver increases the electrical conductivity of the cathode which results in improved performance of the cell, while still maintaining a low TEC mismatch with YSZ. This material should be studied under long term operating conditions to determine if its long-term performance is better than LSC and NSC-based SOFC.

Chapter 4: IT-SOFC with Intergrowth Perovskite Oxides Cathodes: $(La,Sr)_{n+1}(Fe,Co)_nO_{3n+1}$, (n = 2, 3, ∞) cathodes

4.1 INTRODUCTION

Perovskite-related intergrowth oxides from the Ruddlesden-Popper series $(La,Sr)_{n+1}(Fe,Co)_nO_{3n+1}$ with n = 2 [67] and n = 3 [68] have been identified as good candidates for cathode materials for IT-SOFC due to their stability and oxygen ion conductivity. Recently, $Sr_{2.7}La_{0.3}Fe_{2-y}Co_yO_{7-\delta}$ (n =2)[47] and $LaSr_3Fe_{3-y}Co_yO_{10}$ (n = 3)[69] have been explored as cathodes with $La_{0.8}Sr_{0.2}Ga_{0.8}Mn_{0.2}O_{2.8}$ electrolytes for electrolyte-supported IT-SOFC. It was shown that these compositions exhibit good mixed electronic-ionic conductivity and structural stability. From these series, $Sr_{2.7}La_{0.3}Fe_{1.4}Co_{0.6}O_{7-\delta}$ and $LaSr_3Fe_{1.5}Co_{1.5}O_{10}$ exhibited the best performance. In this study we explore the use of the perovskite-related intergrowth oxides $Sr_{2.7}La_{0.3}Fe_{1.4}Co_{0.6}O_{7-\delta}$ (SLFCO7) and $LaSr_3Fe_{1.5}Co_{1.5}O_{10}$ (LSFCO10) as cathodes of IT-SOFC with thin YSZ electrolytes, and compare these cathodes to the $La_{0.6}Sr_{0.4}Co_{0.5}Fe_{0.5}O_3$ (LSCF) perovskite cathode studied in Chapter 3.

The crystalline structures of the Ruddlesden-Popper series consist of n consecutive perovskite layers along the z axis, separated by a double rock salt layer formed by lanthanide and oxygen atoms.[70] A simple perovskite structure results when n = ∞ to produce LSCF. Thus, n = 2 results in SLFCO7 and n = 3 results in LSFCO10. Figure 4.1 shows the crystalline structures for these compounds.

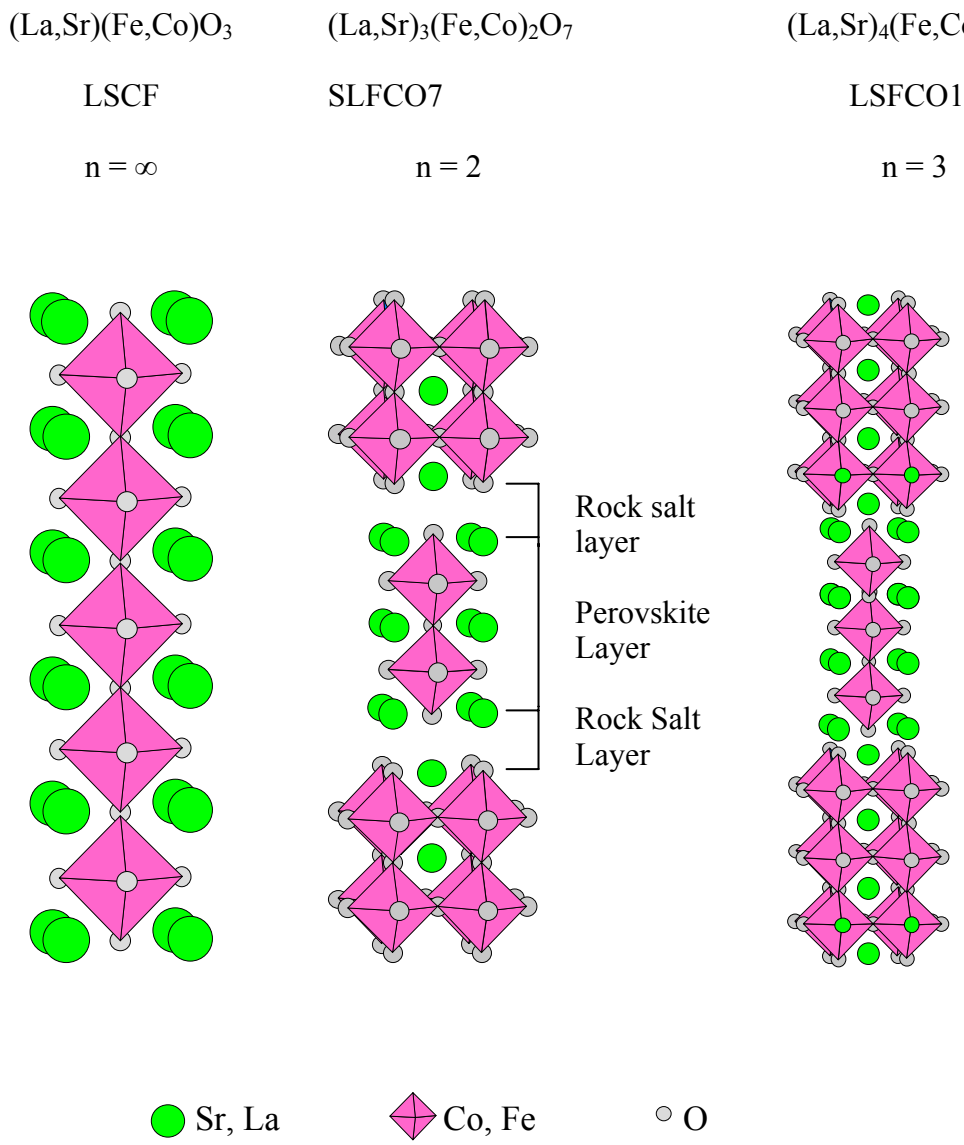

Figure 4.1. Crystalline structures of perovskite (n = ∞) (left) and perovskite related intergrowth oxides (n = 2 and 3) (center and right).

4.2 EXPERIMENTAL

The cathode materials were produced by solid state reaction in air. Stoichiometric amounts of La_2O_3 (Alfa Aesar) , $SrCO_3$ (Alfa Aesar), Fe_2O_3 (Spectrum) and Co_3O_4 (GFS Chemicals) were calcinated in air for 12 h at 900 ºC in the case of SLFCO7 or 1000 ºC in the case of LSFCO10. After grinding using an agate mortar, the powders were fired at 1300 ºC with intermediate steps of grinding in agate mortar. The resulting powders were hand ground with ethanol until reaching a satisfactory particle size. Reactivity tests for SLFCO7 and LSFCO10 with YSZ and GDC were performed to evaluate the use of an interlayer. IT-SOFC were prepared and tested as described in Chapter 2.

4.3 RESULTS

The particle size of the resulting powders was approximately 0.5 - 10 μm. Figure 4.2 shows SEM images of SLFCO7 and LSFCO10 powders after calcining.

Reactivity tests showed that both SLFCO7 and LSFCO10 reacted with YSZ (Figures 4.3 and 4.4), even at low firing temperatures. Reactivity tests with GDC (Figures 4.5 and 4.6) showed that a GDC interlayer can be used at firing temperatures as high as 1000 ºC.

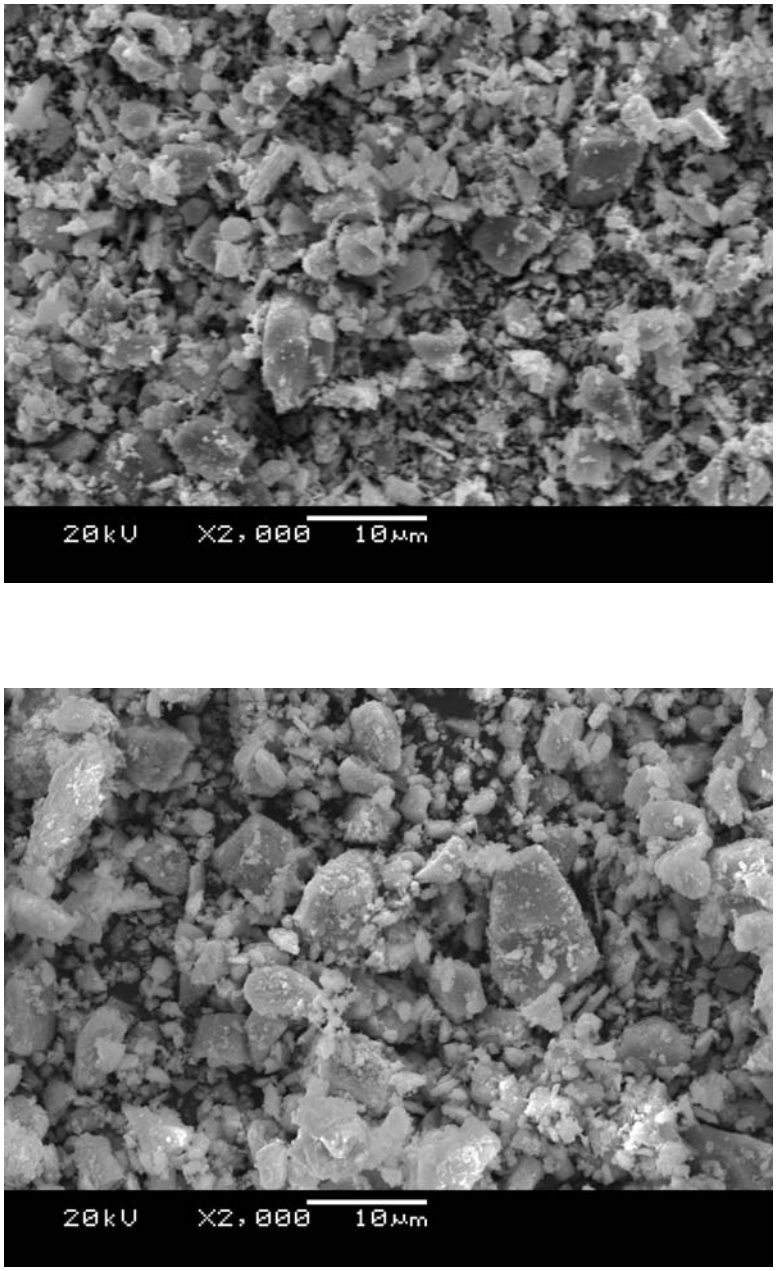

Figure 4.2. SEM of SLFCO7 (top) and LSFCO10 (bottom) powders produced by solid state reaction and hand milled.

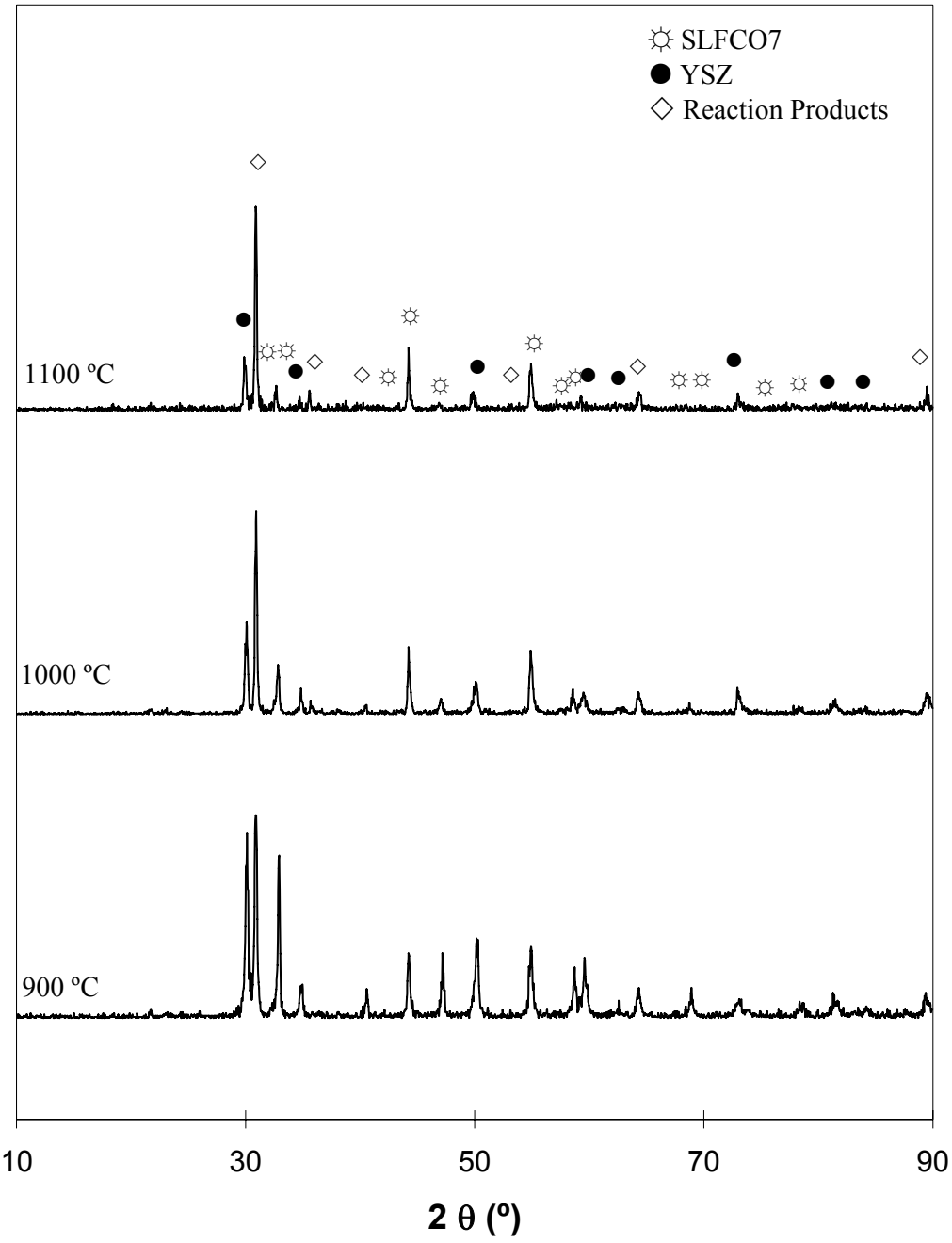

Figure 4.3. Reactivity test for SLFCO7 and YSZ.

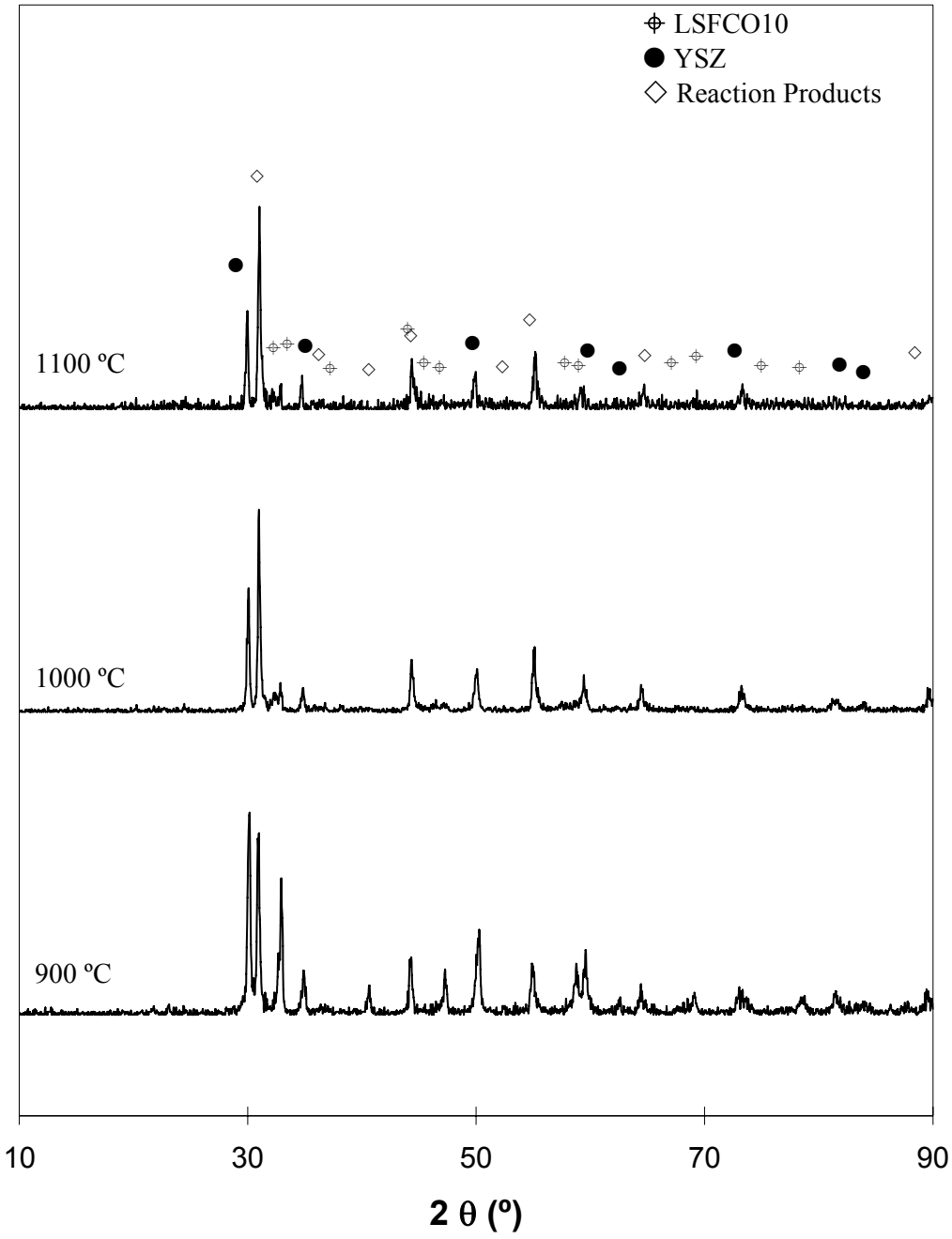

Figure 4.4. Reactivity test for LSFCO10 and YSZ.

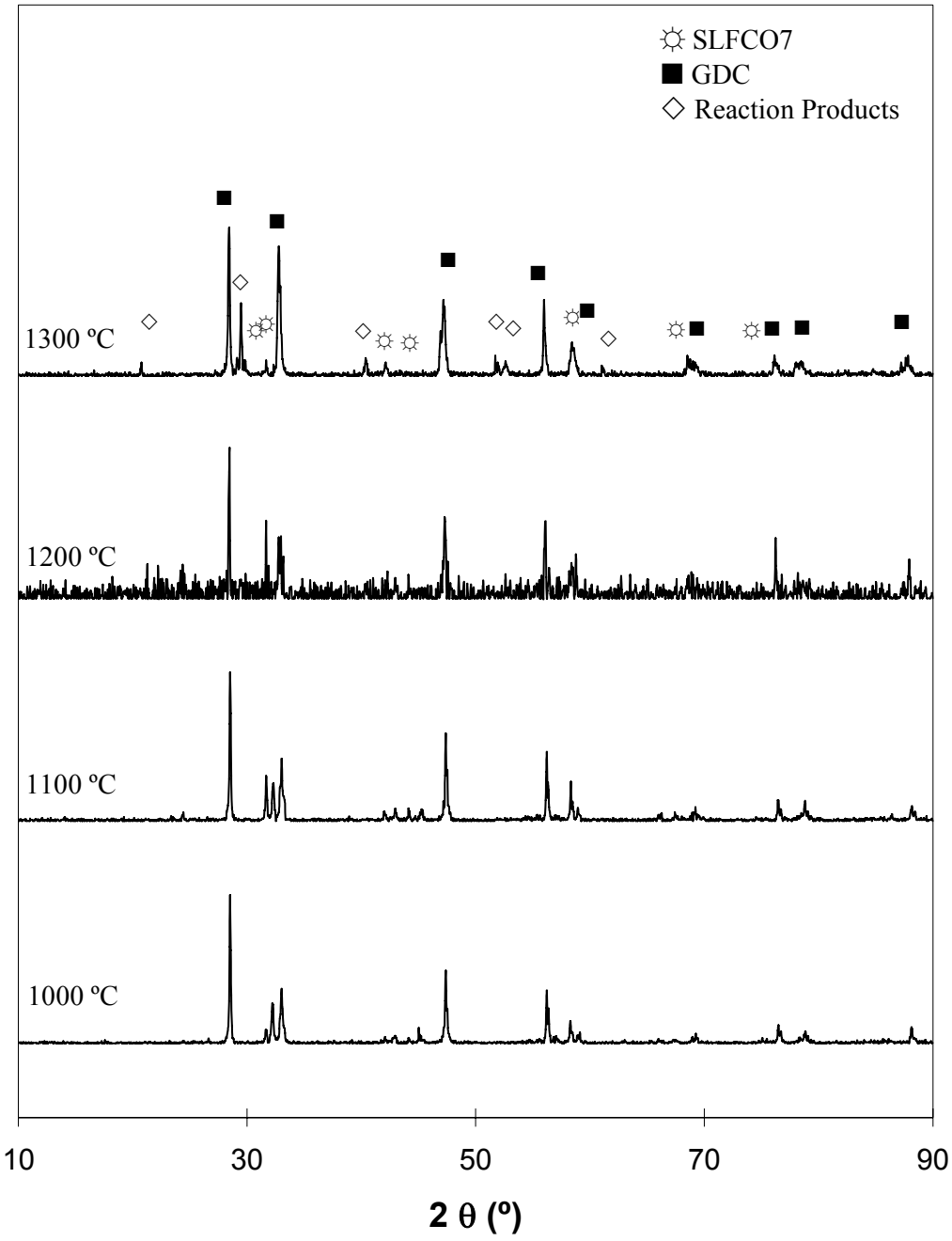

Figure 4.5. Reactivity test for SLFCO7 and GDC.

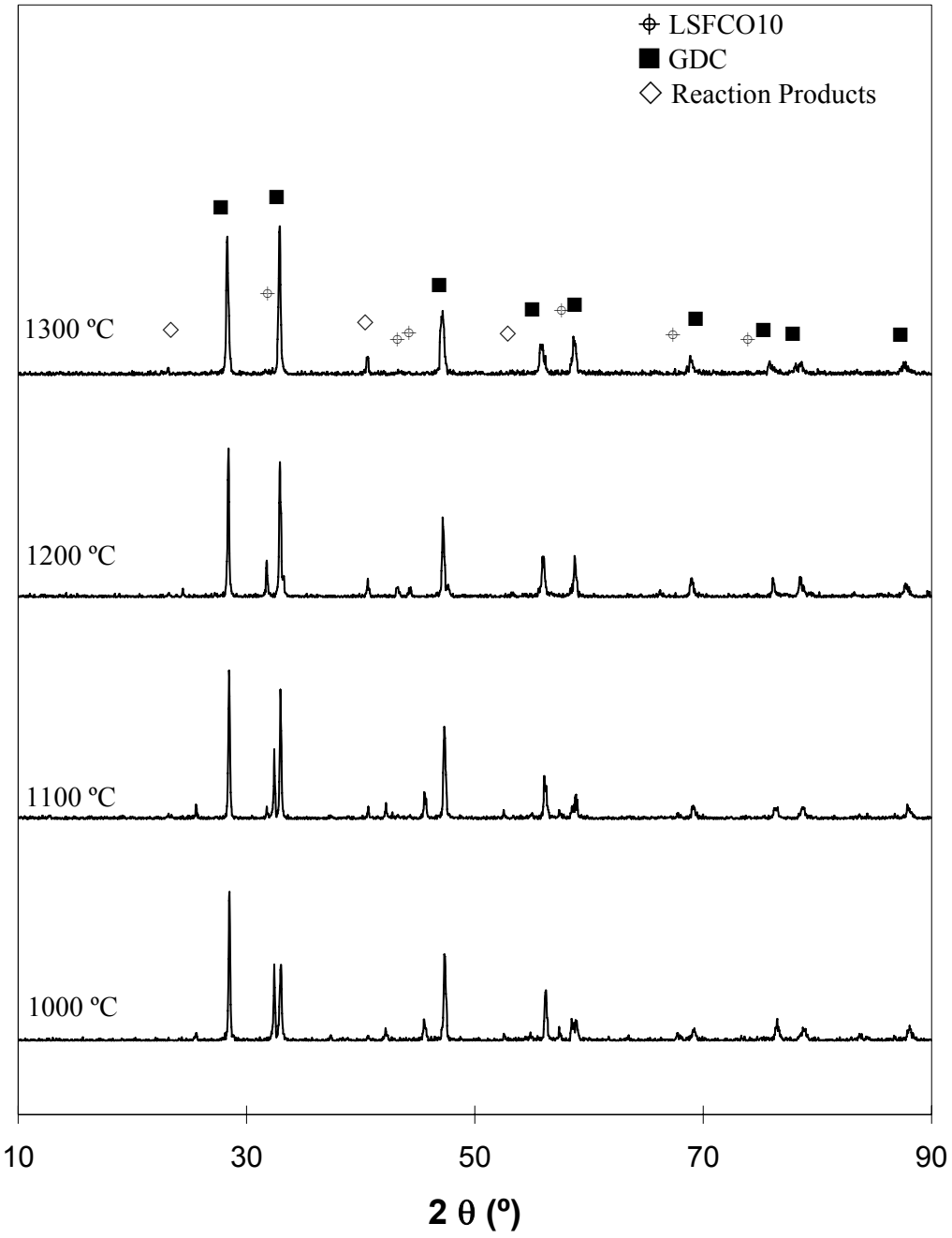

Figure 4.6. Reactivity test for LSFCO10 and GDC.

The electrochemical evaluation of the cells was performed according to the procedures described in Chapter 2. I-V traces and power density curves of individual specimens can be found in Appendix C. The average maximum power densities for each composition are shown in Table 4.1. The values listed for LSCF1000 perovskite cathode correspond to the cells with $La_{0.6}Sr_{0.4}Co_{0.5}Fe_{0.5}O_3$ cathodes fired at 1000 ºC as discussed in Chapter 3. Data collected from electrochemical testing of representative cells are shown in Figures 4.7 and 4.8. Electrochemical performance of LSCF1000 from Chapter 3 is presented in Figure 4.9 to facilitate comparisons to intergrowth compounds.

Table 4.1 Maximum power densities (W/cm^2) obtained at operating temperatures of 600 ºC – 800 ºC, for IT-SOFC using $(La,Sr)_{n+1}(Fe,Co)_nO_{3n+1}$ cathodes.

Cathode	n	800 ºC	700 ºC	600 ºC
SLFCO7	2	0.372	0.150	0.045
LSCFO10	3	0.739	0.338	0.101
LSCF1000	∞	0.378	0.159	0.045

It can be seen in Table 4.1 that the performance for SLFCO7 and LSCF1000 cathodes are similar, although a comparison of the power density vs. current density curves (Figures 3.11 and 4.7) show that the maximum power density values are achieved at lower current densities with SLFCO7 cathodes.

The maximum power density of cells is doubled when using LSFCO10 cathodes compared to SLFCO7 or LSCF1000. Figure 4.8 shows the electrochemical performance of such cells.

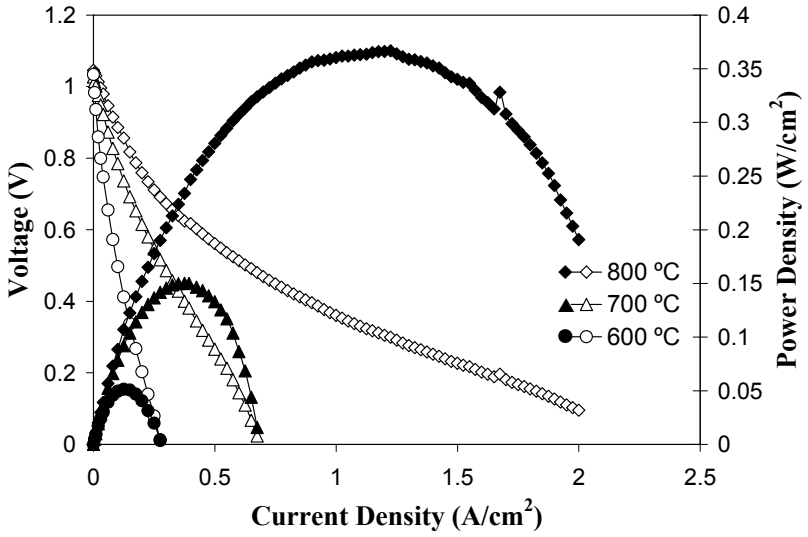

Figure 4.7. I-V curves (open symbols) and power densities (closed symbols) of IT-SOFC with SLFCO7 cathodes.

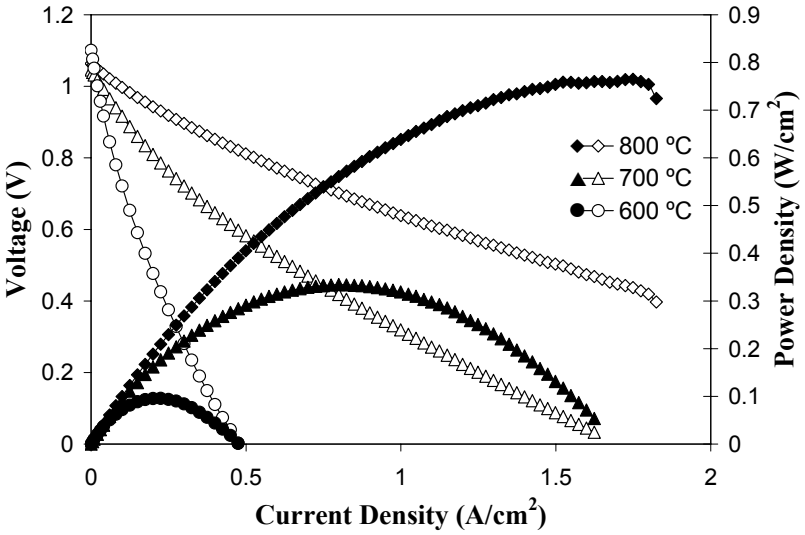

Figure 4.8. I-V curves (open symbols) and power densities (closed symbols) of IT-SOFC with LSFCO10 cathodes.

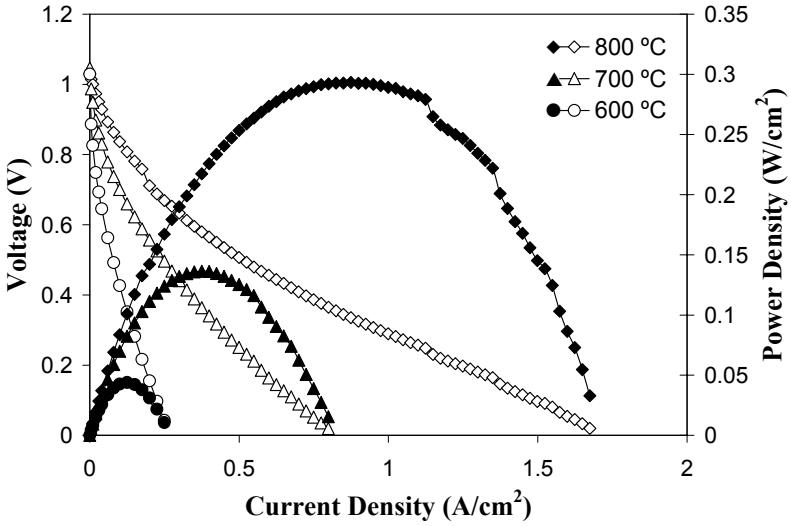

Figure 4.9. I-V curves (open symbols) and power densities (closed symbols) of IT-SOFC with LSCF1000 cathodes. (same as Figure 3.12)

4.4 DISCUSSION

The values of maximum power densities of cells with $(La,Sr)_{n+1}(Fe,Co)_nO_{3n+1}$ cathodes do not follow the trend of the conductivity values for these compositions (see Appendix B). In this series, the highest conductivity values correspond to LSCF1000, followed by much lower values for LSFCO10 and SLFCO7. These conductivities are consistent with the fact that when $n = \infty$ (LSCF1000) the conductivity is isotropic in the material, whereas for lower values of n, the electronic transport along the z-axis is lower than that along the x- and y- directions. However, a closer look to the initial slopes of average I-V traces (Figures 4.10, 4.11 and 4.12), show a slightly larger decay for SLFCO7 than for LSCF1000 and both of them are much steeper than that of LSFCO10. This is related to a higher activation polarization for LSCF1000, followed by SLFCO7, than for LSFCO10.

There are at least two possible reasons for the lower activation polarization for LSFCO10: a) greater catalytic activity and b) more reaction sites. The first cause is related to the chemistry of the compound and the second cause is related to the microstructure. Since all the materials were fired at the same temperature, it is not likely that there should be larger differences in the microstructures which could suggest that the LSFCO10 is more catalytically active than the other two compounds.[67,68]

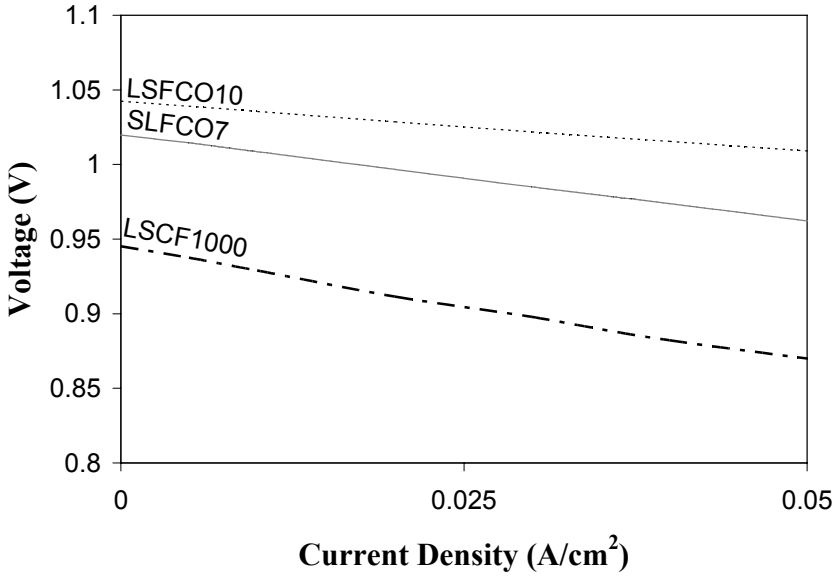

Figure 4.10. Comparison of average I-V traces at low current densities at 800 ºC.

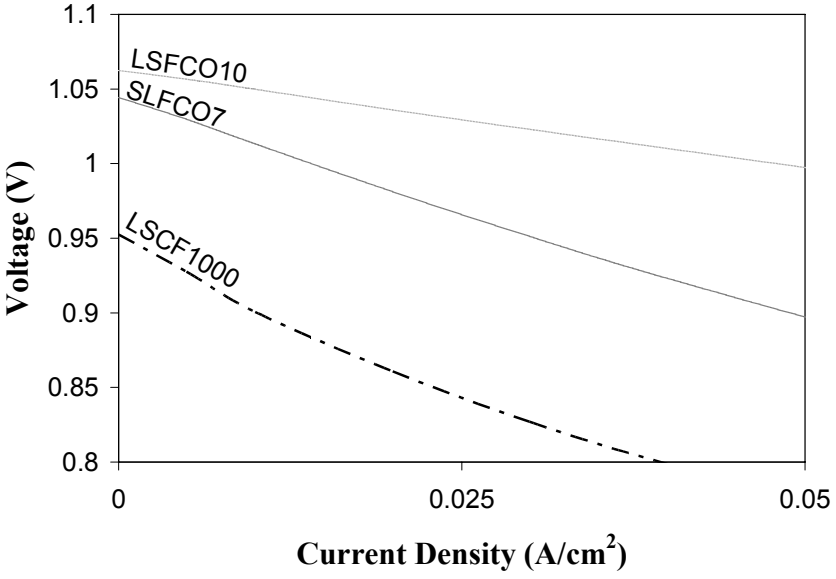

Figure 4.11. Comparison of average I-V traces at low current densities at 700 ºC.

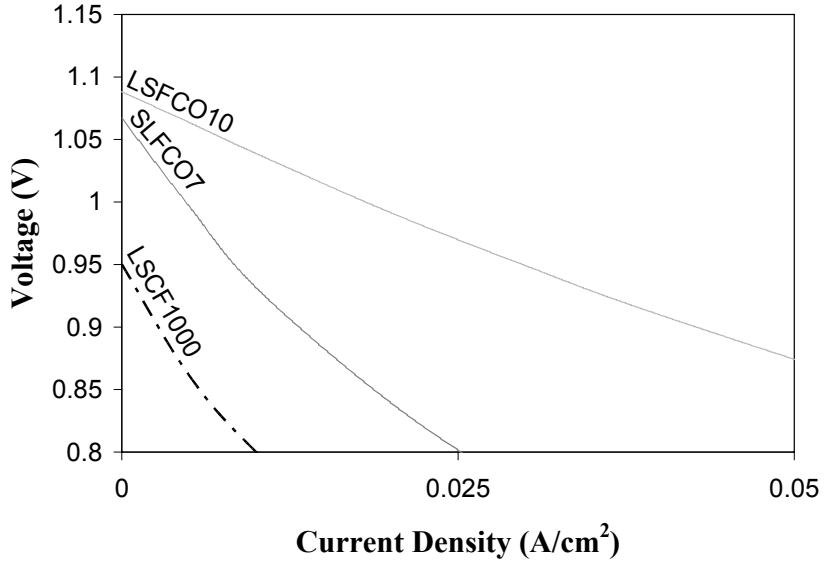

Figure 4.12. Comparison of average I-V traces at low current densities at 600 ºC.

Figure 4.13 shows SEM of the cross-section of fracture surfaces of representative untested IT-SOFC. From these micrographs it is apparent that the electrolyte is gastight and there is good adhesion between the electrolyte and the anode and GDC interlayer. The interlayer is 5-7 μm thick and the thickness of the cathode layer is 15-17 μm. Both the anode and cathode exhibit sufficient porosity to ensure that gas flow can occur through the electrodes. In the left image of Figure 4.12 some delamination is apparent between the SLFCO7 cathode and the GDC interlayer; this delamination likely occurred during fracturing to produce the micrograph rather than during specimen preparation. Increasing the firing temperature during the last step in processing would improve the adhesion of the cathode but higher firing temperatures

lead to reactions at the interface between GDC and SLFCO7, and possible coarsening, which affect the cell performance in a negative way. The poor adhesion between the SLFCO7 cathode and the interlayer make difficult to confirm the effect of the activation polarization in the value of maximum power density, as this is also the cathode composition that presents the lowest conductivity (See Appendix B). The better structural stability of LSFCO10 may also contribute to the higher performance, but this would also be most apparent at moderate currents since delamination would most likely affect the ohmic polarization.

4.5 CONCLUSIONS

SLFCO7 and LSFCO10 are attractive cathode materials for IT-SOFC because they exhibit adequate conductivity. Despite having conductivity values lower than the perovskite material LSCF, their performance in cells using thin YSZ electrolytes and GDC interlayers is comparable (in the case of SLFCO7) or superior (with LSFCO10) than using LSCF. LSFCO10 appears particularly promising for long term testing at intermediate temperatures, given the excellent performance it shows in this and other studies.[47,69]

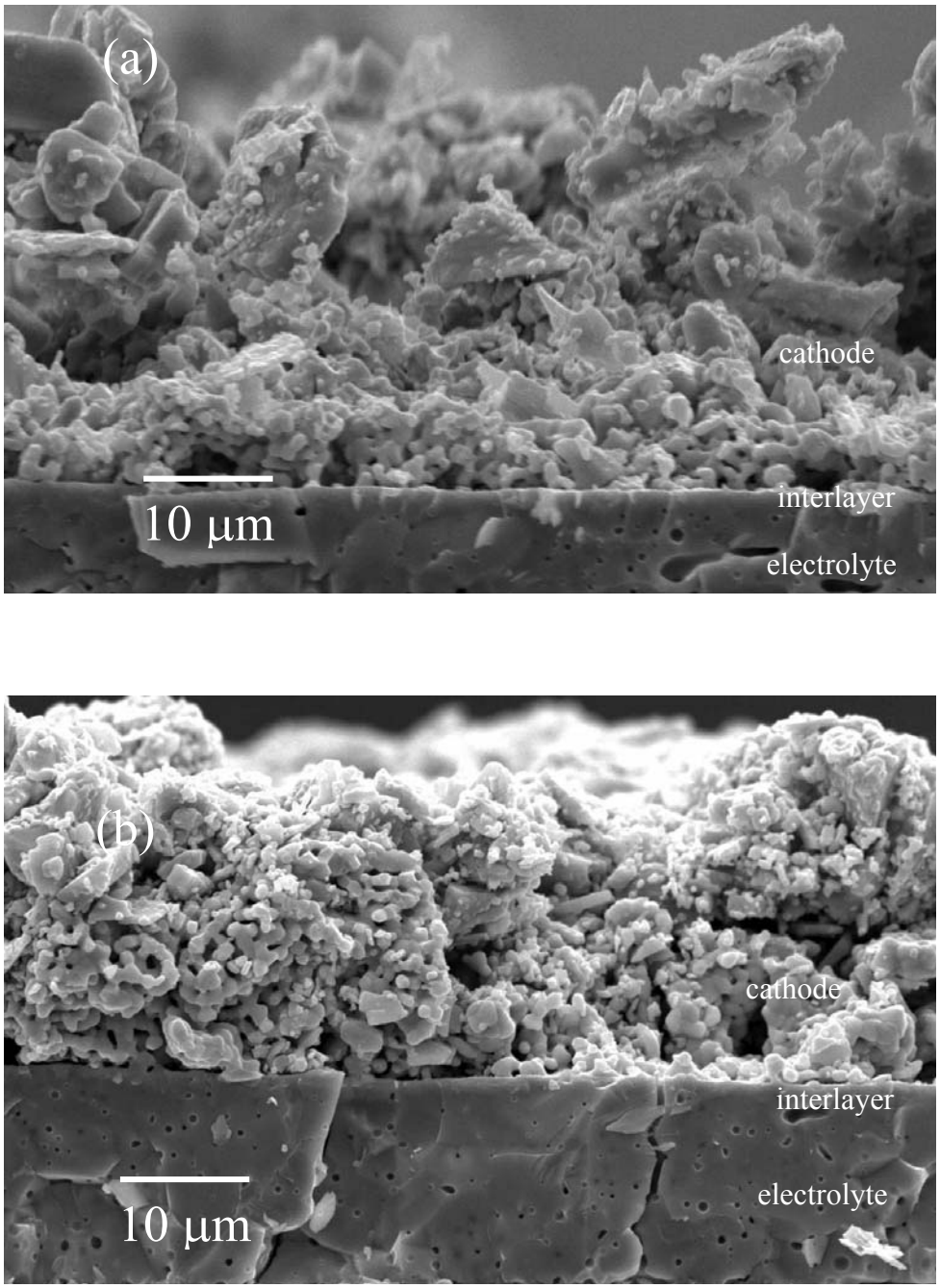

Figure 4.13. SEM of IT-SOFC with SLFCO7 (a) and LSFCO10 (b) cathodes.

Chapter 5: Summary

The increase in the demand for economically available alternative sources of energy has driven the study of SOFC. YSZ has been the preferred electrolyte material for SOFC, but at intermediate temperatures the ionic conductivity of YSZ decreases. Reducing the thickness of the electrolyte allows for a conductance similar to that of thick YSZ electrolytes at elevated temperatures. The production of SOFC with thin YSZ electrolytes has been studied previously, but many of the methods involve complicated steps or suffer from high equipment costs. This work has demonstrated the feasibility of producing SOFC with thin YSZ electrolytes by inexpensive ceramic techniques. The importance of the steps and parameters used during tape casting and co-firing has been evident during this process. The manufacturing process proposed can be easily adapted to an industrial level, where automated processes could help to minimize variances in the final product.

Along with thin YSZ electrolytes, cathodes that exhibit adequate catalytic activity at intermediate temperatures are important for good performance of IT-SOFC. Perovskite materials, like $(La,Sr)(Co,Fe)O_3$ (LSCF) were investigated as cathodes. The effect of cathode sintering temperature was studied, and it was found that at higher sintering temperatures the cathodes exhibited some coarsening, which reduces the number of active sites and increases activation polarization. However, a very low temperature may inhibit the adherence of the cathode to the interlayer, resulting in high

contact resistance. Therefore, it is important to determine the optimal cathode sintering temperature.

Materials with lower TEC are required for IT-SOFC so that they can survive long-term operation, even with multiple thermal cycles. Substitution of Nd by La decreases the TEC due to the more covalent Nd-O bonds, but also decreases the conductivity of the material. The presence of Fe in the B sites contributes to further decrease in TEC and conductivity. Impregnation with a noble metal, like silver, helps to increase the conductivity while retaining a low TEC. The performance of neodymium cobaltites was in general lower than that of cells with lanthanum cobaltites. From these, NSC cathodes showed better performance than NSCF cathodes, although silver impregnation helped to improve the performance of NSCF.

Some intergrowth perovskite oxide cathodes from the Ruddlesden-Popper series $(La,Sr)_{n+1}(Fe,Co)_nO_{3n+1}$, the n = 2 (SLFCO7) and 3 (LSFCO10) members, have been studied as cathode materials for intermediate temperatures given their high oxide ion conductivity and structural stability. Testing of our cells with cathode material SLFCO7 resulted in power density values similar to that of cells with LSFC fired at the same temperature, but LSFCO10 cathode material resulted in power density values twice as large as that of cells with SLFCO7, which is an unexpected result. It was postulated that the reason for the enhanced performance of LSFC10 could be higher catalytic activity.

This work presents further research opportunities. It could be of interest to study how the performance of the cells can be explored as a function of the mechanical

stability and variations in the cathode compositions. In the exploratory work for the present study, cells with anodes made out of two layers of tape cast material were made, but they were too fragile for testing. Subsequent studies can be made on IT-SOFC with different anode (3, 4, 5 layers of tape cast material) and cathode thickness and to learn how this can affect the electrochemical performance of the cell.

In addition, there are a whole variety of compositions that are catalytically active at intermediate temperatures and that can be studied as cathode materials, as well as different materials to be used as interlayers. Since the electrochemical performance of IT-SOFC is highly affected by the microstructure of their components, it would be interesting in particular to examine how different processing routes affect the final performance of cathode materials. Impregnating cathodes with low TEC, such as LSFCO10 with silver would also be interesting to see if further enhancement in performance is possible. Lastly, long term testing is needed to fully appreciate the effect of cathode materials with lower TEC on the performance of IT-SOFC.

Appendix A: Preparation of Anode/Electrolyte assemblies for co-firing

After the tape cast electrolyte and anode material were dried separately, the following steps were taken to obtain flat, cracks-free, anode and electrolyte assemblies after co-firing.

1. Punching: Six layers of the anode material and one disc of the electrolyte material were used per cell. The punch diameter was 22.2 mm (7/8”). A razor blade was used to cut the discs.

Figure A.1. Punching and anode disc.

Figure A.2. Punched disc (bottom).

2. Removing from the glass substrate: The anode discs were removed from the substrate by peeling off the disc from the substrate with a razor blade. Then, the excess of material surrounding the disc was carefully detached. The electrolyte tapes were easier to handle. The cleanest way to take the electrolyte discs off the glass was to remove first the surrounding material, peel one side of the disc with the razor blade; and pull it off.

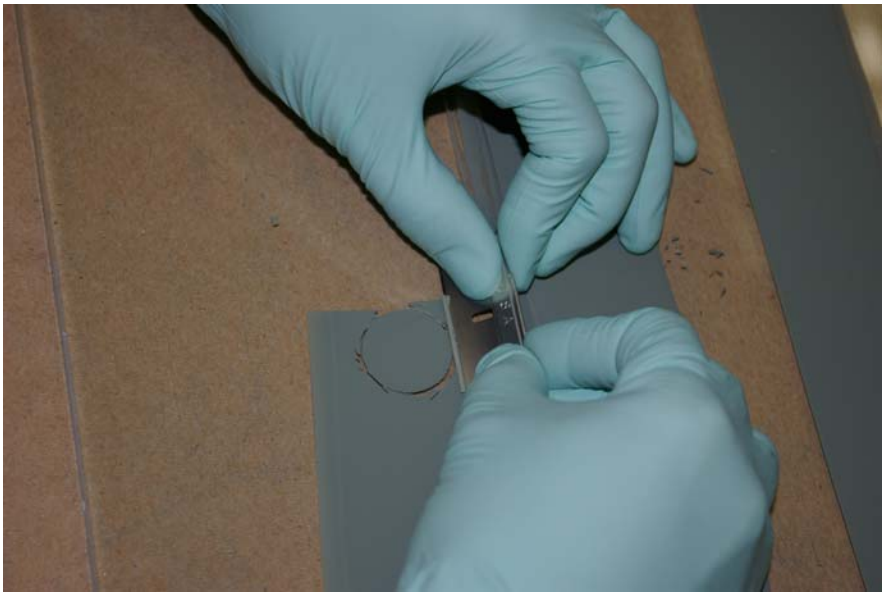

Figure A.3. Removing anode disc and surrounding area from glass substrate.

Figure A.4. Detaching excess material from anode disc.

Figure A.5. Anode disc with side that was in contact with glass up.

Figure A.6. Removing excess material surrounding electrolyte disc.

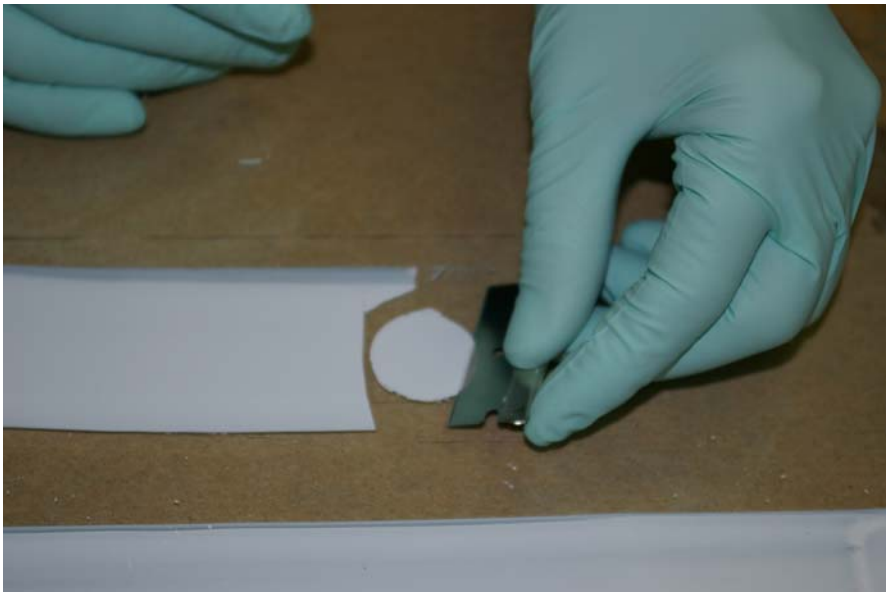

Figure A.7. Removing electrolyte disc from glass substrate.

3. Stacking the assemblies: Six anode discs were stacked up followed by one electrolyte disc. The side of the electrolyte disc that was in contact with the glass substrate was placed on the same side as the anode disc. The stack was covered with non-stick, coated, ultra-heavy duty barbecue aluminum foil (All-Foils, Inc.).

Figure A.8. Anode disks stacked on aluminum foil.

Figure A.9. Electrolyte disk on top of anode disks.

4. Hot lamination: Four anode/electrolyte (A/E) assemblies were laminated simultaneously in a manual 12 ton force Spectropress® at 85 ºC for 10 minutes. The applied force was 3 tons (19.3 MPa / assembly). The assemblies were placed between ¼" thick polycarbonate plates to protect them during lamination. After cooling for several hours, the aluminum foil was easily removed from the anode side first. Special care was taken when removing the foil from the anode side, as some delamination can occur, particularly at the edges.

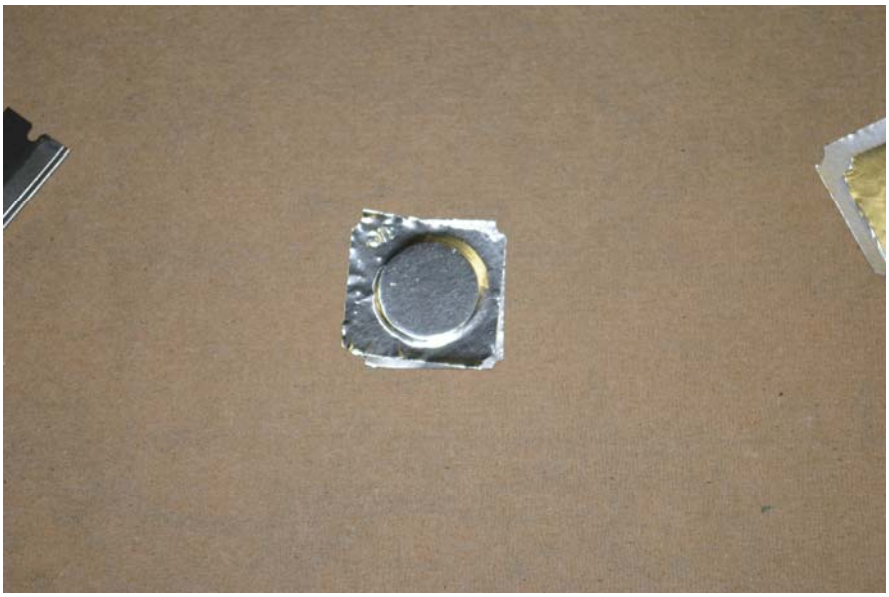

Figure A.10. A/E assembly after lamination.

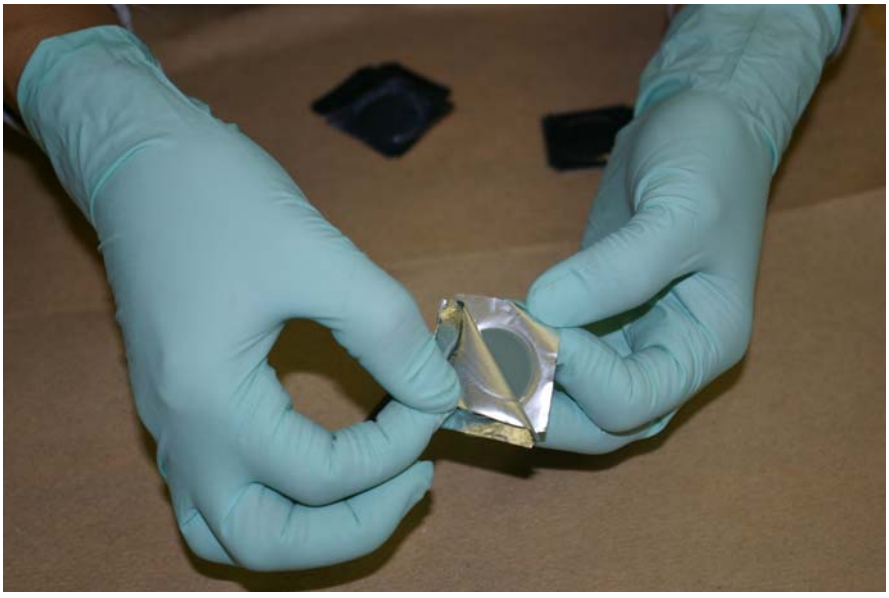

Figure A.11. Removal of the aluminum foil from the anode side.

Figure A.12. Removal of aluminum foil from the electrolyte side.

5. Reshaping the border of the A/E assembly: The A/E assembly contour was trimmed using a razor blade to remove delaminations at the edges of the assembly.

Figure A.13. A/E assembly after hot lamination.

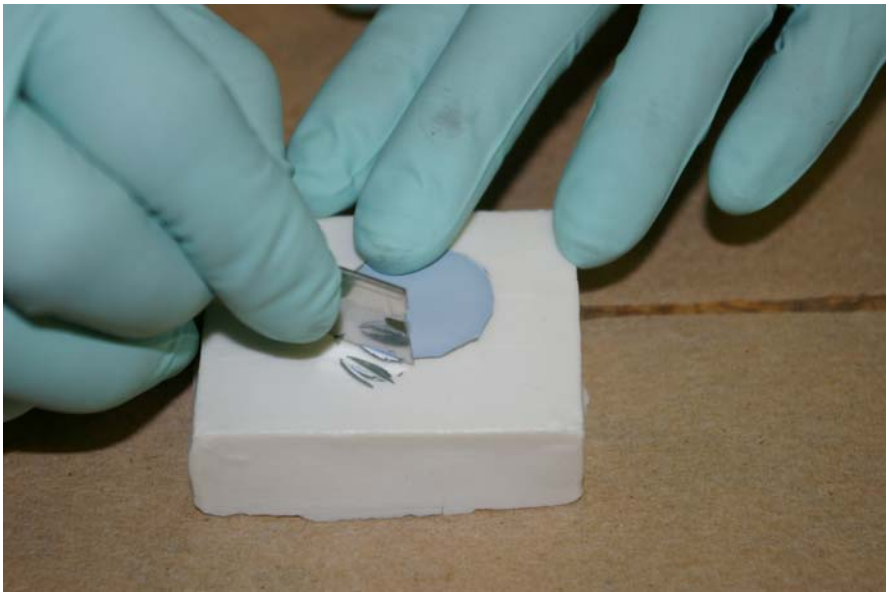

Figure A.14. Edge trimming.

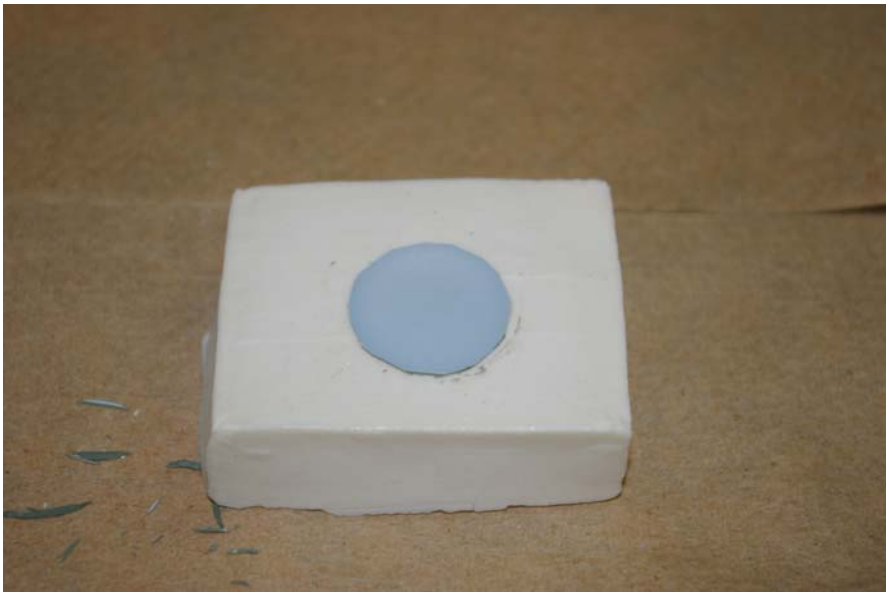

Figure A.15. A/E assembly ready to be co-fired.

6. Setting A/E assembly up for co-firing:

    a. The A/E assemblies were fired on a ground alumina plate. To facilitate the handling when transferring between furnaces, the alumina plate was placed in a crucible; coarsened-alumina powder helped to keep the alumina plate in place in the crucible. A layer of 3 wt% mol yttria-stabilized zirconia (3YSZ) previously coarsened at 1500 ºC was deposited on top of the alumina plate and compressed. This powder layer prevented the A/E assembly from chemically reacting or sticking to the alumina plates.[71]

Figure A.16. Depositing coarsen YSZ.

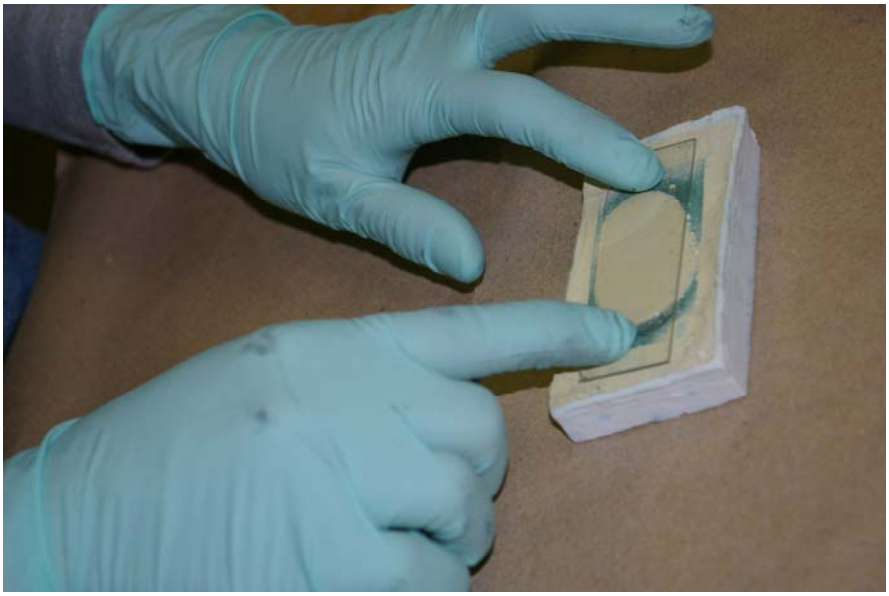

Figure A.17. Flattening coarsen YSZ out on alumina plate.

b. Graphite powder was used to prevent the coarsened YSZ powder from sticking to the A/E assembly during co-firing. Additionally, the graphite powder permitted the planar displacements of the assembly upon shrinking. The A/E assembly was coated with graphite powder and slightly compressed between glass slides before being carefully placed on the coarsened YSZ powder bed. The tensile stresses experienced by the anode and compressive stresses by the electrolyte during sintering tended to curl the assembly toward the electrolyte. To avoid deformations and cracking, the anode side of the A/E assembly was placed side up.

Figure A.18. The A/E assembly is covered with graphite.

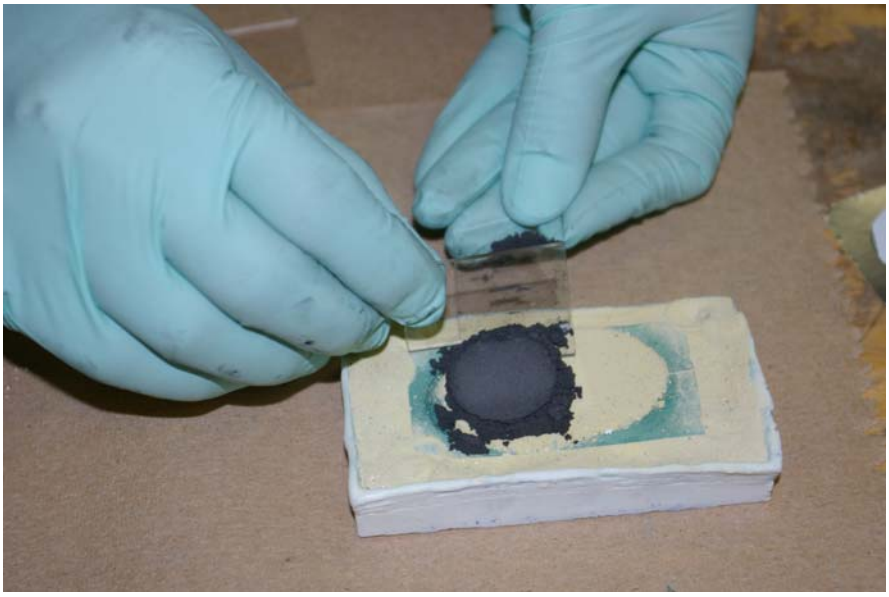

Figure A.19. Placing graphite-covered A/E assembly on coarsen YSZ powder with anode side up.

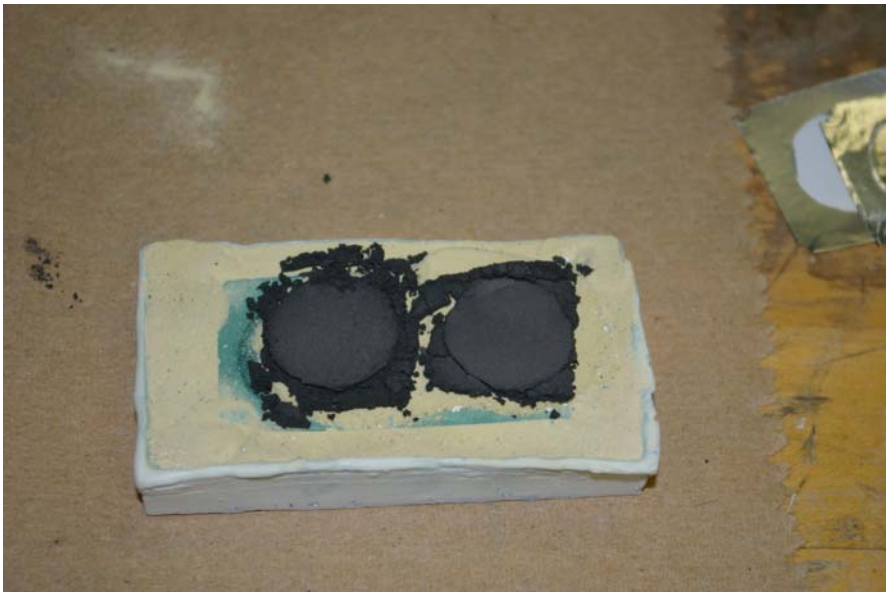

Figure A.20. Two assemblies were fired simultaneously in the same crucible.

c. The A/E assemblies were covered with a layer of coarsened YSZ. This layer was flattened and an alumina plate was placed on top. The specimens were then ready for co-firing.

Figure A.21. The coarsened YSZ layer that covers the cells is flattened.

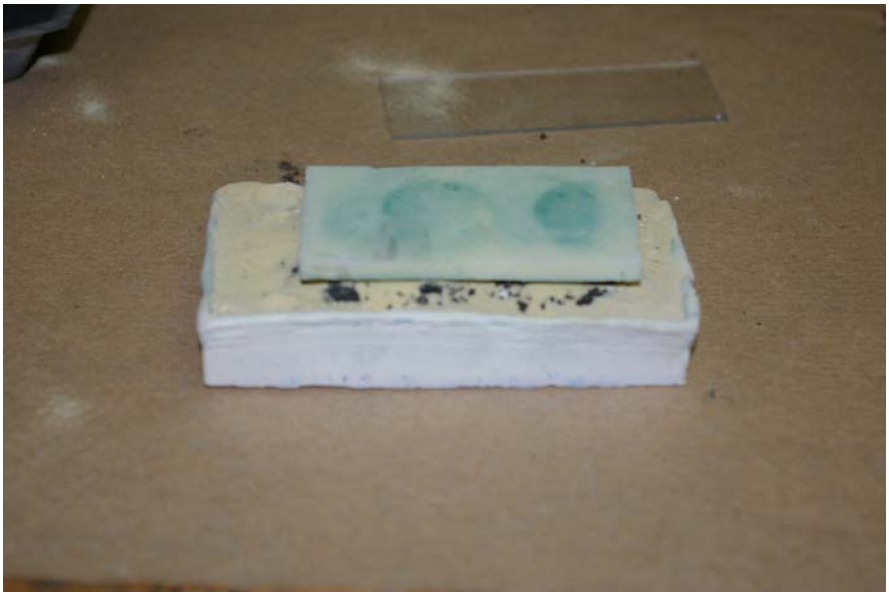

Figure A.22. Alumina plate on top of coarsen YSZ.

7. The co-firing was made in two separate steps. The organics were removed in a tubular furnace. Then, the A/E assemblies were transferred to a box furnace for sintering. At this point the specimens were extremely brittle. An additional mass was placed on top of the crucibles to produce a pressure of about 500 Pa during sintering.
8. A soft plastic spatula can was used to remove any coarsened YSZ that was attached to the specimen after sintering.

Appendix B: Conductivity and Thermal Expansion Coefficients Data

Cathode Material	σ (S/cm)			TEC (10^{-6} ºC^{-1})	Reference
	800 ºC	700 ºC	600 ºC		
LSC	2238	2818	3162	21.3	[61]
LSCF [1]	333		275	17.5	[58]
NSC	1257	1575	1696	18.7	[46,61]
NSCF	363	407	422	16.7	[46]
SLFCO7	54	71	91	21.2	[47]
LSFCO10	148	185	220	20.5	[69]

[1] Data for $La_{0.6}Sr_{0.4}Co_{0.2}Fe_{0.8}O_{3-\delta}$

Appendix C: Electrochemical data of tested cells.

C.1 LSC1000

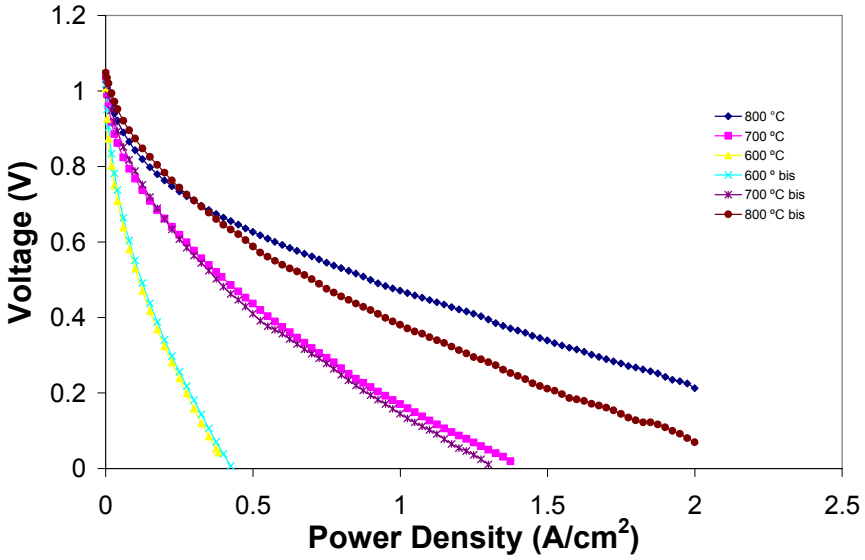

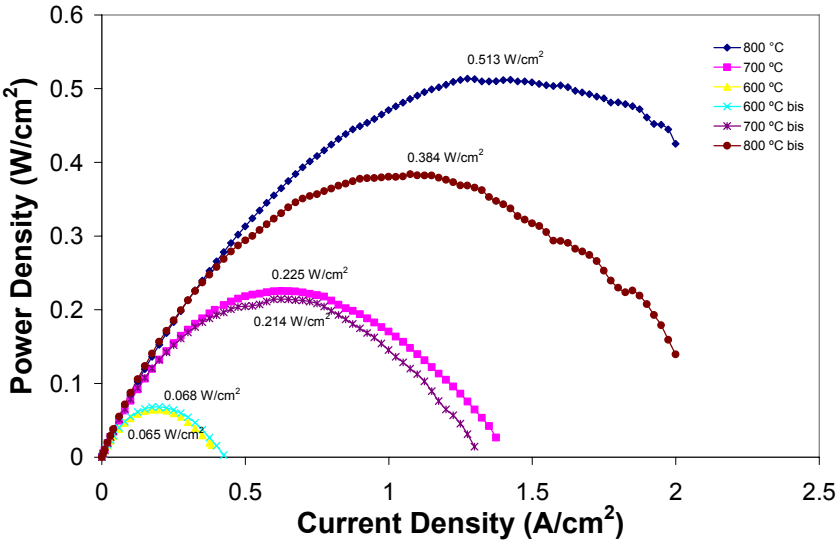

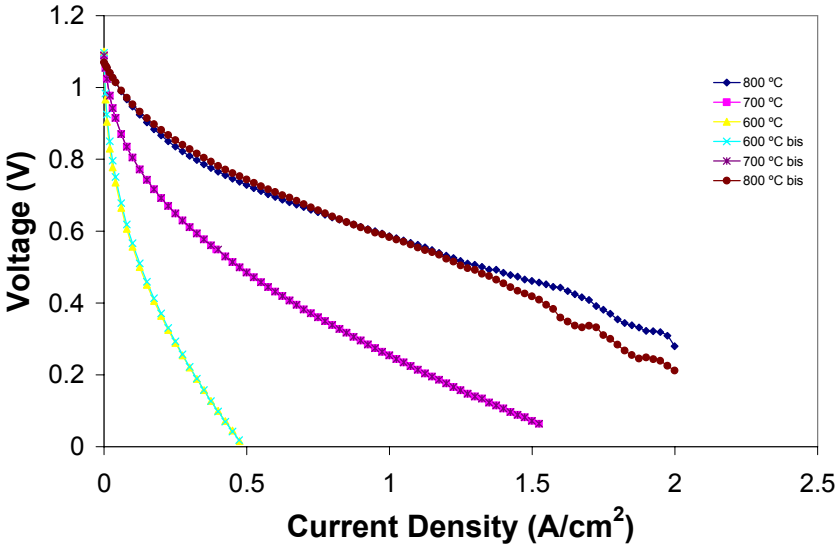
Voltage (V)
Current Density (A/cm2)
800 °C
700 °C
600 °C
600 °C bis
700 °C bis
800 °C bis

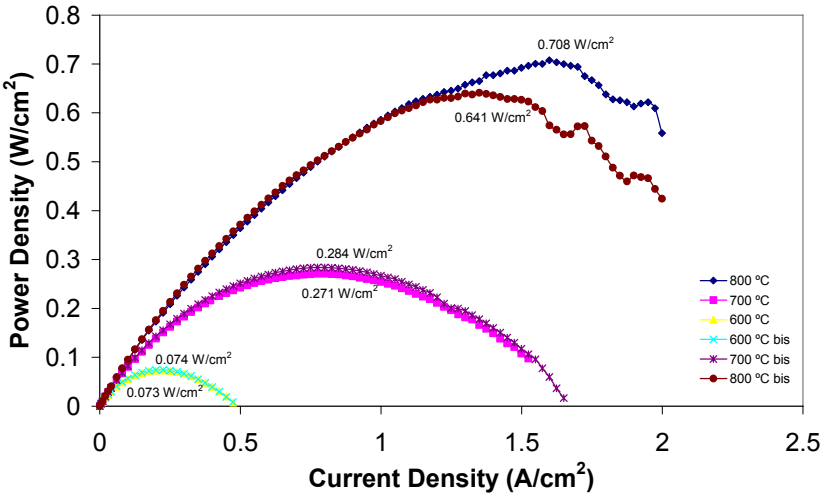
Power Density (W/cm2)
Current Density (A/cm2)
0.708 W/cm2
0.641 W/cm2
0.284 W/cm2
0.271 W/cm2
0.074 W/cm2
0.073 W/cm2
800 °C
700 °C
600 °C
600 °C bis
700 °C bis
800 °C bis

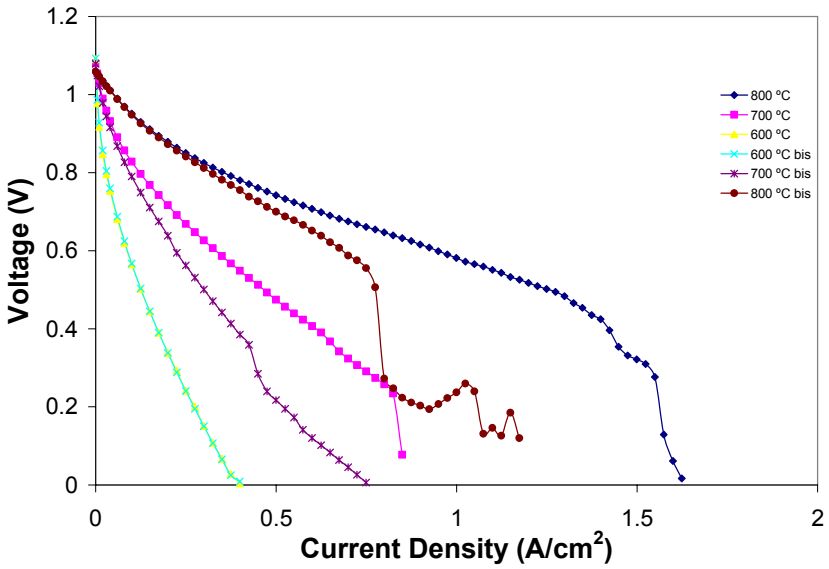
Voltage (V)
Current Density (A/cm²)
800 °C
700 °C
600 °C
600 °C bis
700 °C bis
800 °C bis

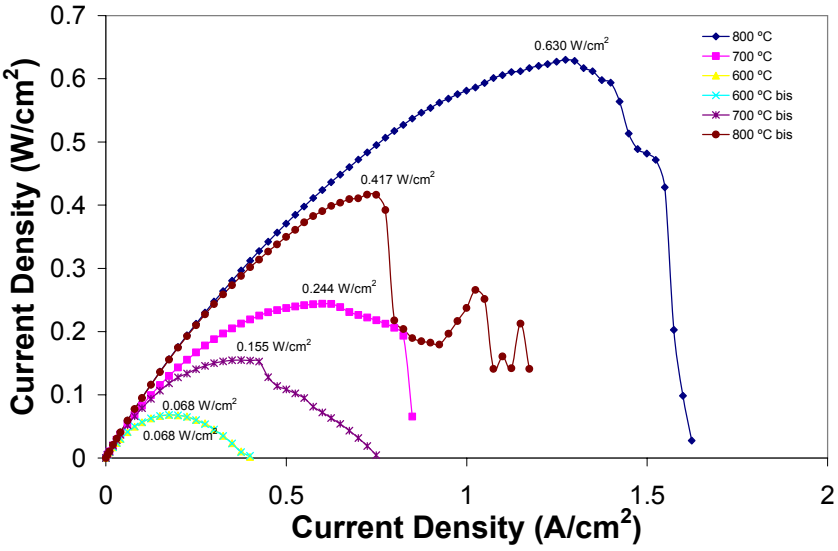
Current Density (W/cm²)
Current Density (A/cm²)
0.630 W/cm²
0.417 W/cm²
0.244 W/cm²
0.155 W/cm²
0.068 W/cm²
0.068 W/cm²
800 °C
700 °C
600 °C
600 °C bis
700 °C bis
800 °C bis

C.2 LSC1100

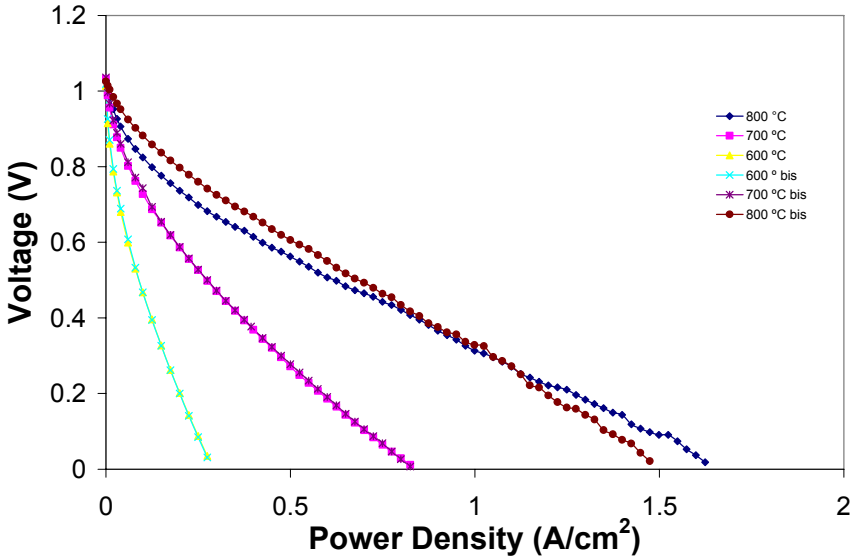
Voltage (V)
Power Density (A/cm2)
800 °C
700 °C
600 °C
600 ° bis
700 °C bis
800 °C bis

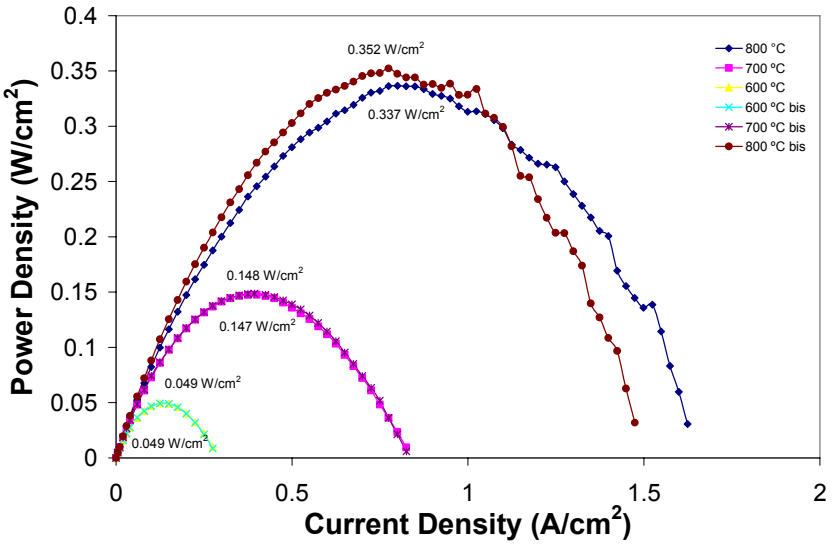
Power Density (W/cm2)
Current Density (A/cm2)
0.352 W/cm2
0.337 W/cm2
0.148 W/cm2
0.147 W/cm2
0.049 W/cm2
0.049 W/cm2
800 °C
700 °C
600 °C
600 °C bis
700 °C bis
800 °C bis

C.3 LSCF1000

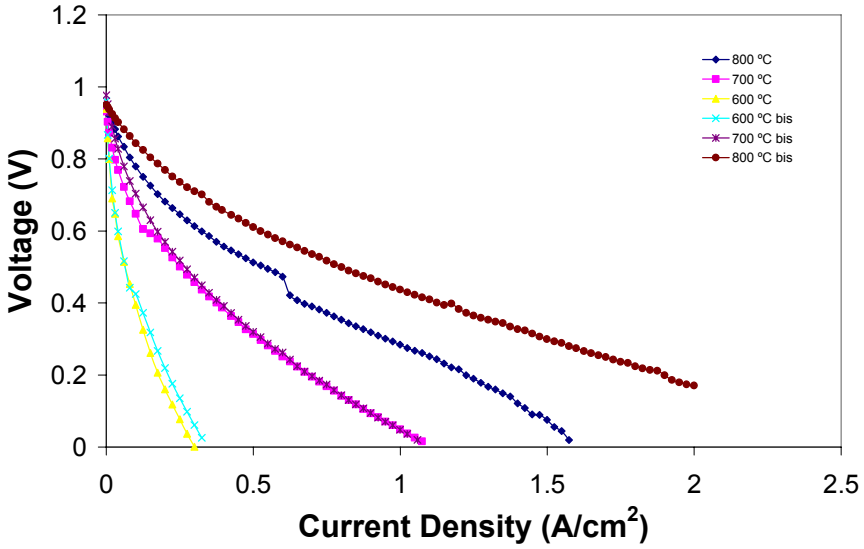
Voltage (V)
Current Density (A/cm2)
800 ºC
700 ºC
600 ºC
600 ºC bis
700 ºC bis
800 ºC bis

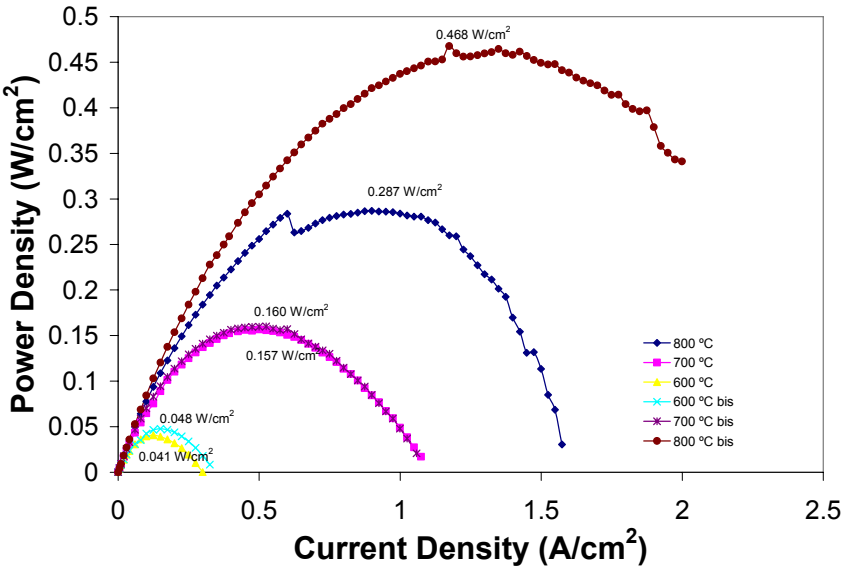
Power Density (W/cm2)
Current Density (A/cm2)
0.468 W/cm2
0.287 W/cm2
0.160 W/cm2
0.157 W/cm2
0.048 W/cm2
0.041 W/cm2
800 ºC
700 ºC
600 ºC
600 ºC bis
700 ºC bis
800 ºC bis

C.4 LSCF1100

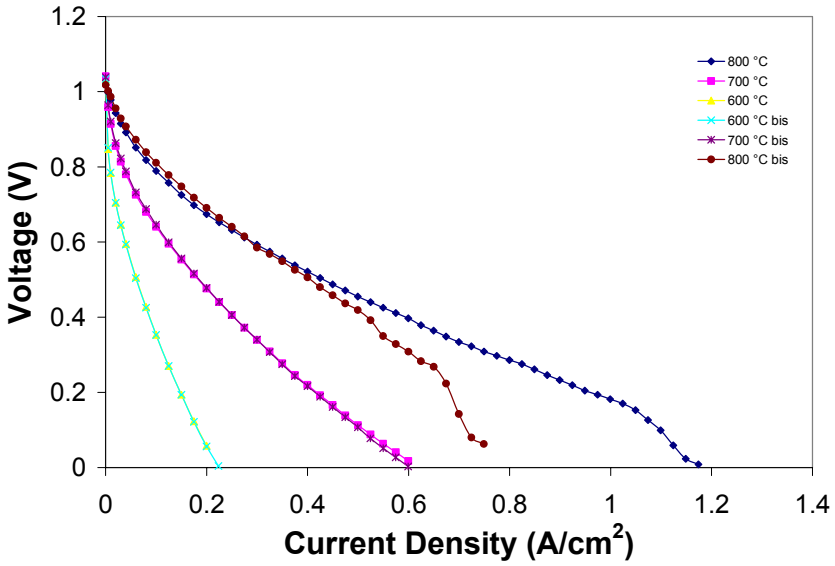
Voltage (V)
Current Density (A/cm2)
800 °C
700 °C
600 °C
600 °C bis
700 °C bis
800 °C bis

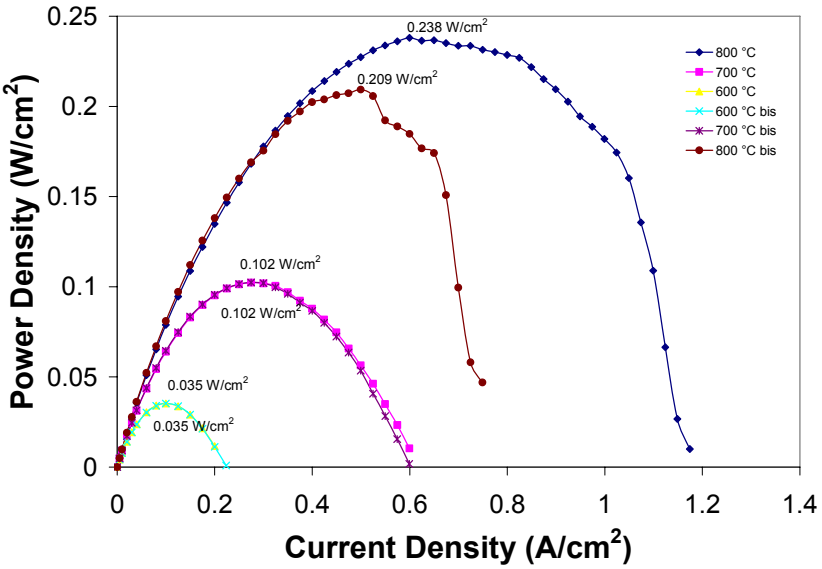
Power Density (W/cm2)
Current Density (A/cm2)
0.238 W/cm2
0.209 W/cm2
0.102 W/cm2
0.102 W/cm2
0.035 W/cm2
0.035 W/cm2
800 °C
700 °C
600 °C
600 °C bis
700 °C bis
800 °C bis

C.5 NSC

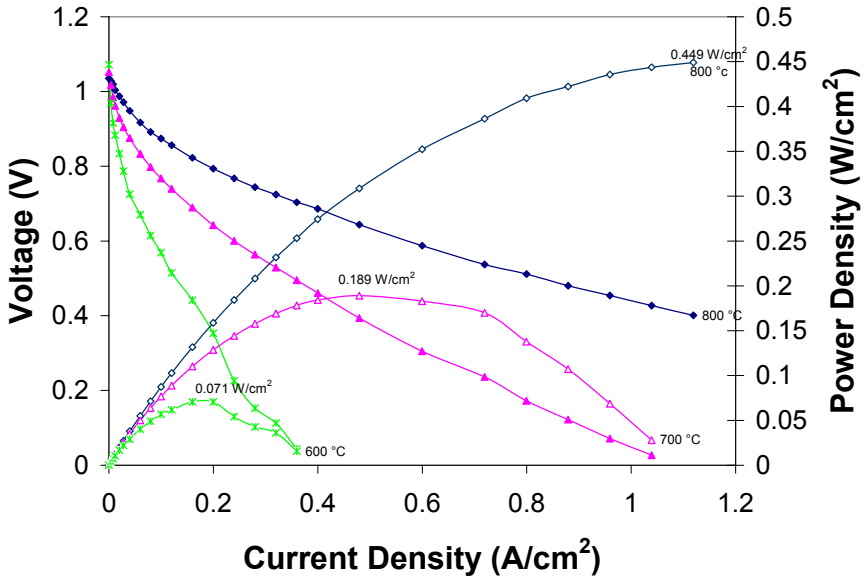
Voltage (V)
Power Density (W/cm2)
Current Density (A/cm2)
0.449 W/cm2
800 °c
0.189 W/cm2
800 °C
0.071 W/cm2
700 °C
600 °C

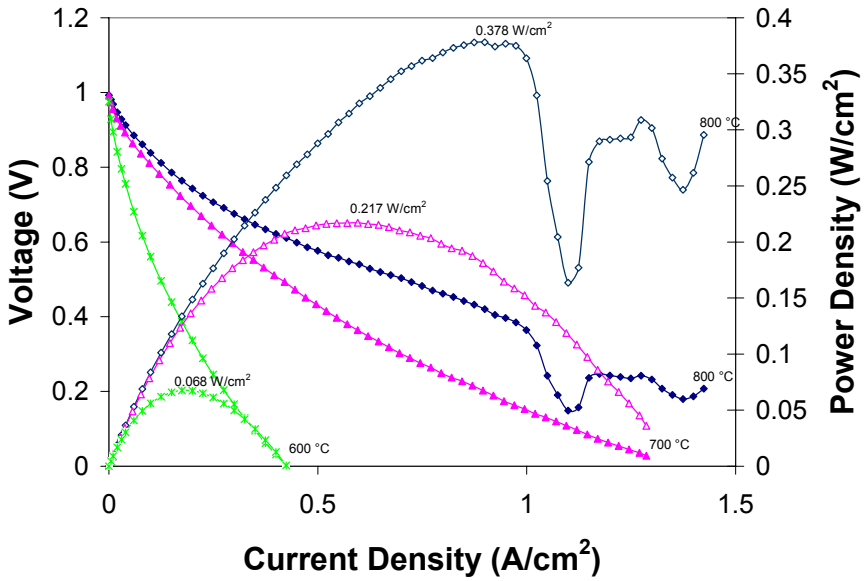
Voltage (V)
Power Density (W/cm2)
Current Density (A/cm2)
0.378 W/cm2
800 °C
0.217 W/cm2
800 °C
0.068 W/cm2
700 °C
600 °C

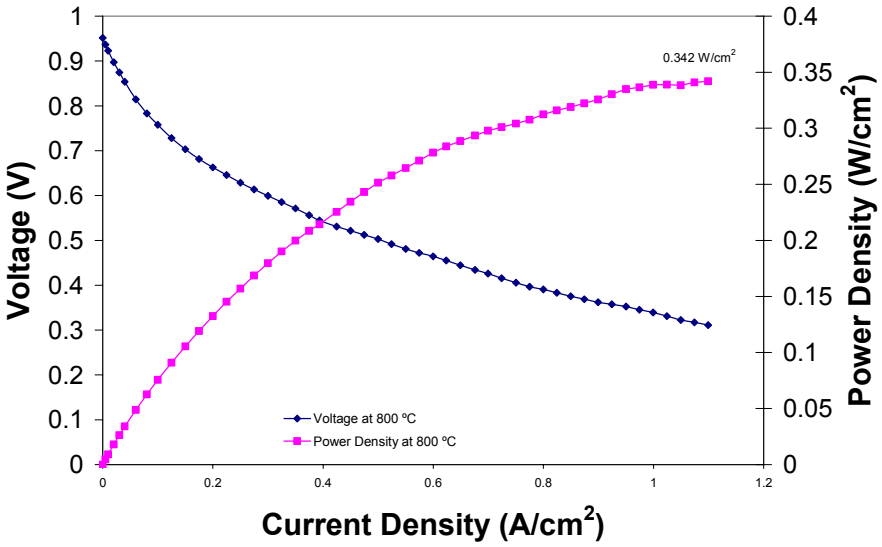
Voltage (V)
Power Density (W/cm2)
Current Density (A/cm2)
0.342 W/cm2
Voltage at 800 ºC
Power Density at 800 ºC

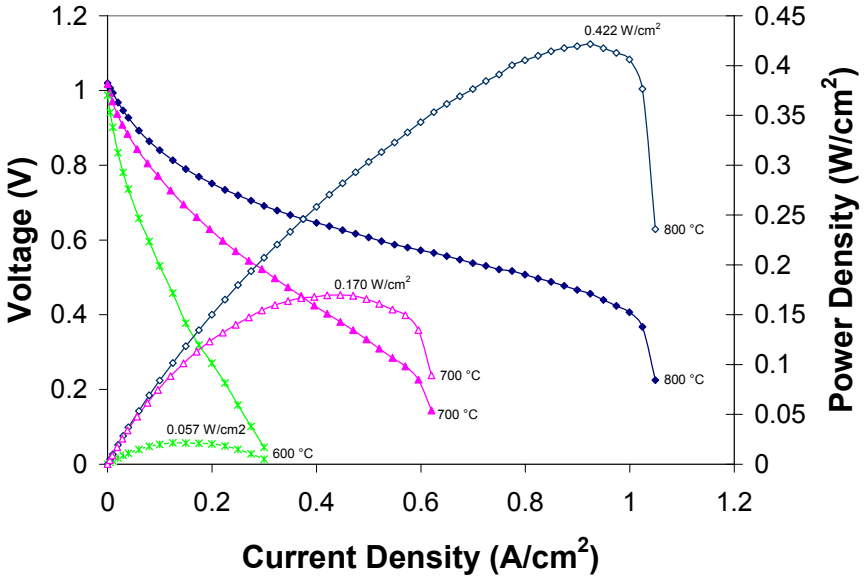
Voltage (V)
Power Density (W/cm2)
Current Density (A/cm2)
0.422 W/cm2
0.170 W/cm2
0.057 W/cm2
800 °C
800 °C
700 °C
700 °C
600 °C

C.6 NSCF

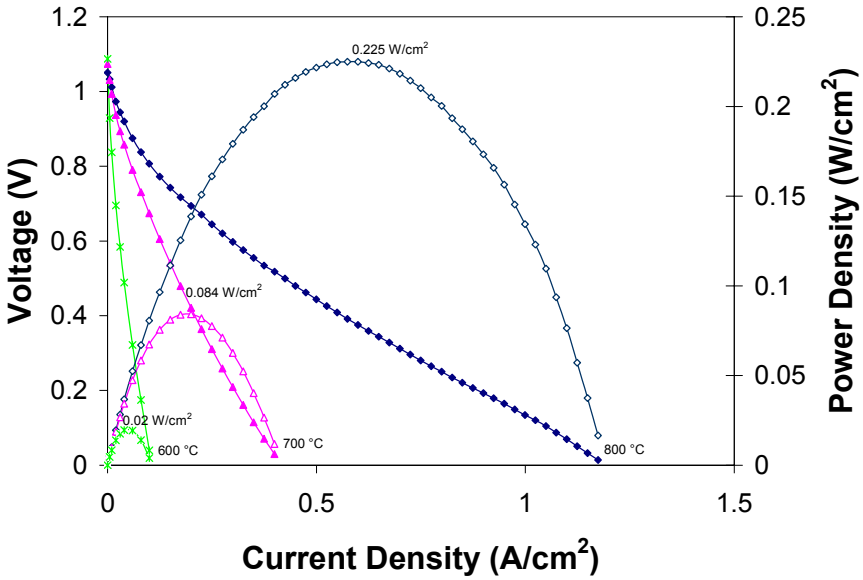
0.225 W/cm2
0.084 W/cm2
0.02 W/cm2
600 °C
700 °C
800 °C
Voltage (V)
Power Density (W/cm2)
Current Density (A/cm2)

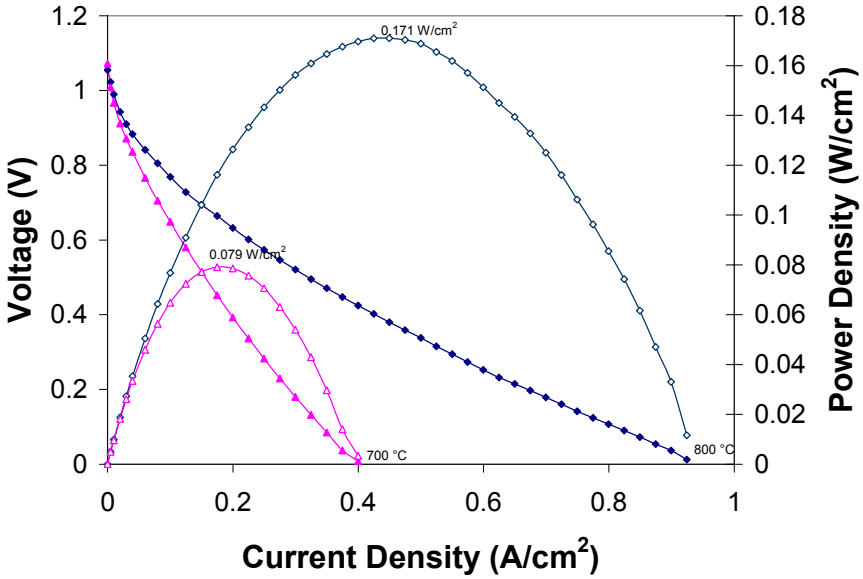
0.171 W/cm2
0.079 W/cm2
700 °C
800 °C
Voltage (V)
Power Density (W/cm2)
Current Density (A/cm2)

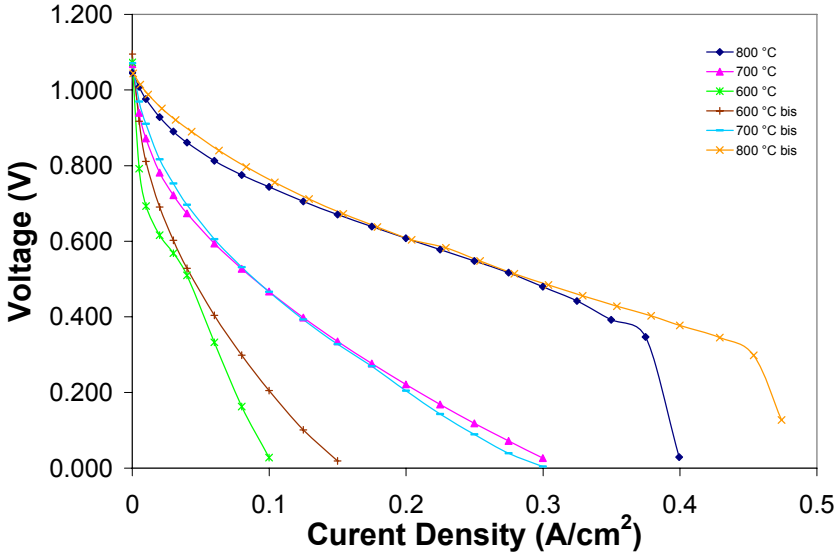
1.200
1.000
0.800
0.600
0.400
0.200
0.000
Voltage (V)
0
0.1
0.2
0.3
0.4
0.5
Curent Density (A/cm2)
800 °C
700 °C
600 °C
600 °C bis
700 °C bis
800 °C bis

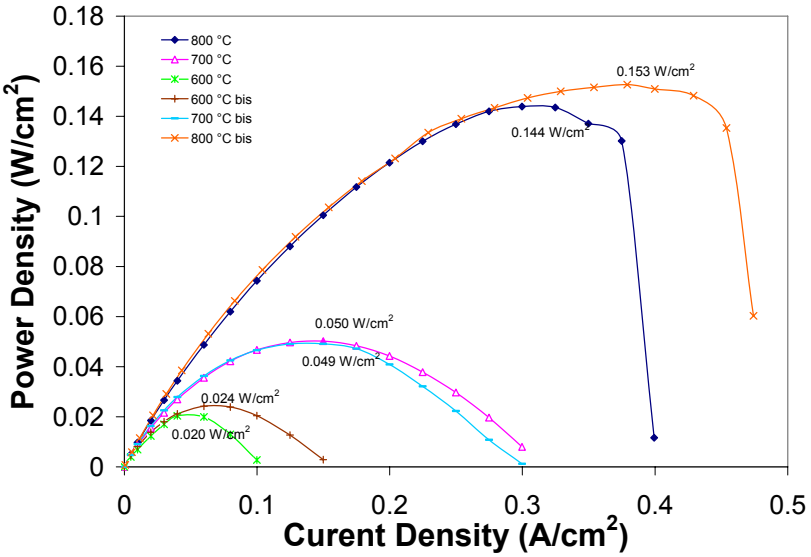
0.18
0.16
0.14
0.12
0.1
0.08
0.06
0.04
0.02
0
Power Density (W/cm2)
0
0.1
0.2
0.3
0.4
0.5
Curent Density (A/cm2)
800 °C
700 °C
600 °C
600 °C bis
700 °C bis
800 °C bis
0.153 W/cm2
0.144 W/cm2
0.050 W/cm2
0.049 W/cm2
0.024 W/cm2
0.020 W/cm2

C7 NSCF-AG

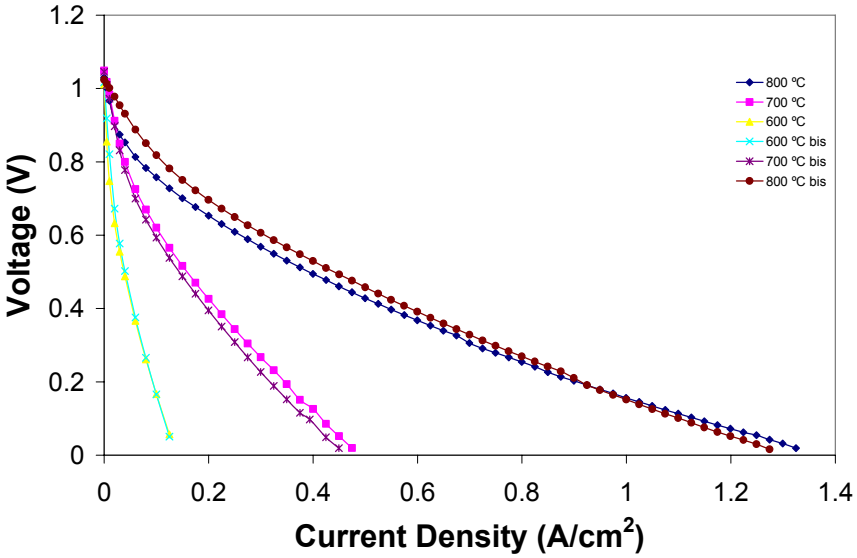
Voltage (V)
Current Density (A/cm2)
800 ºC
700 ºC
600 ºC
600 ºC bis
700 ºC bis
800 ºC bis

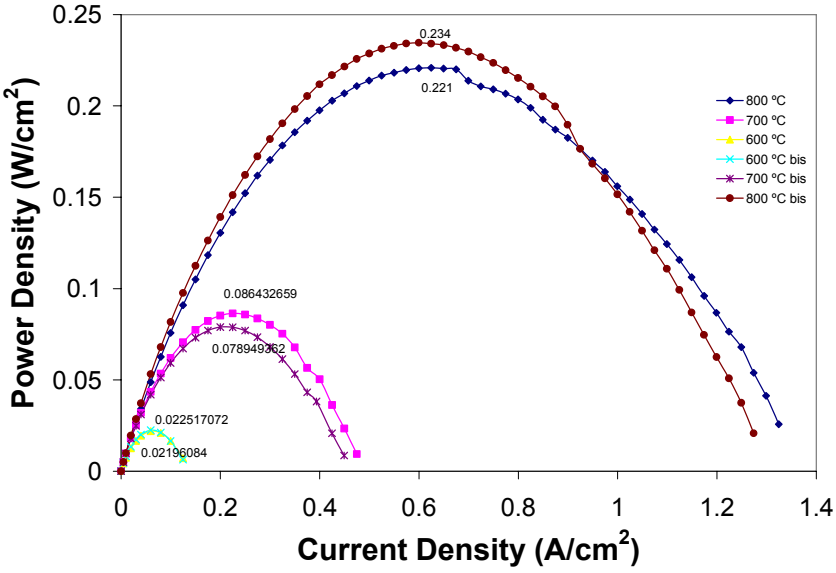
Power Density (W/cm2)
Current Density (A/cm2)
0.234
0.221
0.086432659
0.078949362
0.022517072
0.02196084
800 ºC
700 ºC
600 ºC
600 ºC bis
700 ºC bis
800 ºC bis

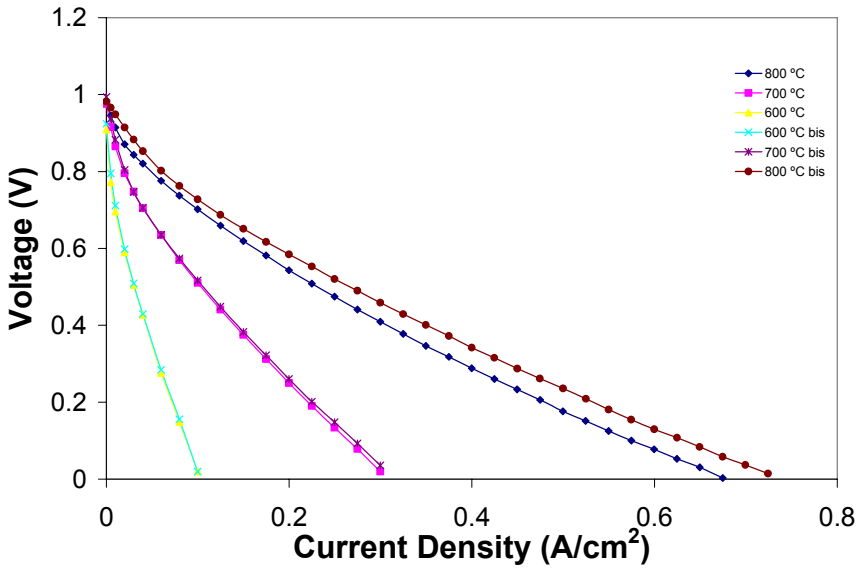
Voltage (V)
Current Density (A/cm2)
800 ºC
700 ºC
600 ºC
600 ºC bis
700 ºC bis
800 ºC bis

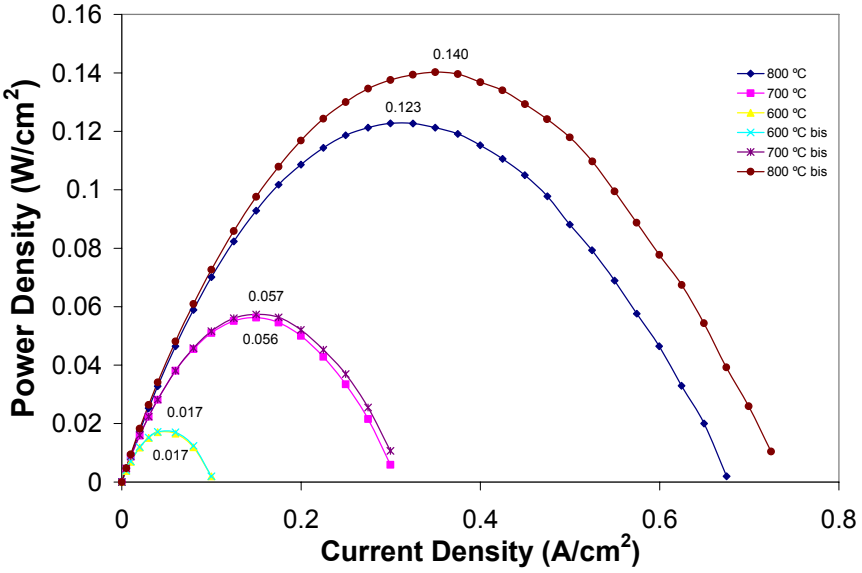
Power Density (W/cm2)
Current Density (A/cm2)
0.140
0.123
0.057
0.056
0.017
0.017
800 ºC
700 ºC
600 ºC
600 ºC bis
700 ºC bis
800 ºC bis

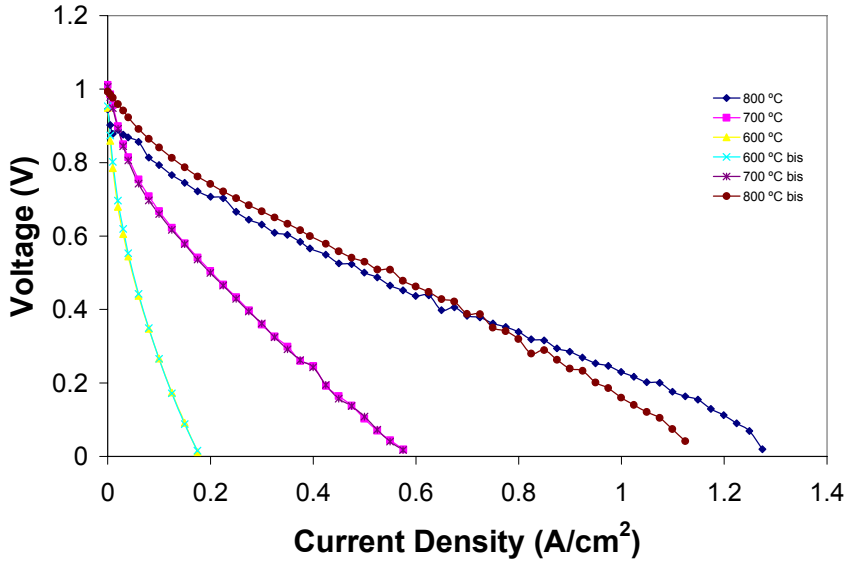
Voltage (V)
Current Density (A/cm2)
800 °C
700 °C
600 °C
600 °C bis
700 °C bis
800 °C bis

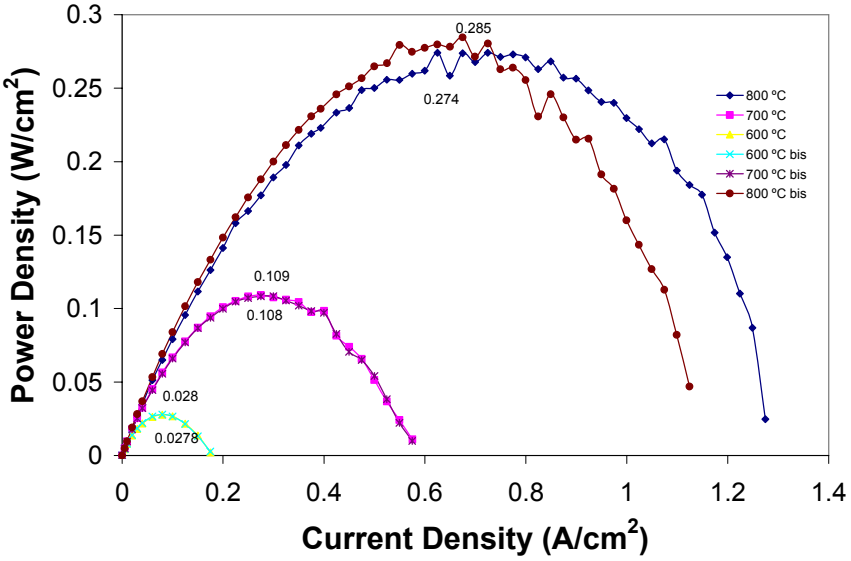
Power Density (W/cm2)
Current Density (A/cm2)
0.285
0.274
0.109
0.108
0.028
0.0278
800 °C
700 °C
600 °C
600 °C bis
700 °C bis
800 °C bis

C.8 SLFCO7

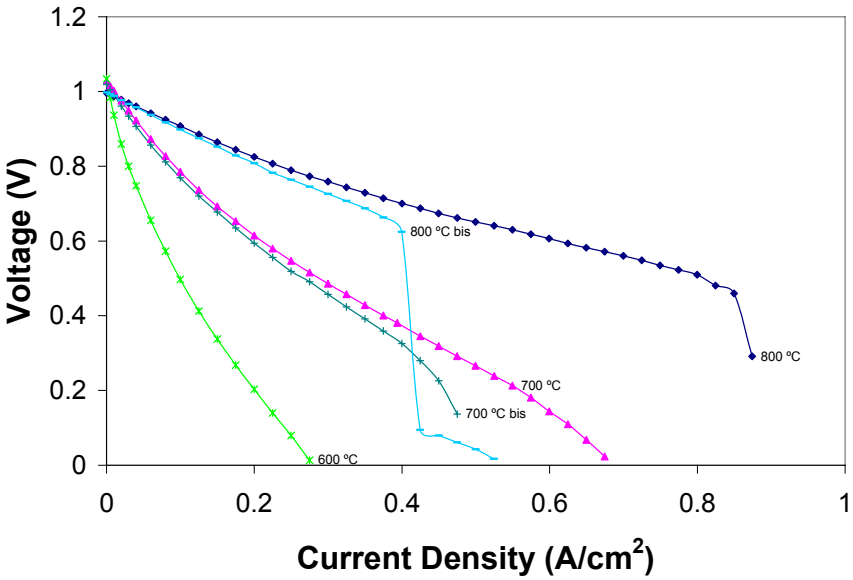
Voltage (V)
Current Density (A/cm²)
800 °C
800 °C bis
700 °C
700 °C bis
600 °C

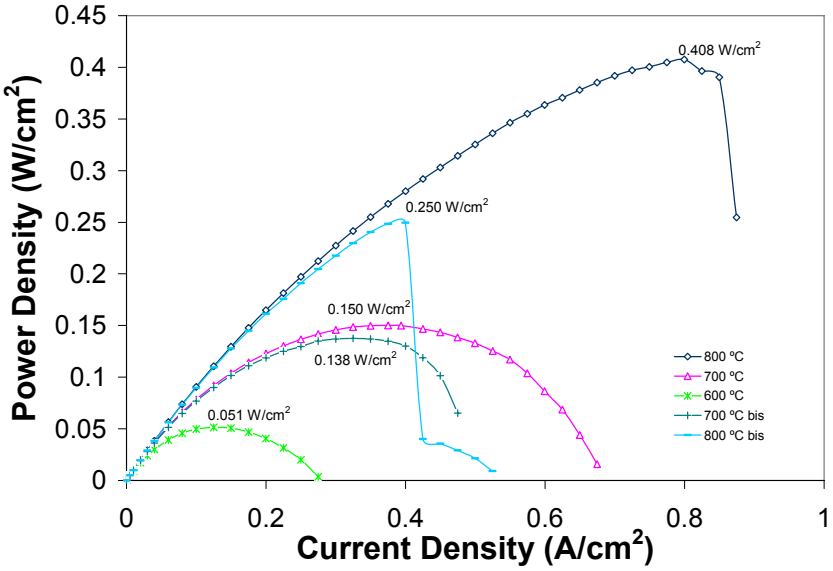
Power Density (W/cm²)
Current Density (A/cm²)
0.408 W/cm²
0.250 W/cm²
0.150 W/cm²
0.138 W/cm²
0.051 W/cm²
800 °C
700 °C
600 °C
700 °C bis
800 °C bis

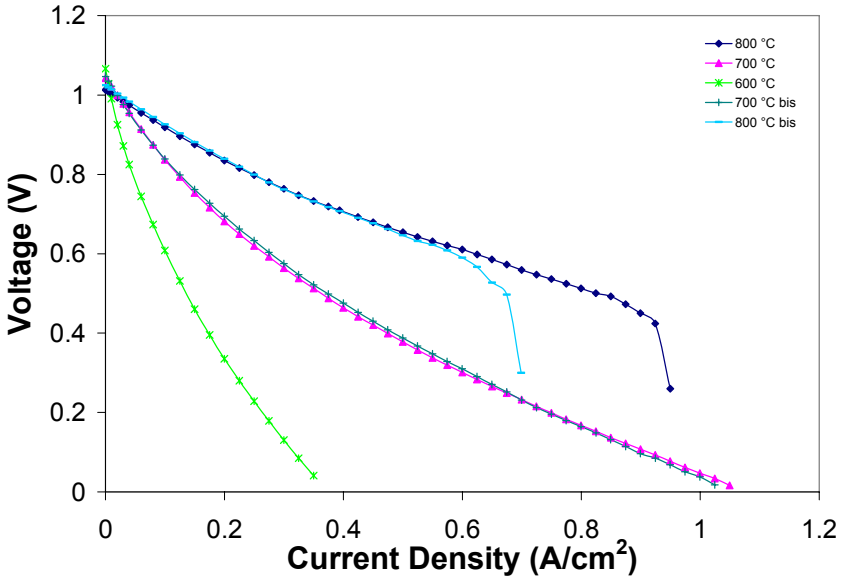
800 °C
700 °C
600 °C
700 °C bis
800 °C bis
Voltage (V)
Current Density (A/cm2)
0
0.2
0.4
0.6
0.8
1
1.2

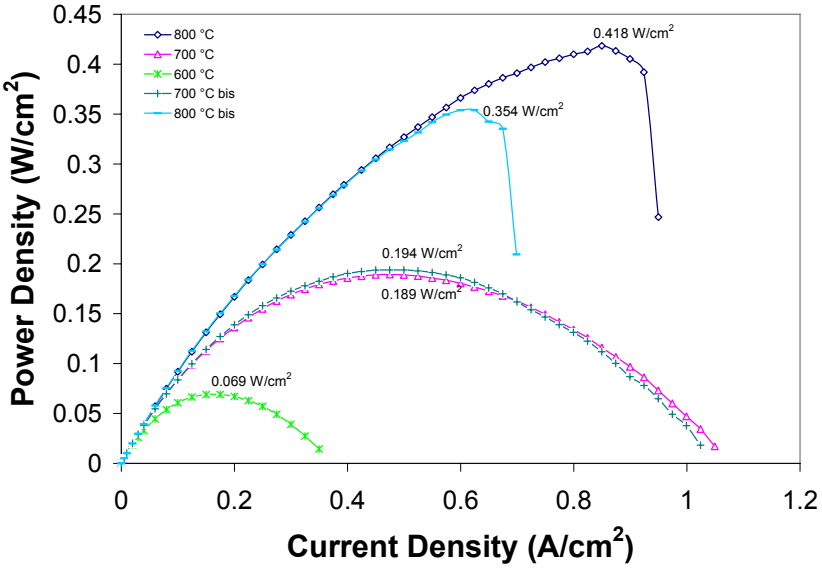
800 °C
700 °C
600 °C
700 °C bis
800 °C bis
0.418 W/cm2
0.354 W/cm2
0.194 W/cm2
0.189 W/cm2
0.069 W/cm2
Power Density (W/cm2)
Current Density (A/cm2)
0
0.05
0.1
0.15
0.2
0.25
0.3
0.35
0.4
0.45
0.6
0.8
1
1.2

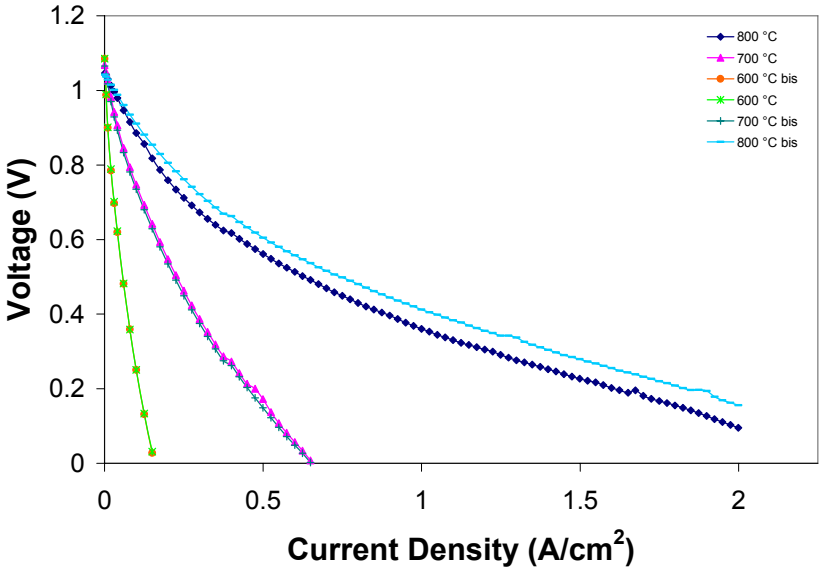
1.2
1
0.8
0.6
0.4
0.2
0
0
0.5
1
1.5
2
Voltage (V)
Current Density (A/cm2)
800 °C
700 °C
600 °C bis
600 °C
700 °C bis
800 °C bis

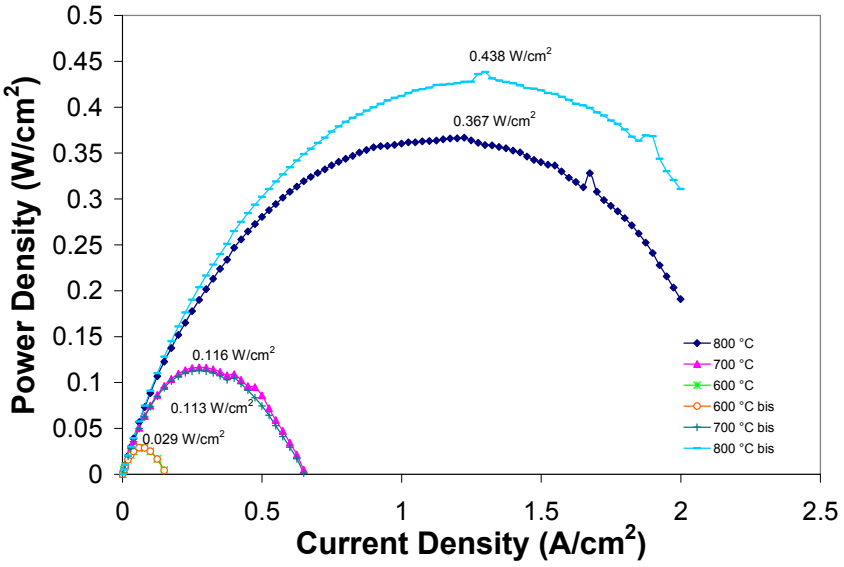
0.5
0.45
0.4
0.35
0.3
0.25
0.2
0.15
0.1
0.05
0
0
0.5
1
1.5
2
2.5
Power Density (W/cm2)
Current Density (A/cm2)
0.438 W/cm2
0.367 W/cm2
0.116 W/cm2
0.113 W/cm2
0.029 W/cm2
800 °C
700 °C
600 °C
600 °C bis
700 °C bis
800 °C bis

C.9 LSFCO10

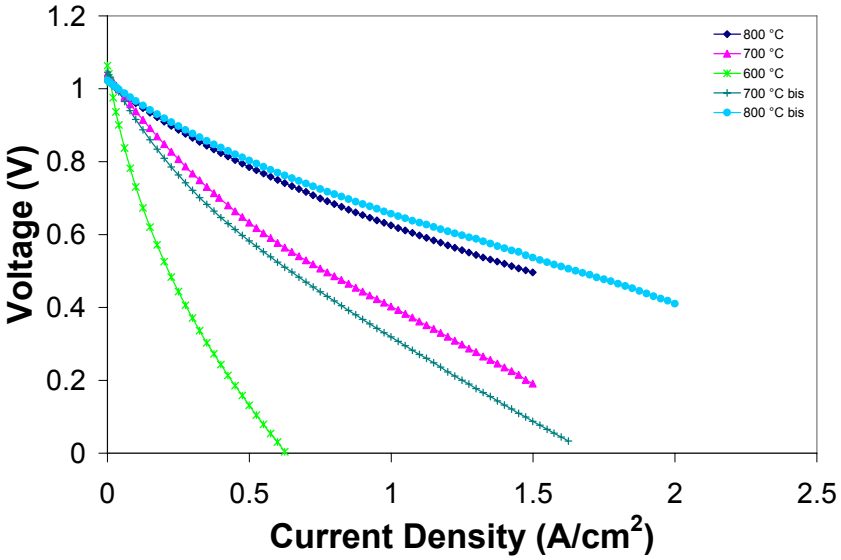
800 °C
700 °C
600 °C
700 °C bis
800 °C bis
Voltage (V)
Current Density (A/cm2)

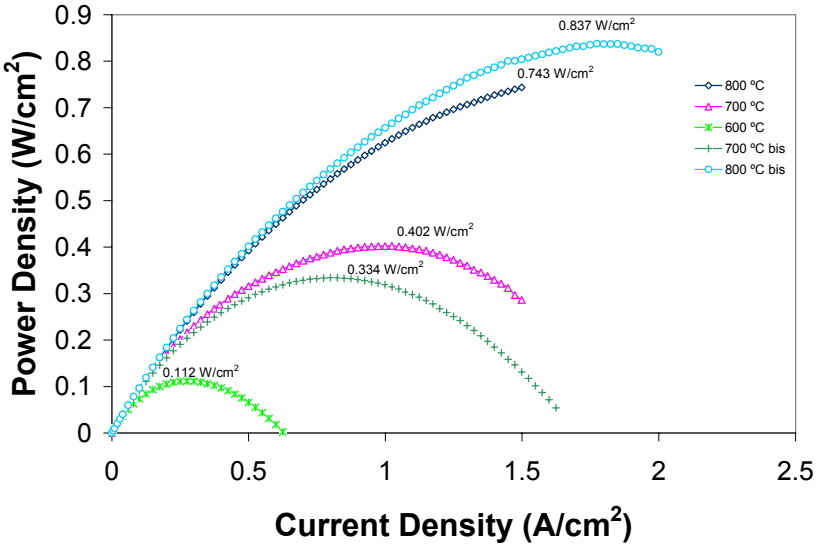
0.837 W/cm2
0.743 W/cm2
0.402 W/cm2
0.334 W/cm2
0.112 W/cm2
800 °C
700 °C
600 °C
700 °C bis
800 °C bis
Power Density (W/cm2)
Current Density (A/cm2)

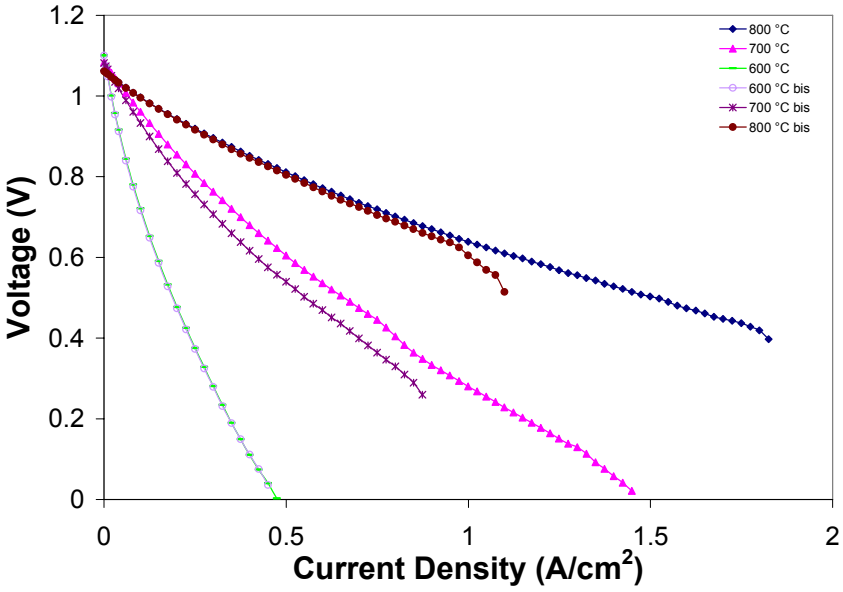
Voltage (V)
Current Density (A/cm2)
800 °C
700 °C
600 °C
600 °C bis
700 °C bis
800 °C bis

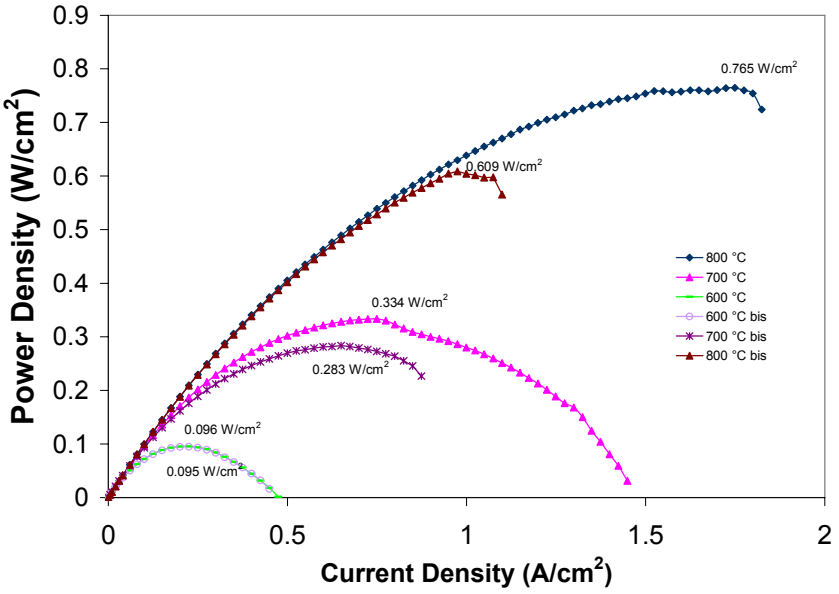
Power Density (W/cm2)
Current Density (A/cm2)
0.765 W/cm2
0.609 W/cm2
0.334 W/cm2
0.283 W/cm2
0.096 W/cm2
0.095 W/cm2
800 °C
700 °C
600 °C
600 °C bis
700 °C bis
800 °C bis

Abbreviations and Symbols

ABBREVIATIONS

A/E	Anode – electrolyte
ASR	Area specific resistance
BBP	Benzyl butyl phthalate
CVD	Chemical vapor deposition
DC	Direct current
EAVD	Electrostatic assisted vapor deposition
emf	Electromotive force
EtOH	Ethanol
EVD	Electrochemical vapor deposition
GDC	Gadolinium-doped ceria
IT-SOFC	Intermediate temperature solid oxide fuel cell
LSFCO10	$La_{2.7}Sr_{0.3}Fe_{1.4}Co_{0.6}O_{10-\delta}$
LSGM	$La_{0.8}Sr_{0.2}Ga_{0.8}Mg_{0.2}O_{3-\delta}$
LSM	$(La,Sr)MnO_3$
MEK	Methyl ethyl ketone
NSC	$Nd_{0.6}Sr_{0.4}CoO_3$

NSCF	$Nd_{0.6}Sr_{0.4}Co_{0.5}Fe_{0.5}O_3$
NSCF-Ag	Silver-impregnated $Nd_{0.6}Sr_{0.4}Co_{0.5}Fe_{0.5}O_3$
OCV	Open circuit voltage
PE	Phosphate ester
PEG	Polyethylene glycol
PVB	Polyvinyl butyral
sccm	Standard centimeter cubic per minute
SEM	Scanning electron microscope
SLFCO7	$Sr_3LaFe_{1.5}Co_{1.5}O_{7-\delta}$
SOFC	Solid oxide fuel cell
TEC	Thermal expansion coefficient
TPB	Triple phase boundaries
XRD	X-ray diffraction
YSZ	Yttria-stabilized zirconia

SYMBOLS

E_{cell}	Reversible cell voltage
F	Faraday's constant (96485.3 C)
I_L	Limiting current density (A/cm^2)
l_e	Electrolyte thickness

n	Number of electrons involved in a reaction
$p(X)$	Partial pressure of X
R	Molar gas constant (8.3144 J mol^{-1} K^{-1})
T	Temperature
V	Real voltage output (V)
ΔG	Gibbs free energy change
ΔG^o	Standard Gibbs free energy change
ΔH	Enthalpy change
ΔS	Entropy change
E^o	Standard cell voltage (V)
I	Current density (A/cm^2)
I_0	Exchange current density (A/cm^2)
ε	Efficiency
η	Polarization (V)
η_a	Activation polarization (V)
η_c	Concentration polarization (V)
η_Ω	Ohmic polarization (V)
ρ_e	Ionic resistivity of the electrolyte ($\Omega \cdot cm$)
σ	Conductivity (S/cm)

References

1. Appleby, A. J. and Foulkes, F. R., *Fuel Cell Handbook*, Krieger Publishing Company, Malabar, FL, (1993).

2. Minh, N. Q. and Takahashi, T., *Science and Technology of Ceramic Fuel Cells*, Elsevier, The Netherlands, (1995).

3. Thomas, S. and Zalbowitz, M., *Fuel Cells - Green Power*, Los Alamos National Laboratory, http://education.lanl.gov/resources/fuelcells/ (1999).

4. Williams, M. C. In *ASM Handbook. Corrosion: Fundamentals, Testing and Protection*; Cramer, S. D. and Covino, B. S., Jr., Eds.; ASM International: Materials Park, OH 44073-0002, Vol. 13-A, p. 178 (2003).

5. Hart, A. B. and Womack, G. J., *Fuel Cells: Theory and Application*, London, Chapman & Hall, (1967).

6. Will, J., Mitterdorfer, A., Kleinlogel, C., Perednis, D. and Gauckler, L. J., *Solid State Ionics*, **131**, 79 (2000).

7. Mukherjee, A., Maiti, B., Das Sharma, A., Basu, R. N. and Maiti, H. S., *Ceram. Int.*, **27**, 731 (2001).

8. Singhal, S. C. and Kendall, K., *High temperature solid oxide fuel cells: fundamentals, design and applications*, Elsevier Advanced Technology, Oxford, (2003).

9. Grove, W. R., *Philos. Mag.*, **14**, 127 (1839).

10. Nernst, W. H., *Z. Elektrochem.*, **6**, 41 (1899).

11. Schottky, W., *Wiss. Veröff. Siemens Werken*, **14**, 1 (1935).

12. Baur, E. and Preis, H., *Z. Elektrochem.*, **43**, 727 (1937).

13. McDougall, A., *Fuel Cells*, John Wiley & Sons, New York, (1976).

14. Pukrushpan, J. T., Stefanopoulou, A. G. and Peng, H., *Control of fuel cell power systems: principles, modeling, analysis and feedback design.*, Springer-Verlag, London, (2004).

15. Ivers-Tiffee, E. and Virkar, A. V. In *High temperature solid oxide fuel cells: fundamentals, design and applications*; Singhal, S. C. and Kendall, K., Eds.; Elsevier Advanced Technology: Oxford, p. 229 (2003).

16. Liu, J. and Barnett, S. A., *J. Am. Ceram. Soc.*, **85**, 3096 (2002).

17. Singhal, S. C., *Solid State Ionics*, **135**, 305 (2000).

18. Ishihara, T., Sammes, N. M. and Yamamoto, O. In *High temperature solid oxide fuel cells: fundamentals, design and applications*; Singhal, S. C. and Kendall, K., Eds.; Elsevier Advanced Technology: Oxford, p. 83 (2003).

19. Mori, M., Yamamoto, T. and Itoh, H. in *Considerations on Thermal Expansion of Nickel-Zirconia Anode in SOFC during Fabrication and Operation,* Stimming, U., Singhal, S. C., Tagawa, H. and Lehnert, W., editors, PV 97-40, p. 869, Solid Oxide Fuel Cells V, Aachen, Germany (1997).

20. Zhu, W. Z. and Deevi, S. C., *Mater. Sci. Eng., A*, **362**, 228 (2003).

21. Minh, N. Q., *J. Am. Ceram. Soc.*, **76**, 563 (1993).

22. Koide, H., Someya, Y., Yoshida, T. and Maruyama, T., *Solid State Ionics*, **132**, 253 (2000).

23. Van Roosmalen, J. A. M. and Cordfunke, E. H. P., *Solid State Ionics*, **52**, 303 (1992).

24. Hammouche, A., Siebert, E. and Hammou, A., *Mater. Res. Bull.*, **24**, 367 (1989).

25. De Souza, R. A. and Kliner, J. A., *Solid State Ionics*, **106**, 175 (1998).

26. Skinner, S. J., *Int. J. Inorg. Mat.*, **3**, 113 (2001).

27. Krist, K. and Wright, J. D. in *Fabrication methods for reduced temperature solid oxide fuel cells,* Singhal, S. C. and Iwahara, H., editors, PV 93-4, p. 782, Third International Symposium on Solid Oxide Fuel Cells, Honolulu, HI (1993).

28. Itoh, H., Mori, M., Mori, N. and Abe, T., *J. Pow. Sour.*, **49**, 315 (1994).

29. Mogensen, M. and Hendriksen, P. V. In *High temperature solid oxide fuel cells: fundamentals, design and applications*; Singhal, S. C. and Kendall, K., Eds.; Elsevier Advanced Technology: Oxford, p. 261 (2003).

30. Brown, F. T., *Energy*, **11**, 209 (1986).

31. Barnett, S. A., *Energy*, **15**, 1 (1990).

32. Tietz, F., Buchkremer, H. P. and Stöver, D., *Solid State Ionics*, **152-153**, 373 (2002).

33. Van Dieten, V. E. J. and Schoonman, J., *Solid State Ionics*, **57**, 141 (1992).

34. Bai, W., Choy, K. L., Rudkin, R. A. and Steele, B. C. H., *Solid State Ionics*, **113-115**, 259 (1998).

35. Ishihara, T., Shimose, K., Kudo, T., Nishiguchi, H., Akbay, T. and Takita, Y., *J. Am. Ceram. Soc.*, **83**, 1921 (2000).

36. Zhitomirsky, I. and Petric, A., *Mater. Sci. Eng., B*, **78**, 125 (2000).

37. De Souza, S., Visco, S. J. and De Jonghe, L. C., *J. Electrochem. Soc.*, **144**, L35 (1997).

38. Chen, X. J., Khor, K. A., Chan, S. H. and Yu, L. G., *Mater. Sci. Eng., A*, **341**, 43 (2003).

39. Chen, C. C., Nasrallah, M. M. and Anderson, H. U., *Solid State Ionics*, **70/71**, 101 (1994).

40. Wang, C., Worrell, W. L., Park, S., Vohs, J. M. and Gorte, R. J., *J. Electrochem. Soc.*, **148**, A864 (2001).

41. Minh, N. Q. and Montgomery, K. in *Performance of Reduced-Temperature SOFC stacks,* Stimming, U., Singhal, S. C., H., T. and Lehnert, W., editors, PV 97-40, p. 153, Fifth International Symposium on Solid Oxide Fuel Cells (SOFC-V), Aachen, Germany (1997).

42. Srivastava, P. K., Quach, T., Duan, Y. Y., Donelson, R., Jiang, S. P., Ciacchi, F. T. and Badwal, S. P. S., *Solid State Ionics*, **99**, 311 (1997).

43. Otoshi, S., Sasaki, Y., Ohnishi, H., Hase, M., Ishimaru, K., Ippommatsu, M., Higuchi, T., Miyayama, M. and Yanagida, H., *J. Electrochem. Soc.*, **138**, 1519 (1991).

44. Simner, S. P., Stevenson, J. W., Meinhardt, K. D. and Canfield, N. L. in *Development of Fabrication Techniques and Electrodes for Solid Oxide Fuel Cells*, Singhal, S. C. and Yokokawa, H., editors, PV 2001-16, p. 1051, Seventh International Symposium on Solid Oxide Fuel Cells (SOFC-VII), Tsukuba, Ibaraki, Japan (2001).

45. Lee, K. T. and Manthiram, A. in *Investigation of $Nd_{0.6}Sr_{0.4}Co_{1-y}M_yO_{3-\delta}$ (M = Fe and Mn) as cathode materials for intermediate temperature solid oxide fuel cells*, editors, 179, p. 131, Baltimore, MD, United States (2006).

46. Lee, K. T. and Manthiram, A., *Solid State Ionics*, **176**, 1521 (2005).

47. Lee, K. T., Bierschenk, D. M. and Manthiram, A., *J. Electrochem. Soc.*, **153**, A1255 (2006).

48. Ohrui, H., Matsushima, T. and Hirai, T., *J. Pow. Sour.*, **71**, 185 (1998).

49. Lee, K. T. and Manthiram, A. in *Investigation of $Nd_{1-x}Sr_xCoO_3$ as cathodes for intermediate temperature solid oxide fuel cells*, editors, p. 5, San Antonio, TX, United States (2004).

50. Zhitomirsky, I. and Petric, A., *J. Eur. Ceram. Soc.*, **20**, 2055 (2000).

51. Mistler, R. E. and Twiname, E. R., *Tape Casting: theory and practice*, The American Ceramic Society, Westerville, OH 43081, (2000).

52. Cassidy, M., Lindsay, G. and Kendall, K., *J. Pow. Sour.*, **61**, 189 (1996).

53. Dees, D. W., Claar, T. D., Easler, T. E., Fee, D. C. and Mrazek, F. C., *J. Electrochem. Soc.*, **134**, 2141 (1987).

54. Chick, L. A., Pederson, L. R., Maupin, G. D., Bates, J. L., Thomas, L. E. and Exarhos, G. J., *Mater. Lett.*, **10**, 6 (1990).

55. Yokokawa, H. and Horita, T. In *High Temperature Solid Oxide Fuel Cells: Fundamentals, Design and Applications*; Singhal, S. C. and Kendall, K., Eds.; Elsevier Advanced Technology: Oxford, UK, (2003).

56. Adler, S. B., *Solid State Ionics*, **111**, 125 (1998).

57. Badwal, S. P. S., Jiang, S. P., Love, J., Nowotny, J., Rekas, M. and Vance, E. R., *Ceram. Int.*, **27**, 419 (2001).

58. Petric, A., Huang, P. and Tietz, F., *Solid State Ionics*, **135**, 719 (2000).

59. Sakaki, Y., Takeda, Y., Kato, A., Imanishi, N., Yamamoto, O., Hattori, M., Iio, M. and Esaki, Y., *Solid State Ionics*, **118**, 187 (1999).

60. Tu, H. Y., Takeda, Y., Imanishi, N. and Yamamoto, O., *Solid State Ionics*, **117**, 277 (1999).

61. Lee, K. T. and Manthiram, A., *J. Electrochem. Soc.*, **153**, A794 (2006).

62. Lee, K. T. and Manthiram, A., *J. Electrochem. Soc.*, **152**, A197 (2005).

63. Lee, K. T. and Manthiram, A., *J. Pow. Sour.*, **160**, 903 (2006).

64. Steele, B. C. H., *Solid State Ionics*, **129**, 95 (2000).

65. Mogensen, M., Sammes, N. M. and Tompsett, G. A., *Solid State Ionics*, **129**, 63 (2000).

66. Mai, A., Haanappel, V. A. C., Uhlenbruck, S., Tietz, F. and Stover, D., *Solid State Ionics*, **176**, 1341 (2005).

67. Prado, F., Armstrong, T., Caneiro, A. and Manthiram, A., *J. Electrochem. Soc.*, **148**, J7 (2001).

68. Armstrong, T., Prado, F. and Manthiram, A., *Solid State Ionics*, **140**, 89 (2001).

69. Lee, K. T. and Manthiram, A., *Chem. Mater.*, **18**, 1621 (2006).

70. Ruddelsen, S. N. and Popper, P., *Acta Crystallogr.*, **11**, 54 (1958).

71. Hellebrand, H. In *Materials science and technology : a comprehensive treatment* Cahn, R. W., Haasen, P. and Kramer, E. J., Eds.; VCH: New York, Vol. 17A, p. 195 (1991).

Vita

Claudia Isela Torres Garibay was born on April 26th, 1972 in Chihuahua, Chihuahua, Mexico to Armando Torres Magallanes and Elia Garibay Sosa. She got a B.S. in Electrical and Industrial Engineering from the Instituto Tecnológico de Chihuahua in 1996 and a M.S. in Materials Science from the Centro de Investigacion en Materiales Avanzados (Advanced Materials Research Center) in 2000; both institutions located in her hometown. Between her undergraduate studies and master studies, she worked in industry in different engineering departments for three and half years. After the completion of her master degree, she lectured Vectorial Calculus and Physics Fundamentals at the Institute Tecnológico de Chihuahua for one year. She joined the University of Texas at Austin in Fall 2001. During her doctoral studies she worked as teaching assistant of Materials Engineering Laboratory and research assistant for the Institute of Advanced Technology.

Permanent address: Santo Domingo # 2920
Parques de San Felipe
Chihuahua, Chih.
31203 Mexico

This dissertation was typed by the author.